TECHNISCHE UNIVERSITÄT WIEN

**DIPLOMARBEIT**

# Optimizing Continuous Gas Fermentation of *Thermoanaerobacter kivui*: From Gasses to Acetate

Ausgeführt zum Zwecke der Erlangung des akademischen Grades eines Diplom-Ingenieurs unter der Leitung von

Univ. Ass. Prof. Dipl.-Ing. (FH) Dr. Stefan Pflügl

Betreut durch

Dipl.-Ing. Josef A. Horvath

am Institut für Verfahrenstechnik, Umwelttechnik und Technische Biowissenschaften

Technische Universität Wien

von

Ismail Cem Oktay, BSc.

| Wien, am | Unterschrift des Betreuers | eigenhändige Unterschrift |
|---|---|---|

## Eidesstattliche Erklärung

Hiermit erkläre ich, dass ich diese Diplomarbeit selbstständig verfasst habe, dass ich die verwendeten Quellen vollständig angegeben habe und dass ich Zitate die anderen Publikationen im Wortlaut oder dem Sinn nach entnommen sind, unter Angabe der Herkunft als Entlehnung kenntlich gemacht habe.

| | |
|---|---|
| Wien, am | eigenhändige Unterschrift |

# I. Abstract

As the world grapples with the pressing challenges of climate change and exceeding planetary boundaries, innovative approaches to carbon recycling are becoming increasingly relevant. This study investigates the potential of *Thermoanaerobacter kivui*, an acetogenic bacterium, to efficiently convert gaseous carbon substrates into organic compounds through gas fermentation. The primary aim of this research is to optimize the continuous gas fermentation process by focusing on critical operational parameters and the influence of various feeding strategies.

In this study, a CO-adapted *T. kivui* strain (CO1), previously developed by the research group, was employed in a series of experiments. The effects of medium composition, stirrer speed, and substrate types were evaluated. Results demonstrated that increasing the FeSO4*7H2O concentration to 33 mg/L in Moon Medium facilitated the transition to continuous operation. The established continuous cultures exhibited a maximum growth rate (μMax) of 0.143 $h^{-1}$, with $CO_2$ utilization rates ($CO_2$UR) and $H_2$ utilization rates (HUR) of 62.1 and 43.29 mmol $g^{-1}_{CDM}$ $h^{-1}$, respectively, under autotrophic conditions.

While continuous fermentation data for *T. kivui* is scarce in the literature, these rates are approximately 1.5 times higher than those reported for the comparable acetogen *Acetobacterium woodii* in steady-state continuous cultures, as reported by Novak et al. (2021). Furthermore, specific acetate productivities for *T. kivui* were found to be 43.29 mmol $g^{-1}_{CDM}$ $h^{-1}$, compared to 21.1 ± 2 mmol $g^{-1}_{CDM}$ $h^{-1}$ for *A. woodii*.

The results indicate that *T. kivui* holds significant promise for advancing carbon recycling efforts in practical applications. By addressing challenges related to scalability and reactor performance, *T. kivui* can serve as a viable candidate for sustainable carbon management strategies. The findings presented in this study could facilitate further research utilizing omics data to enhance our understanding of metabolic pathways and promote the development of value-added products and robust strains for industrial applications.

## II. Acknowledgements

I would like to express my deepest gratitude to everyone who supported me throughout the course of this thesis. This work would not have been possible without the guidance, encouragement, and assistance of several individuals.

First and foremost, I would like to thank my advisors Dipl.-Ing. Josef A. Horvath and Univ. Ass. Prof. Dipl.-Ing. (FH) Dr. Stefan Pflügl for their invaluable guidance, patience, and support throughout this process. Their insightful feedback and expertise were crucial to shaping my research and helping me overcome the many challenges I faced.

I am also deeply grateful to the Institute of Chemical, Environmental and Bioscience Engineering for the resources and opportunities provided to me.

On a personal note, I would like to thank my family for their constant encouragement, understanding, and love. To my dear wife, Mirjam Helena Schweiger, my mother, Fatos Oktay and my dear friends, Aaron Josef Gangl and Uliana Smirnova, your unwavering support and countless hours of distraction and encouragement made this journey more manageable. I truly appreciate the times when you lifted my spirits.

Finally, I want to thank everyone who contributed to this work, directly or indirectly, whose names may not appear here but whose support has been invaluable.

# Contents

# List of Figures

# List of Tables

# 1. Introduction

The era where topics such as deficiencies in raw materials or exceeding the planetary boundaries are being brushed off as “conspiracy theories” is coming to a fast end. Today a myriad of multidisciplinary researchers, civil circles, and governments are determined to analyze, halt, and eventually reverse the effects of human transgressions upon the natural world for over a century.

One interpretation of the overshot of planetary boundaries and the shortfall of the social foundation is proposed by Kate Raworth with the Doughnut Economic Model (2012). The work compares the planetary boundaries suggested by Rockström et al., (2009) and recently updated by Richardson et al., (2023) with shortcomings in the social foundation that is to support the suggested prosperity. Both the doughnut economic model and the planetary boundaries charts can be seen in Figure. 1.1.

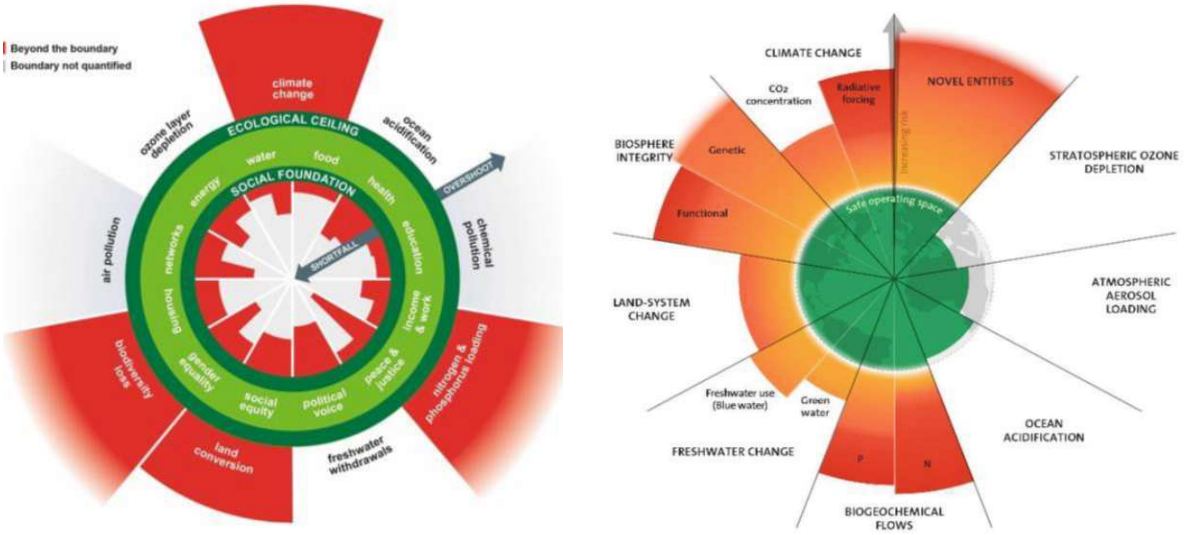


**Figure 1. 1 Doughnut *Economic Model (Raworth, K. 2017) and Planetary Boundaries (Richardson et al., 2023)***

The planetary boundaries chart shows that six out of the nine determined planetary boundaries have been exceeded by significant margins. Even as the most pressing concerns seemingly are the loss of novel entities, and biosphere integrity, alongside Phosphorus and Nitrogen accumulation that happens mostly in underground waters, it is important to note that the earth is an intricate biosystem tightly interwoven. Any crossed boundary is bound to have a cascade of effects on the other boundaries.

One of the most infamous indicators is the change in local and global temperatures. An effect caused by the radiative forcing of greenhouse gases, as these gases increase in their concentration in the atmosphere the reflectivity of the atmosphere against electromagnetic radiation increases. As the reflectivity increases, less energy can cross through the atmosphere, effectively trapping the electromagnetic radiation within.

Approximately 50% of this effect is caused by water vapors (Schmidt et al., 2010), followed by approximately 25% by clouds and close to 20% by $CO_2$. All other absorbers play minor roles. Even as the direct effect of $CO_2$ may be relatively small, the minor contribution to raising average temperatures is reflected in more water vapor and therefore further increase in temperatures. The human effect on climate change is very complex to measure with a high level of accuracy and is still a topic of debate in terms of causes and effects (Alsarhan et al., 2021) and many of the industries that form the backbone of our society cause a certain amount of carbon emissions in various forms. The issue becomes more complex still when the current economic state and goals for the growth of developing countries are considered (Yilmaz et al., 2023).

In recent years the determination to limit carbon emissions has changed form to limiting net carbon emissions by employing a circular carbon economy (CCE) (Saputra et al., 2022) through the utilization of the “4Rs” framework consisting of reduce, reuse, recycle, and remove approaches.

Carbon fixation in terms of incorporation of inorganic carbon into organic compounds is an essential part of our biosphere (Gleizer et al., 2020) enabling all life, as well as producing the fossil fuels that make up the majority of energy use worldwide. As such, the solutions to produce nutrients and fuels from C1- sources through gas fermentation (Section 1.2.1) are becoming increasingly popular. Gas fermenting microbes can metabolize gaseous feedstocks (Figure 1.2) such as carbon monoxide, carbon dioxide and methane (Dürre & Eikmanns, 2015; Lv et al., 2023).

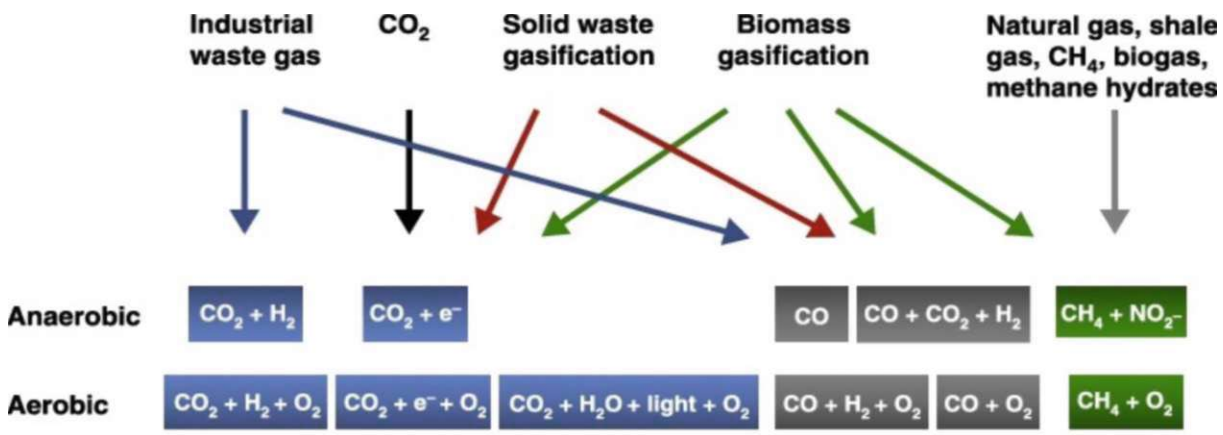


**Figure 1. 2 Gaseous C1-feedstocks and sources (Dürre & Eikmanns, 2015)**

Formate and methanol are two potential substrates for future applications as liquid sources of C1-feedstocks. As formate can be produced electrochemically from $CO_2$ and molecular hydrogen (Chen et al., 2008) or through biocatalysis (Nguyen et al., 2023). Using formate instead of the gas mixes (CO, $CO_2$, and $H_2$) also provides a safer alternative in terms of storage and operation. Formate oxidation, however, results in net $CO_2$ production. Müller et al., (2019) suggests that this disadvantage in biotechnological applications can be overcome by adding reductants such as $H_2$, especially in the case of mixotrophic acetogens.

$CO_2$ can be processed either through abiotic processes employing photocatalysis (Tan et al., 2018), electrocatalysis in terms of electrochemical $CO_2$ recycling (ECR) (Ross et al., 2019), chemical reforming such as Fischer-Tropfsch processes (Appel et al., 2013) or biologically by employing aerobic and anaerobic pathways. Yet even though abiotic methods have shown significant development in recent years (Appel et al., 2013), the feasible use of these methods remains limited by the issues with low product selectivity due to the thermodynamic stability of $CO_2$ (Ulmer et al., 2019; Zhao et al., 2021), difficulties in scaling due to extreme conditions with temperature and pressure, and sensitivity to the composition of the feedstock (Gleizer et al., 2020).

Biological systems, in contrast, require ambient or milder conditions (Onyenwoke & Wiegel, 2015; Schwarz et al., 2018), are highly specific in product formation, and are relatively robust against chemical impurities and environmental fluctuations (Gleizer et al., 2020).

Among the biological pathways to assimilate $CO_2$ (Table 1.1) and other C1 feedstocks into more complex hydrocarbons e.g. fuels and other chemicals, acetogenic bacteria have been regarded as having the highest industrial potential (Redl et al., 2017) particularly due to their higher efficiency and, depending on the source of the feedstock, non-competing nature with agricultural resources (Hawkins et al., 2013).

**Table 1. 1 Summary of seven natural $CO_2$-fixation pathways (Gong et al., 2016; Claassens 2021; Kim et al., 2020)**

| Pathway | Energy Source | ATP/$CO_2$ [mol/mol] | NAD(P)Ha/ $CO_2$ [mol/mol] | $CO_2$-fixing enzymes | Organisms | Type |
|---|---|---|---|---|---|---|
| **Calvin cycle** | Light | 3 | 2 | RuBisCo | Plant, Algae, Cyanobacteria | Aerobic |
| **3-hydroxypropionate cylcle** | Light | 1.67 | 1.67 | Acetyl-CoA carboxylase Propionyl-CoA carboxylase | Green nonsulfur bacteria | Aerobic |
| **3-hydroxypropionate-4-hydroxybutyrate cycle** | Sulfur Hydrogen | 2 | 2 | Acetyl-CoA carboxylase Propionyl-CoA carboxylase | Archaea | Aerobic |
| **Wood-Ljungdahl Pathway** | Hydrogen | 0.5 | 2 | Formate Dehydrogenase CODH/Acetyl-CoA synthase | Anaerobic bacteria (mainly Acetogens) | Anaerobic |
| **Reductive TCA cycle** | Light Sulfur | 1 | 2 | 2-Oxoglutarate synthase Isocitrate dehydrogenase | Green sulfur bacteria, Anaerobic bacteria | Anaerobic |
| **Dicarboxlate/4-hydroxybutyrate cycle** | Sulfur Hydrogen | 2 | 2 | Acetyl-CoA carboxylase Propionyl-CoA carboxylase | Archaea | Anaerobic |
| **Reductive Glysine Pathway** | Hydrogen Sulphate | 0.5 | 2 | Formate Dehydrogenase Glycine Synthase | Bacteria | Anaerobic |

## 1.1. Acetogens

Acetogenic bacteria are one of the most ancient organisms that have evolved to survive. As such, the acetogens have been isolated from a variety of habitats including soil, sediments, and the intestinal tracts of animals including humans, and are found worldwide. The scarcity of the nutrients in the environments in that the acetogens are often seen as well as the energy limitations have led them to evolve the most efficient $CO_2$-fixing metabolic pathway (Fast et al., 2015). The group employs the Wood-Ljungdahl pathway (WLP), an ancient carbon dioxide fixation pathway (Figure 1. 3) which is intricately linked to energy conservation through a chemiosmotic mechanism for ATP synthesis (Katsvy et al., 2021). The WLP is responsible for fixing $CO_2$, containing two branches leading to the formation of the methyl and carbonyl groups of acetyl-CoA from a single molecule of $CO_2$ each (Wood et al., 1986). The convergence of these branches forms a C–C bond, yielding acetyl-CoA (Ragsdale and Pierce, 2008). In the anabolic route, acetyl-CoA is carboxylated to pyruvate, diverting carbon towards typical biosynthetic pathways such as the incomplete reductive tricarboxylic acid cycle (Furdui and Ragsdale, 2000). In the catabolic route, acetyl-CoA is converted to acetate via acetyl-phosphate, generating one mol of ATP per mol of acetate (Katsvy et al., 2021).

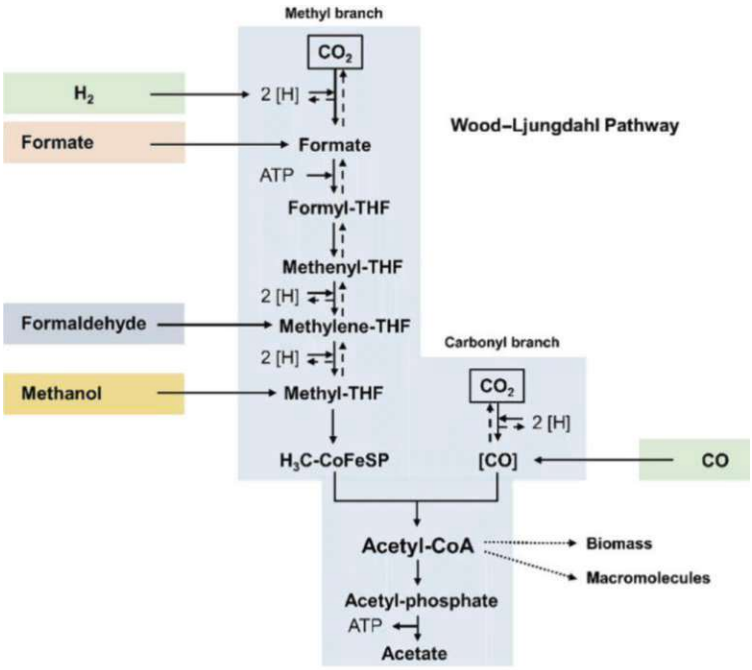


**Figure 1. 3 Wood-Ljungdahl Pathway of $CO_2$ reduction, reducing equivalents [H]; oxidative direction of the pathway shown in dashed arrows (Müller, 2019)**

As the second step of the methyl branch consumes one ATP (Katsvy et al., 2021), the overall ATP balance via substrate-level phosphorylation is zero. To achieve net cellular ATP,

acetogens employ electron bifurcation for ATP synthesis (Schoelmerich and Müller, 2019; Müller, 2019).

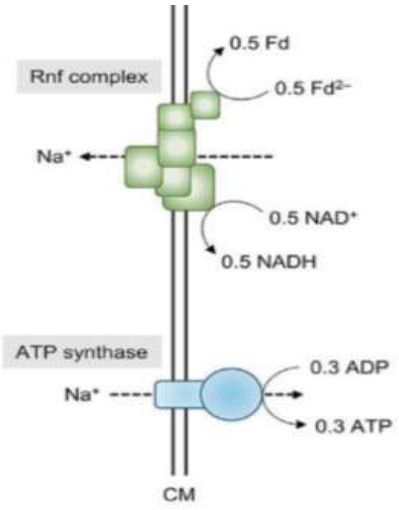


**Figure 1. 4 Coupling of Rnf complex with ATP synthase (Müller, 2019)**

Electron bifurcation is a mechanism of energetic coupling that saves cellular ATP. An exergonic redox reaction is the driving force of an endergonic redox reaction using the same electron donor (Müller, 2019), as an exergonic electron flow drives the endergonic uphill transport from $H_2$ ($E_0$'= -414 mV) to ferredoxin ($E_0$'= -450 to -500 mV). In order to achieve this chemiosmotic mechanism, acetogens possess two types of respiratory enzymes utilizing reduced ferredoxin ($Fd^{2-}$) as the electron donor. The electron acceptor can be either $H^+$, in which case the Ech complex (Section 2.2.2) acts as a $Fd^{2-}$:$H^+$ oxidoreductase (Schoelmerich and Müller, 2019) or $NAD^+$, where the Rnf complex (Figure 1.3) is a $Fd^{2-}$:$NAD^+$ oxidoreductase (Biegel and Müller, 2010). Electron transfer from reduced Fd to the electron acceptor results in an ion transport ($H^+$, $Na^+$) across the cytoplasmic membrane, therefore establishing a transmembrane electrochemical ion potential that drives ATP synthesis through a membrane-integral F1F0 ATP synthase (Hess et al., 2014; Schoelmerich and Müller, 2019; Kuhns et al., 2020). Importantly, the acetogens establish the necessary transmembrane ion transport through either Ech or Rnf complexes, they are classified as Rnf- or Ech- acetogens as to date, no acetogen has been discovered to contain both (Schuchmann and Müller, 2014). In either case, the number of moles of reduced Fd available plays a pivotal role in influencing the energetics of acetogens as reduced ferredoxin not only fuels the Rnf/Ech complexes but also is the electron donor for the reduction of $CO_2$ to CO, a key reaction in WLP pathway (Schuhmann and Müller, 2012).

Molecular hydrogen serves as the ultimate electron source, oxidized by electron-bifurcating hydrogenases (Schuchmann and Müller, 2012; Wang et al., 2013a; b). Four moles of hydrogen oxidation result in the simultaneous reduction of two moles of pyridine

nucleotides (NAD(P)H) and two moles of reduced Fd. If multiple WLP enzymes necessitate reduced Fd as a reductant, a shortage of electrons for the electron transport chain occurs. Therefore, understanding the electron carrier specificity of WLP enzymes in a given species is crucial for calculating ATP yields.

The side products of these respiratory processes are $H_2$ or NADH, subsequently re-oxidized during autotrophic growth which in turn will act as a reducing agent for the production of acetyl-CoA (Müller, 2003; Katsyv and Müller, 2020).

$$2\ CO_2 + 4\ H_2 + nADP + nP_i \rightarrow CH_3COOH + 2\ H_2O + nATP \quad (1)$$

Autotrophic growth of acetogens on $H_2$ and $CO_2$ (equation 1) constitutes a free energy change of only -95 kJ/mol under standard conditions, which approaches the thermodynamic limit. (Müller, 2003).

### 1.1.1. Thermoanaerobacter kivui

*Thermoanaerobacer kivui*, formerly known as *Acetogenium kivui*, is a chemolithotrophic, thermophilic anaerobe that stains Gram-negative even though the cell wall suggests a Gram-positive structure. It was isolated from Lake Kivu which lies on the border between the Democratic Republic of Congo and Rwanda (Leigh et al., 1981) and is a non-motile, non-spore-forming, rod-shaped organism often occurring in pairs or chains.

The optimum temperature for *T. kivui* is 66 ˚C while growth occurs from 50 ˚C to 72 ˚C (Onyenwoke & Wiegel, 2015). The optimum pH is 6.4. while the cells have the ability to grow between 5.3 and 7.3. The thermophilic nature of *T. kivui* brings certain advantages to fermentation as cooling of the fermenter is not necessary, thus sparing potentially high expenses during operation as well as preventing possible contamination.

Growth is obligately anaerobic, so that it requires a reducing agent such as cysteine present in the medium. The cells can tolerate the presence of oxygen in room temperatures as there is no apparent metabolic activity under such conditions (Basen et al., 2017).

*T. kivui* can utilize several compounds as a carbon source to varying degrees (Section 2.1). In addition to the organic compounds *T. kivui* can utilize $CO_2$ and $H_2$ as a substrate and recently has been adapted to use CO as a sole substrate (Weghoff & Müller, 2016).

The width of the cells is approximately 0.7 µm, while the length of the cells varies between 2 and 7.5 µm. The length of the cells is dependent on the substrate used for growth, cells grown on $H_2$ and $CO_2$ vary in their length between 2 and 3.5 µm, while the cells grown on glucose have a length of 5.5 and 7.5 µm (Leigh et al. 1981). Glucose-grown cells are reported to have an abundance of densely staining spherical inclusions. Even though the cells are Gram-negative, the cell wall is of the Gram-positive structure covered by a hexagonal S-layer composed of 80 kDa subunits (Onyenwoke & Wiegel, 2015).

A recent study by Schwarz et al., (2021) suggested that higher pressures could have a stimulatory effect on *T. kivui* to explain the cell densities achieved in serum bottles as opposed to bioreactors. As the cells have been isolated from the sediments of Lake Kivu it is not unlikely that the wild cells are more accustomed to higher pressures and therefore benefit from a stimulatory effect.

### 1.2. Acetogens in Process Engineering

Even as the metabolic versatility, as well as the flexibility of substrates, allows for a myriad of potential applications, the acetogens' use on an industrial scale remains limited to ethanol production from syngas utilizing *C. autoethanogenum* as the biocatalyst in processes pioneered by LanzaTech (Pavan et al., 2022).

Factories that currently operate in China, India and Belgium utilize captured gasses from off-gas streams of steel mills, ferroalloy mills and refineries have been used in capturing more than 240,000 tons of CO according to LanzaTech management, producing ethanol as a primary product.

The recent review by Bengelsdorf et al., (2018) verifies the conversion of acetyl-CoA to a product in a reaction sequence that does not yield additional ATP is not possible as $CO_2$ reduction has a net ATP demand. *C. ljungdahlii*, *C. ragsdalei*, *C. autoethanogenum* and, *A. bacchi* have all been reported to produce ethanol with *C. ljungdahlii* producing the highest

concentration of 48 g $L^{-1}$ (Daniell et al., 2012). With acetogens that can metabolize, or adapt to metabolize CO directly, such as *T. kivui* or *A. woodii*, the energetics improve to a certain extent, however neither species are reported to produce ethanol naturally (Bertsch & Müller, 2019). Even with CO as an electron donor, many products can only be produced as a byproduct due to the unfavorable energetics of the pathways (Müller, 2019).

Acetogens' ability to hydrogenate $CO_2$ to formic acid and the corresponding base formate also provides a nontoxic, stable choice to store hydrogen, since hydrogen is a promising and widely considered alternative to fossil fuels in a sustainable future (Brandon & Kurban, 2017). This process is close to equilibrium with a free energy change ($\Delta G^\circ$) of -3 kJ/mol (Müller, 2019). This low energy demand is further beneficial for a hydrogen storage application since the reaction is easily reversible to release hydrogen on demand. Formic acid contains 4.4 wt% of hydrogen and is in equilibrium with $H_2$ and $CO_2$ by the equation:

$$H_2 + CO_2 \rightleftharpoons HCOO^- + H^+ \qquad G_0' = 3.5\ kJmol^{-1} \qquad (2)$$

This reaction according to eq. 2 is the first reaction of WLP (Fig. 1.2.) and is catalyzed by the hydrogen-dependent $CO_2$ reductase (HDCR). These notable enzymes can use molecular hydrogen directly to reduce $CO_2$, without the need for external soluble cofactors as opposed to other formate dehydrogenases (Schwarz & Müller, 2020). Both *A. woodii* and *T. kivui* possess HDCR enzymes with a [FeFe]-hydrogenase module (HydA2), a formate dehydrogenase module, and two small iron-sulfur-containing subunits. While *A. woodii* possesses two isoenzymes, one with cysteine and the other with selenocysteine in the formate dehydrogenase module, *T. kivui* has only the cysteine form (Müller, 2019). The formate dehydrogenase modules are further differentiated by molybdenum content in *A. woodii* and with tungsten content in *T. kivui*. Both enzymes are highly stable and CO tolerant, even though the enzymes are strongly inhibited by CO ($K_i$ (CO)= 0.11 µM), they are fully reactivated upon removal of it. However, both enzymes are highly oxygen sensitive, and any industrial application must ensure a strict absence of oxygen and low redox potential in the environment (Müller, 2019).

The *A. woodii* HDCR catalyzes hydrogenation of $CO_2$ at 30 ˚C, and 0.8 bar of $H_2$ and 0.2 bar of $CO_2$ partial pressures at an astonishing turnover frequency (TOF) 101.600 $h^{-1}$ (Schuhmann and Müller, 2013). Whereas the even superior enzyme from *T. kivui* catalyzes at 60 ˚C and 1 bar of $H_2$+$CO_2$, with a TOF of 9.556.000 $h^{-1}$ (Schwarz et al., 2018). Both enzymes provide turnover frequencies significantly higher than state-of-the-art chemical catalysts, given the important problem of hydrogen storage, these reversible catalysts offer a promising step towards the efficient conversion of hydrogen into the liquid organic hydrogen carrier formic acid/formate and the subsequent release of the gas for the following utilization as an energy source (Schwarz et al., 2018).

In recent years, significant strides have been made in developing acetogens through metabolic engineering for the conversion of syngas into biofuels and other bio-commodities such as degradable bioplastics (Daniel et al., 2012). Where acetyl-CoA generated by the Wood-Ljungdahl pathway serves as a key intermediate for the synthesis of cell mass as well as products (Liew et al., 2013). Ethanol, butanol, lactic acid, 2,3-butanediol, isopropanol and isopropene have been suggested as direct sources of fuel, or as precursors to other hydrocarbon fuels, pharmaceuticals, nutrients, cosmetics and biodegradable polymers (Bertsch & Müller, 2019; Sokic-Lazic et al., 2011; Tokiwa et al., 2009).

Methods such as adaptive laboratory evolution (ALE) and genetic modification through plasmid-based engineering, ClosTron, transposon mutagenesis, homologous recombination, and CRISPR-Cas genome editing have been employed to establish more favorable bioenergetics and products in acetogens including *A. woodii*, *C. ljungdahlii*, *C. autoethanogenum*, *M. thermoacetica*, *E. limosum* Jin et al., 2020).

### 1.2.1. Gas Fermentation

Gas fermentation involves the fixation of gaseous carbon through gas-fermenting microorganisms and different operation strategies. Up until 2010, research on gas fermentation was negligible. However, with the rising concerns about climate change, scientific and industrial interest in the microbial conversion of CO and $CO_2$ has surged, leading to the evaluation of different methods and processes (Bajracharya et al., 2022).

Gas fermentation is a promising technology for the production of chemicals, fuels and nutrients (Köpke & Simpson, 2020) using toxic or greenhouse gases as it can be used with a single or a mixture of gasses such as CO, $CO_2$, or syngas. However, for the process to be economically viable, especially in the case of *T. kivui*, a much better understanding of the organism and operation techniques must be established through research.

The main parameters that influence gas fermentation are the selection of biocatalyst, medium composition, pH, temperature, partial and headspace pressure, reactor design and configuration, and mode of operation.

For the biocatalysts to utilize the gas feedstock, substrates need to first pass into a liquid culture medium via gas-to-liquid mass transfer, the rate-limiting step in gas fermentation processes (Bajracharya et al., 2022).

The rate of diffusion of a component between phases is dependent on the mass transfer coefficient, this coefficient is based on the notion that the mass transfer between two phases takes place through a boundary layer that is referred to as the two-film theory (Whitman, 1962). For liquids, the mass transfer coefficient is conventionally written as '$k_L$', and the overall rate of mass transfer is also dependent on the contact area between two phases often termed 'a, the volumetric gas transfer coefficient therefore is referred to as the '$k_L a$' value. The $k_L a$ value can be represented mathematically according to eq. 3.

$$dC_i/dt = k_L a\,(C_i^* - C_{iL}) \tag{3}$$

where, $C_i^*$ is the saturated concentration of the dissolved component *i*, and $C_{iL}$ is the current concentration of the dissolved component *i* in the media. Experimental determination of $k_L a$ can however be difficult and therefore it may be more sensible to measure gas uptake rates and fit the data in mass balances to calculate rates and yields.

Effective gas-to-liquid transfer can be energy intensive, requiring repeated recirculation of feed gas or elevated mechanical forces.

#### 1.2.1.1. Continuous Stirred-Tank Reactor

Continuous stirred tank reactors (CSTR) use mechanical force, typically through a turbine propellor situated above the sparger, to sheer gas bubbles into bubbles of smaller size. Both

increase the available interface for mass transfer and increase the retention time due to the smaller equivalent diameter of the bubbles (Park et al., 2017). Even as the CSTR enables a high gas-to-liquid mass transfer and uniform mixing, the elevated power input per reactor volume is required for stirring (Kaiser et al., 2018). The shear forces created by the stirrers can also influence microorganisms in several ways, such as changes in morphology, variation in growth and metabolite formation, and even causing damage to cell structures (Zhou et al., 2018).

#### 1.2.1.2. Bubble Column

Bubble columns are typically cylindrical vessels fixed with a sparger at the bottom. The convective flow of the gas supplied from the bottom facilitates both mixing and improved gas-to-liquid mass transfer (Bajracharya et al., 2022). The simple setup results in a lower capital investment and depending on the mode of operation lower operating costs. Length to diameter ratio is a crucial factor for both design and scaling (Asimakopoulos et al., 2018). A specific type of bubble column where a circulating liquid flow promotes mixing is called a gas lift reactor.

#### 1.2.1.3. Trickle Bed Reactor

A trickle bed reactor is packed with an inert material on which the microbial biofilm is grown. The liquid is sprayed from the top of the reactor and trickles down the film surface, while the gas can either be supplied cocurrently or countercrurrently. The large surface area to volume ratio allows for an exceptionally large gas-to-liquid interface and therefore allows for high gas-to-liquid mass transfer without necessitating mechanical agitation. Due to these effects, the reactors require lower gas and liquid flow rates (Liew et al., 2013; Dutta et al., 2023).

#### 1.2.1.4. Hollow Fiber Membrane Reactor

Similar to trickle bed reactors, hollow fiber membrane reactors use a membrane system that provides a highly specific interface that provides support for microbial growth. Even as the hollow fiber membrane reactors achieve very high gas-to-liquid mass transfer and smaller

volumes, the nature of the reactors makes them prone to biofouling caused by microbial growth causing a thick biofilm formation and therefore negatively impacting the reactor performance (Asimakopoulos et al., 2018).

### 1.2.2. Operation Strategies

Operation strategies can be summarized under three groups, batch, fed-batch, and continuous. Each operation strategy comes with its own advantages and disadvantages, and the choice of the reactor and operating strategies influences product concentration, yields, and amount of impurities. Since the reactor selection can be a major component of the initial and operating costs, some compromises are necessary in the choice while still considering, the substrate, biocatalyst type and activity, productivity and conversion rates, and downstream processing (Liu, 2017).

#### 1.2.2.1. Batch Process

Batch mode implies that there is no mass flow through the borders of the working system, in terms of gas fermentation this means that the medium, biocatalyst, and the gaseous substrate are sealed in a controlled volume. This state is almost exclusive to serum bottles and Hungate tubes. In this regard, the batch cultures are usually used to grow pre-cultures to inoculate a more elaborate fermentation system, or for experimental purposes. As no control is necessary, batch cultures are very easy to operate and also to replicate, however, the conditions such as substrate availability, levels of metabolites, and pH in the batch are always changing (Liu, 2017; Bajracharya et al., 2022). Industrially the downtime periods of reactor preparation and prolonged lag phases can lead to an overall lower productivity (Liu, 2017).

#### 1.2.2.2. Fed-Batch Process

Fed-batch operation is when the gaseous substrate is continuously supplied to the controlled volume. This is achieved through one of the bioreactor setups explained in section 2.3.1, working with a bioreactor offers further control options in terms of pH and gas flow. These control options provide new opportunities such as maintaining optimum

conditions to obtain higher concentrations of biomass or manipulating the conditions to achieve specific results such as forcing the microorganisms to produce secondary metabolites and limiting the growth rates (Burger et al., 2022; Liu, 2017). The accumulation of the metabolites is, however, still a limiting factor with fed-batch operations, and often leads to toxic levels and inhibits the growth and substrate formation (Klemps et al., 1987). Since the cultures under fed-batch conditions also have a limited lifespan, the downtimes are comparable to batch operations.

#### 1.2.2.3. Continuous Processes

The continuous processes can be regarded as the most controlled type of operation. Unlike in the batch and fed-batch operations, the medium is constantly replaced with a fresh medium while the reactor broth, containing metabolites and cells in case of no cell retention, is removed from the reactor, keeping the reactor volume constant. After a certain period of time, the system can reach a steady state where cell, metabolite, and substrate concentrations remain constant (Liu, 2017). Therefore, achieving continuous processes is very significant in terms of industry as a product with uniform quality could be supplied through extended periods of time where the steady product formation facilitates steady downstream processing and therefore reduces the downtimes to a minimum. Continuous processing is also highly relevant for scientific studies, as conditions can be manipulated to obtain experimental data for a better understanding of transitions in metabolism through various approaches such as omics analysis. The data obtained can then be used to generate more knowledge and be used for future improvements. However, establishing and maintaining continuous cultures are more demanding in terms of process control as opposed to other modes of operation, and keeping strictly anaerobic conditions requires increased attention from the operators, especially in cases where toxic or explosive gasses are involved such as $H_2$ or CO.

Given the urgency of mitigating carbon emissions to stay within planetary boundaries, the need for sustainable carbon recycling processes is more critical than ever. Among the promising strategies, biological carbon recycling, particularly through the use of acetogenic bacteria, has emerged as a potential solution. These bacteria can convert gaseous carbon compounds, such as $CO_2$ and CO, into organic compounds, offering a circular approach to carbon management. One such acetogen, *Thermoanaerobacter kivui*, stands out due to its high efficiency in gas fermentation processes, its ability to thrive in thermophilic environments, and its promising role in industrial-scale biofuel production. Its capability to utilize gaseous feedstocks, such as $CO_2$ and $H_2$, positions it as a key organism in the development of sustainable carbon recycling technologies. This study seeks to optimize the continuous gas fermentation process using T. kivui, focusing on operational parameters that could enhance the efficiency of carbon fixation. By addressing key challenges in scalability and reactor performance, this research aims to contribute to the development of sustainable biotechnological solutions to global carbon management.

## 1.3. Goals of this study

The primary aim of this study was to establish and optimize continuous gas fermentation with the extremophile acetogen *T. kivui*.

To this purpose, following sub-goals and research questions were established:

**Optimization of Continuous Gas Fermentation**

Objective: To establish and optimize continuous gas fermentation processes using *T. kivui*, focusing on operational parameters and the influence of different feeding strategies.

- What are the critical operational parameters for establishing continuous gas fermentation in a Continuous Stirred Tank Reactor (CSTR)?
- How does the inclusion of glucose in the feed affect the performance of continuous gas fermentation in terms of growth, metabolic activity, and product formation?

**Scalability and Reactor Comparison**

Objective: To assess the scalability of continuous fermentation processes and compare the performance of different reactor types.

- What are the growth profiles and scalability potential of *T. kivui* in a bubble column reactor compared to other reactor types?

**Evaluation of Strains and Substrate Utilization**

Objective: To select the most suitable strain of *T. kivui* and understand its performance with various substrates under different conditions.

- Which strain of *T. kivui* exhibits the highest growth rates and cell density under various gaseous substrate compositions?
- How does the selected strain perform under different pH levels and acetate concentrations when using gaseous substrates?

- What is the growth profile and adaptability of the selected strain when formate is used as the sole substrate?

# 2. Theoretical Principles

## 2.1. *Thermoanaerobacter kivui* Growth and Substrates

*T. kivui* has a naturally high doubling rate with respect to other acetogens at approximately 2.7 hours (Daniell et al., 1990). The suggested stoichiometry for growth under chemolithotrophic conditions is as follows:

$$4.1H_2 + 2.4CO_2 \rightarrow CH_3COOH + 0.1 \text{ cell C} + 0.3 \text{ unrecovered C} \quad (4)$$

$$6.8CO \rightarrow CH_3COOH + 3.5CO_2 + 0.4 \text{ cell C} + 0.9 \text{ unrecovered C} \quad (5)$$

For the glucose-cultivated cells:

$$C_6H_{12}O_6 + 0.7CO_2 \rightarrow 2.7CH_3COOH + 0.4 \text{ cell C} + 0.9 \text{ unrecovered C} \quad (6)$$

**Table 2. 1 Average Maximal Optical Densities from stationary phase cultures of *T. kivui* DSM2030 (Jain et al., 2020)**

| Substrate | $OD_{600}$ |
|---|---|
| No substrate | n.d. |
| 25 mM Glucose | 2.64±0.11 |
| 25 mM Glucose + 50 mM Formate | 2.86±0.14 |
| $H_2 + CO_2$ (1 bar) | 0.57±0.02 |
| $H_2 + CO_2$ (1 bar) + 50 mM Formate | 0.8±0.02 |
| 25 mM Mannitol | 2.46±0 |
| 25 mM Mannitol + 50 mM Formate | 2.45±0 |
| 300 mM Formate | 0.22±0.017 |
| 50 mM Pyruvate | 0.15±0.01 |

Production of acetate is comparable regardless of chemolithotrophic and heterotrophic feeding profiles, 14.5 mM and 15.2 mM respectively. Cell yields however strongly vary depending on the feeding profile as dry cell yields as high as 0.43 g/L have been recorded under heterotrophic conditions as opposed to 0.07 g/L under chemolithotrophic conditions, yielding an acetate to dry weight ratio of 35 and 207 respectively. As energy production and biomass synthesis are obligately coupled to acetogenesis, the ratio of acetate formed to biomass synthesized is a direct reflection of cell energetics which demonstrates that cells experience an increasing energy demand under increasingly minimal conditions. It is also recognized that minimal amounts of (0.2 mM) $H_2$ were produced alongside acetate in cells that were cultivated with CO or glucose.

*T. kivui* is not naturally able to grow on CO as a sole substrate. However, cells that were pre-grown on $H_2$ and $CO_2$ can be adapted to grow on CO alone through multiple passages with increasing CO percentages (Weghoff & Müller, 2016). It is noted that a lag phase occurs through each transfer to a higher CO concentration resulting in increased doubling times. The lag phase subsides however after at least three passages under the same conditions. Table 2.1. can be referred to for growth under different feeding regimes.

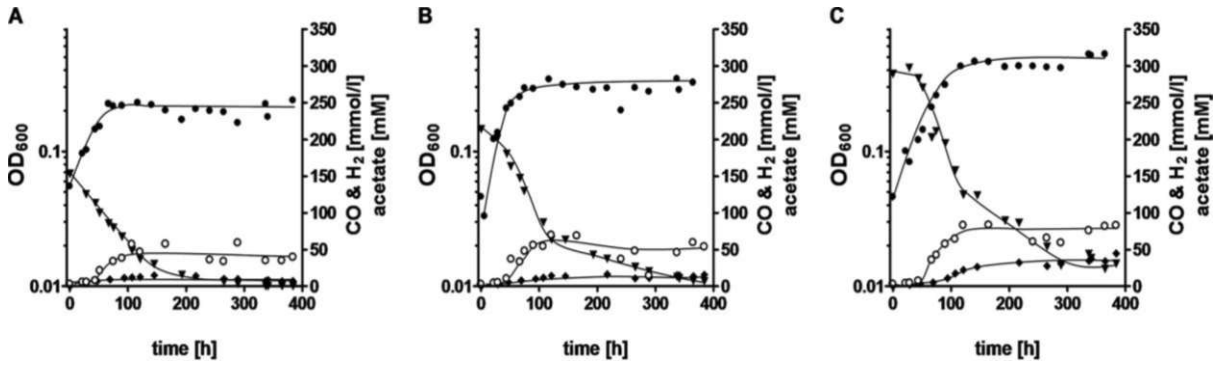


**Figure 2. 1 CO *consumption, acetate production, and H2 formation in cells growing on increasing concentrations of CO. The gas phase consisted of 30% CO (A), 50% CO (B), or 70% CO (C). N2 plus CO2 (80:20 [vol/vol]) was used as the makeup gas at a final pressure of 2 x 10$^5$ Pa. All cultures were grown in a complex medium, and growth was measured by monitoring the optical density (•) at 600 nm. The concentrations of CO (▼) and H2 (⧫) in the gas phase and of acetate in the liquid phase (○) were determined by gas chromatography. Shown are data from one representative experiment out of three independent replicates. (Weghoff & Müller, 2016)***

*T. kivui* also has the ability to grow on formate as a sole substrate as formate synthesis is the first step of the WLP. This ability is relevant as formate can be produced readily from $H_2$ and $CO_2$ and as opposed to the gas mixture it is a stable liquid that can be safely stored. The final cell densities are inferior in comparison to gas fermentation which could be the result of an inhibitory effect of formate in higher concentrations particularly with the HDCR enzyme. Alternatively, this could be the result of an increased energy demand for the metabolism. Figure 2.1 and Table 2.1 can be referred to for growth profiles and achieved cell densities under different feeding regimes.

## 2.2. Important Proteins, Their Functions and Inhibitions in *T. kivui*

### 2.2.1. Hydrogen-Dependent Carbon Dioxide Reductase (HDCR)

The HDCR complex found in *T. kivui* consists of 2 catalytic subunits, formate dehydrogenase and a [FeFe]-hydrogenase (FDH) as well as 2 small subunits carrying iron-sulfur [FeS]-clusters (Schwarz & Müller, 2020; Jain et al., 2020). HDCR catalyzes formate-dependent hydrogen formation or hydrogen-dependent formate formation depending on the concentrations of $H_2$, $CO_2$, and formate (Jain et al., 2020) as well as accepting CO as an electron donor via ferredoxin (Schwarz & Müller, 2020).

HDCR in *T. kivui* requires strictly anoxic conditions. The reduction of $CO_2$ to formate with hydrogen as the electron donor is close to thermodynamic equilibrium ($E_0$' [$CO_2$/formate] = –432 mV; $E_0$' [2 $H^+/H_2$] = –414 mV).

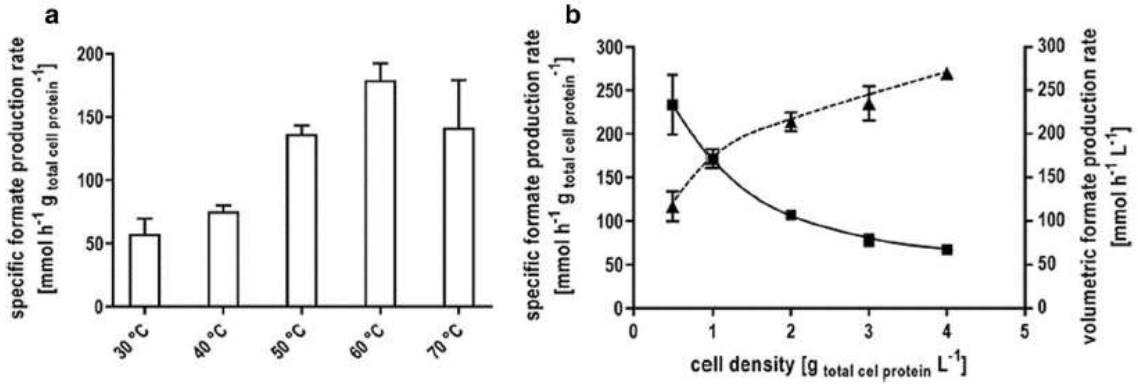


**Figure 2. 2 Characterization of hydrogen dependent $CO_2$ reduction by whole cells of T. kivui. (A) resting cells of T. kivui (1mg/mL) (B) the influence of the cell density on formate production (■) initial formate production rates, (▲) volumetric production rates(Schwarz & Müller, 2020).**

The reaction occurs according to eq. 2 and as the K value is close to one, the chemical equilibrium can be manipulated by pH, pressure, and substrate/product concentrations. Alkaline environments serve as proton scavengers and therefore pull the reaction on the product side (Schwarz & Müller, 2020). *T. kivui* resting cells have been reported to produce formate at the rate of 152 mmol $g^{-1}h^{-1}$ (Figure 2.2), impressive as it is, when the direction of the reaction is shifted towards $H_2$ + $CO_2$, production rates as high as 685 mmol $g^{-1}h^{-1}$ have been reported under ideal conditions. Even as the ideal temperature for growth is 66 ˚C for *T. kivui*, specific formate production is shown to be highest at 60 ˚C by Schwarz and Müller.

### 2.2.2. Energy-converting hydrogenase (Ech)

Energy-converting hydrogenases (Ech) are a group of membrane-bound respiratory enzyme complexes that couple the oxidation of reduced Fd with the reduction of protons and vice versa (Katsvy & Müller, 2022).

*T. kivui* has two Ech-type complexes, Ech1 and Ech2 composed of 9 and 8 subunits respectively. Both protein complexes consist of three modules, the electron input module, an electron output module comprising a [NiFe]-hydrogenase, and a membrane integral domain for ion translocation (Schoelmerich and Müller, 2019; Katsvy & Müller, 2022).

Reduced ferredoxin is oxidized by the reduction of protons to hydrogen gas is an exergonic reaction, and most likely, the liberated redox energy is used to pump $H^+$ outside of the cells, establishing a $H^+$ gradient (Schoelmerich & Müller, 2019). The reaction catalyzed is bidirectional, and when the conditions require it the Ech can reduce ferredoxin with $H_2$ as the electron donor. Even though it was originally thought that the Ech-type complexes in *T. kivui* transport only $H^+$ ions, a recent study by Schoelmerich and Müller, (2019) shows that *T. kivui* has also established a $Na^+$ gradient. According to this study, inverted membrane vesicles revealed both $H^+$ and $Na^+$ transport is coupled in cases where CO is oxidized, it has not been established however if one or both Ech complexes are involved in this process. This study further shows both Ech clusters are transcriptionally upregulated in the case of autotrophic growth. Since ATP is much more limited in the case of autotrophic growth, the $H^+$ gradient and the reduction of Fd become much more important for the *T. kivui*. The relative transcript levels of ech1 and ech2 have been shown to increase 6- and 16-fold respectively in cells grown on $H_2$ and 31- and 43-fold in cells grown on CO, as opposed to glucose-grown cells. This up-regulation is argued to be a crucial reason for the successful adaptation of *T. kivui* to grow on CO, and it is also likely that it is crucial for the adaptation to autotrophic growth in terms of continuous fermentations.

### 2.2.3. ATP-Synthase

The $F_1F_0$ ATP-Synthase is another group of membrane integral enzyme complexes. The $F_1F_0$ ATP-synthase is universally accepted as a rotary motor that uses a proton gradient to drive ATP synthesis (Capaldi & Aggeler, 2002; Schoelmerich & Müller, 2019). The function of this complex is especially important in case of autotrophic growth, as the energy limitations imposed by the conditions leave it as the sole source of net ATP gain. Even though the Ech activity does lead to $Na^+$ transport, $Na^+$ dependency for growth has not been encountered (Hess et al., 2014; Schoelmerich & Müller, 2019), and the ATP synthase does not contain a conserved $Na^+$ binding motif (Hess et al., 2014). The ATP-synthase in *T. kivui* solely consumes the $H^+$ gradient established by the Ech complex.

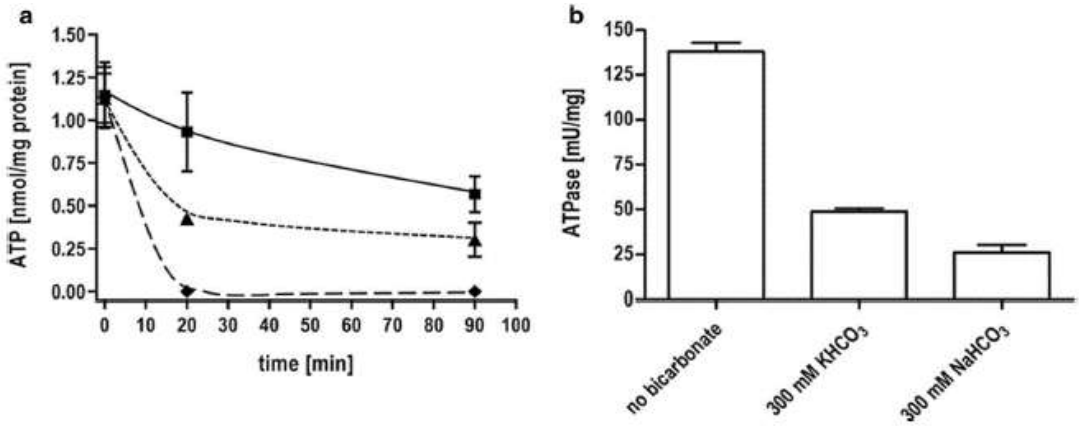


**Figure 2. 3 Effect of bicarbonate on the ATP content of resting cells and ATP hydrolysis catalyzed by membranes of T. kivui. (A) resting cells of T. kivui (1mg/mL) (■) without bicarbonate, (▲) 50mM $KHCO_3$, (♦) 300mM $KHCO_3$ (B) Memranes from T. kivui (Schwarz & Müller, 2020).**

A recent study by Schwarz and Müller, (2020) has shown that ATP hydrolysis may be inhibited by the presence of bicarbonate (Figure 2.3) where both resting cells and cell membranes have been tested for ATP synthesis. Intracellular ATP content of the whole cells has been shown to decrease by 38% in the presence of 50 mM $KHCO_3$ and by 81% with 300 mM $KHCO_3$.

### 2.2.4. [FeFe]-Hydrogenase Complex HydABC

The electron bifurcating [FeFe]-hydrogenase in *T. kivui* is an enzyme that produces $H_2$ during fermentation using NADPH and reduced ferredoxin. However, the enzyme can also operate in the reverse direction if the conditions demand it, as is the case for autotrophic growth (Müller et al., 2018). The low potential electron donor Fd is required for the function of both Ech-type complexes and for the reduction of $CO_2$ to CO which is the precursor of the carbonyl group of acetate (Schuhman & Müller, 2014). A recent study by Katsvy et al., (2023) has shown that the HydABC complex from *T. kivui* catalyzes the electron bifurcation from $H_2$ to Fd and $NADP^+$ with an activity of 20.5 ± 2.8 U $mg^{-1}$. In this study, a model for the catalytic cycle of HydABC is also proposed (Figure 2.4). In which, oxidation of hydrogen gas by the H-cluster in the HydA subunit leads to the reduction of flavin mononucleotide (FMN) and subsequent electron transfer to B2 and C1. Reduction of B2 increases the binding affinity of $NADP^+$. Reduction of C1 triggers conformational changes in HydC that open toward the HydB C-ter domain. Another $H_2$ oxidation step leads to electron transfer to the nucleotide-binding site, and the formation of NADPH. Reduction and dissociation of the nucleotide decrease the C1–B3 distance, which allows for electron transfer to the HydB C-terminal (C-ter) domain. NADPH dissociates and HydC transitions into a closed state that prevents electron backflow to the FMN site. Fd binding allows for electron transfer from the HydB C-ter domain, leading to oxidized HydABC, and reinitiation of a new catalytic cycle.

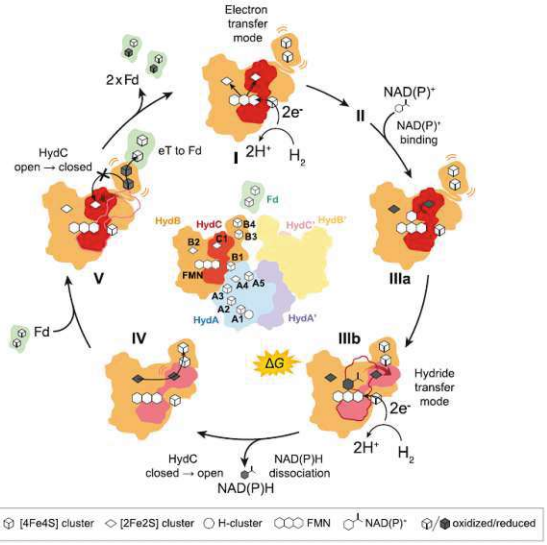


***Figure 2. 4 Suggested electron bifurcating mechanism of HydABC (Katsvy et al., 2023)***

### 2.2.5. PFOR and CODH/Acs

Two enzyme complexes are located in the central switch point of catabolic and anabolic processes. The bifunctional carbon monoxide dehydrogenase/Acetyl-CoA synthase (CODH/Acs) unites both branches of the WLP by fusing a methyl group with enzyme-bound CO (Katsvy et al., 2021b).

Under heterotrophic conditions using sugars, PFOR's role is to provide acetyl-CoA and reduced Fd from pyruvate, which then can be used by Ech-complexes to establish a chemiosmotic proton gradient (Schoelmeric & Müller, 2019). It has been shown that PFOR, alongside acetate kinase is inhibited by the existence of acetate within the medium (Figure 2.11.).

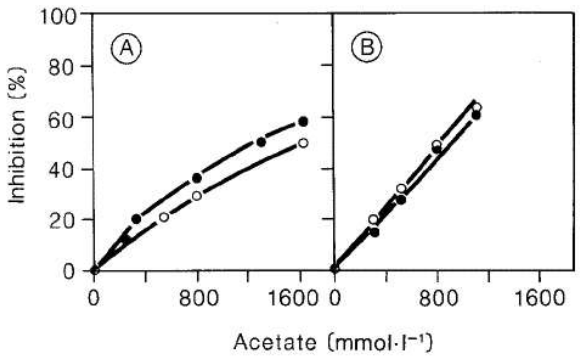


**Figure 2. 5 Effects of potassium-(○) or sodium-(●) acetate on PFOR (A) and acetate kinase (B) (Klemps et al. 1987)**

The bifunctional CODH/Acs enzyme complex, on the other hand, brings methyl and carbonyl branches of the WLP to provide acetyl-CoA which in turn is either converted to acetate for energy conservation or utilized for biomass synthesis. However, the CODH/Acs complex is also responsible for the reduction of $CO_2$ to enzyme-bound CO (Jain et al., 2021). The oxidation of CO to $CO_2$ is accomplished by the monofunctional CODH (Jain et al., 2021).

## 2.3. *T. kivui* metabolism

*T. Kivui* is an Ech- complex containing (Hess et al., 2014) thermophilic acetogen, that can grow chemolitoautotrophically with high rates on $CO_2$+$H_2$, CO, or a mixture of all three gasses (Leigh et al., 1981; Klemps et al., 1987; Hess et al., 2014) in addition to the other organic substrates mentioned in the substrates section.

The catabolism of *T. kivui* can be considered under three modules. The oxidative module deals with the oxidation of organic substrates to acetate while providing ATP, reduced Fd, and NADH (Figure 2.8). The WLP can be considered as an energy-neutral, cytoplasmic enzyme system for reoxidation of NADPH and reduced Fd (Figures 2.6 ; 2.7 ; 2.8). Finally, the

redox balancing module consists of Ech complexes, ATP synthase, and electron-bifurcating hydrogenase enzymes. The electrochemical $H^+$ (Hess et al., 2014) gradient is used for ferredoxin (ox/red) and ATP production by Ech complexes and ATP synthase, respectively. The hydrogenase enzyme balances the redox pools of ferredoxin (ox/red) and $NADP^+$/NADPH (Figures 2.6, 2.7, and 2.8).

### 2.3.1. Metabolism with Autotrophic Feeding

When $CO_2$ and $H_2$ are used as a substrate, $CO_2$ is reduced in the methyl branch to formate by the HDCR complex that contains a formate dehydrogenase (Ragsdale and Pierce, 2008; Schoelmerich & Müller, 2019; Jain et al. 2020). The formate is then bound by formyl-THF-synthetase, in an ATP-dependent reaction to formyl-THF (Weghoff & Müller, 2016). The formyl group is then further reduced to a methenyl group by the methenyl-THF-cyclohydrolase (Schoelmerich & Müller, 2019; Hess et al., 2014). Methenyl-THF is further converted to methylene-THF by an NADPH-dependent methylene-THF dehydrogenase (Schoelmeric & Müller, 2019; Katsvy et al., 2021; Hess et al., 2014). The branch continues with the reduction of the methylene-THF to methyl-THF by the methylene-THF reductase(Hess et al. 2014) which according to Katsvy et al., (2021) is catalyzed by a coupling of methylene-THF reductase with the membrane-bound Ech complex and uses reduced Fd as an electron donor and not NADPH or NADH. The methyl branch then concludes with the methyl group being bound to corrinoid/FeS protein (CoFeSP) by the methyl transferase (Hess et al., 2014; Katsvy et al., 2021; Jain et al., 2020).

On the carbonyl branch, $CO_2$ is reduced by the CO dehydrogenase/acetyl-CoA (CODH/Acs) synthase to enzyme-bound CO in a reduced ferredoxin-dependent reaction (Schoelmerich & Müller, 2019; Katsvy et al., 2021). The two branches come together as the enzyme-bound CO is combined with the methyl group and CoA on the CODH/Acs to form acetyl-CoA. From there on, acetyl-CoA can be utilized either in an anabolic fashion by being used in biosynthetic pathways or can be converted to acetyl phosphate by phosphotransactylase and eventually to acetate by acetyl kinase resulting in an ATP gain (Hess et al., 2014). The overall equation is according to eq. 7.

$$4\ H_2 + 2\ CO_2 \rightarrow CH_3COOH + 2\ H_2O\ \ (\Delta G_0' = -95\ kJ/mol.) \qquad (7)$$

It is important to note that WLP results in no net ATP gain for the whole cell (Schuhmann and Müller, 2014), *T. kivui* uses the respiratory enzyme Ech to create a chemiosmotic mechanism for ATP synthesis (Hess et al., 2014).

Should CO be the substrate available the metabolism follows the same principles with the exception of CO to $CO_2$ oxidation that is facilitated either by CODH (Katsvy et al., 2021) or CODH/Acs (Weghoff & Müller, 2016) according to the eq. 8.

$$4CO + 4H_2O \rightarrow 4CO_2 + 4H_2 \qquad (\Delta G_0' = -20\ kJ/mol.) \qquad (8)$$

The overall reaction occurs according to eq. 9.

$$4\ CO + 2\ H_2O \rightarrow 2\ CO_2 + CH_3COOH \qquad (\Delta G_0' = -165.6\ kJ/mol.) \qquad (9)$$

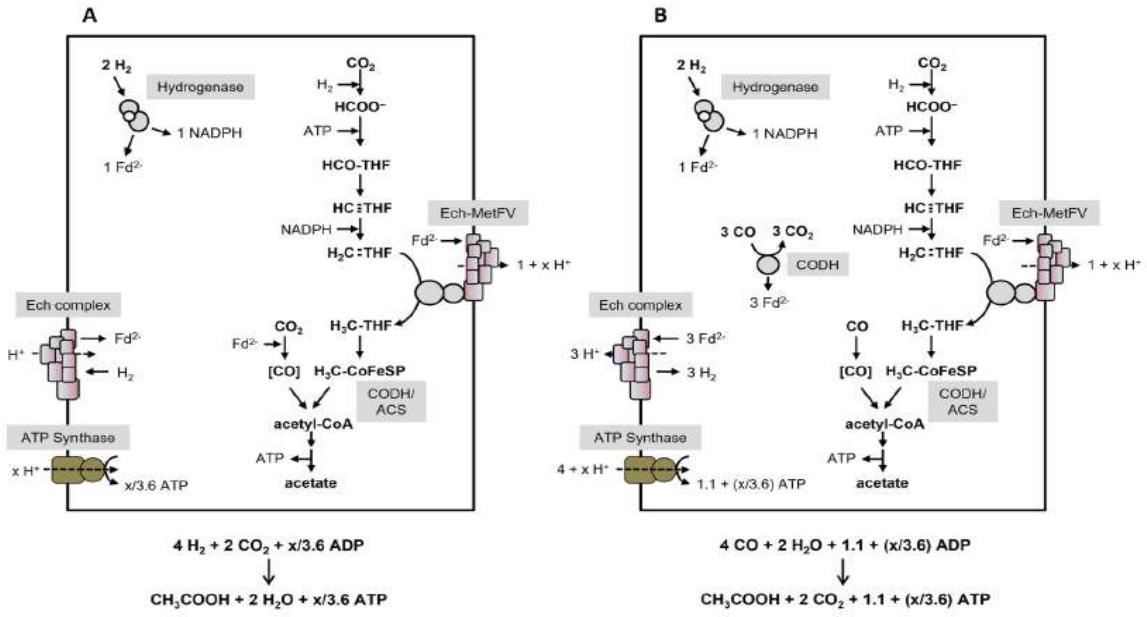


***Figure 2. 6*** **WLP pathway and bioenergetics of acetate formation from $H_2$ + $CO_2$ (A) or CO (B) in T. kivui (Katsvy et al. , 2021).**

An iteration of the WLP in *T. kivui* is depicted in Figure 2.6, the coupling of MetFV type MTHFR with the Ech complex is a hypothesis by Katsvy et al., (2021). It is important to note that the Ech complex changes the function depending on the substrate type, $CO_2$ + $H_2$ or CO, to either use the extracellular $H^+$ gradient to provide reduced Fd or use the reduced Fd to establish an

$H^+$ gradient respectively. The exact stoichiometry behind the electrons and energy conservation remains unknown, and further research is necessary to establish a definitive mapping of the metabolic pathway.

In addition to the gasses mentioned in this section, *T. kivui* can also adapt to utilize formate via WLP as the sole energy and carbon source for growth. Acetogenesis in this case follows the same principles, with the exception of HDCR reversing its function (Burger et al., 2022) to produce essential $CO_2$ for the carboxyl branch of the WLP, and $H_2$ for reduced Fd, NADPH, and ATP. Growth based on formate as the sole substrate is limited (Table 2.1.). It is noted however, that once glucose-grown cells reach the resting phase, introducing formate to the medium drives the cells to almost oxidize formate completely into $H_2$ and $CO_2$ and not towards the production of acetate (Burger et al., 2022). The optimum conditions for driving the resting cells to $H_2$ production are noted as 70˚C and a pH of 7. Figure 2.7 depicts a further iteration of the WLP pathway with formate as a sole substrate. Table 2.2. can be reviewed for experimental results of whole-cell $H_2$ production.

***Table 2. 2 $qH_2$ and HER of formate based $H_2$ production by whole T. kivui cells under optimized reaction conditions (Burger et al., 2022).***

| **$H_2$ Production** | **Condition: 0.3 mg $mL^{-1}$ cells in 300 mM sodium formate** | **Condition: 4 mh $mL^{-1}$ cells 600 mM sodium formate** |
|---|---|---|
| $qH_2$ (mmol $g^{-1}$ $h^{-1}$) | 685 ± 87 | 250 ± 2 |
| HER (mmol $L^{-1}$ $h^{-1}$) | 205 ± 26 | 999 ± 6 |

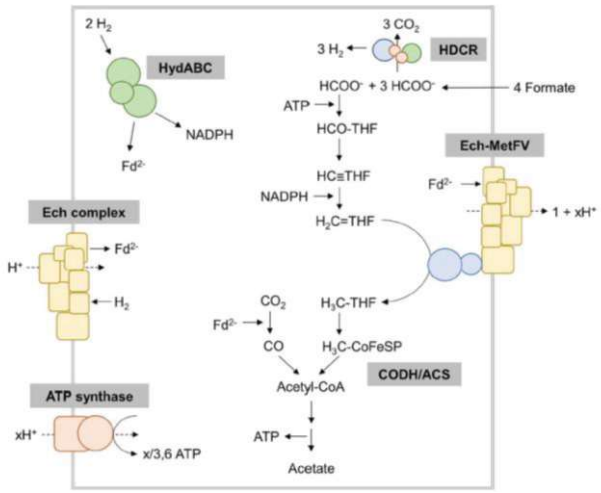


***Figure 2. 7 WLP pathway and bioenergetics of acetate formation from Formate in T. kivui (Burger et al., 2022).***

### 2.3.2. Metabolism with Heterotrophic Feeding

The availability of glucose greatly enhances the ability to produce energy, as glucose is converted to acetate via glycolysis. Glucose is first converted to pyruvate which in turn provides 2 ATP and 2 NADH conversion of the said pyruvate to acetyl-CoA further provides 2 $CO_2$ and 2 reduced Fd, finally in the case of the catabolic route, acetyl-CoA is converted to acetate producing again 2 additional ATP. The produced $CO_2$ is further utilized by the WLP to produce additional acetate. Ech complex uses $H_2$ to produce necessary $Fd^{2-}$ which is oxidized by the bifurcating hydrogenase and the Nfn complex to produce $H_2$ and to reduce $NADP^+$, respectively. The rest of the WLP functions as it would under $CO_2 + H_2$ metabolism. The abundance of energy is reflected in the achieved cell densities (Table 2.1.). The described pathway including glycolysis is depicted in Figure 2.8.

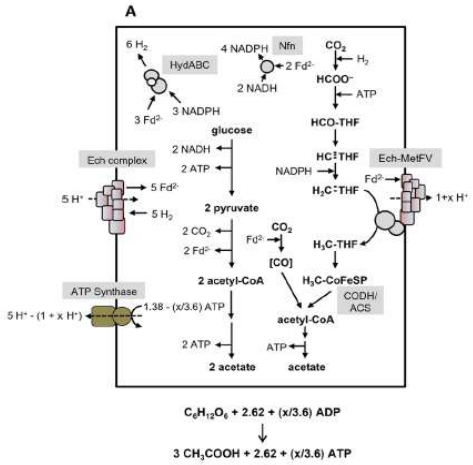


***Figure 2. 8 WLP pathway and bioenergetics of acetate formation from Glucose in T. kivui (Katsvy et al., 2021).***

# 3. Materials and Methods

## 3.1. Strains, media, and trace elements

*Thermoanaerobacter kivui* strains used in this study are listed in Table 3.1.

***Table 3. 1 List of T. kivui strains used in this study.***

| ***T. kivui* Strain** | **Source** |
|---|---|
| CO Adapted | TU Wien |
| $H_2/CO_2$ Adapted | TU Wien |
| Glucose Adapted | TU Wien |
| CO1 | TU Wien |
| Wild Type | DSM 2030 |

***Table 3. 2 Media used in this study***

| **Media** | **Purpose** | **Component** | **Concentration** |
|---|---|---|---|
| Moon Medium | Precultures, serum bottle experiments, fermentations | $Na_2HPO_4*2H_2O$<br>$NaH_2PO_4*H_2O$<br>$K_2HPO_4$<br>$KH_2PO_4$<br>$NH_4Cl$<br>$(NH_4)_2SO_4$<br>NaCl<br>$MgSO_4*7H_2O$<br>$CaCl_2*2H_2O$<br>$FeSO_4*7H_2O$<br>$KHCO_3$<br>Cysteine-HCl*$H_2O$<br>Resazurin (0.2%)<br>Traces DSM141 | 7.8 g/L<br>6.9 g/L<br>0.21 g/L<br>0.16 g/L<br>0.25 g/L<br>0.225 g/L<br>0.438 g/L<br>0.091 g/L<br>0.0060 g/L<br>0.0020 g/L<br>5.41 g/L<br>0.527 g/L<br>0.5 mL/L<br>10 mL/L |
| Eysmondt Medium | Precultures, fermentations | $(NH_4)_2SO_4$<br>$MgSO_4x7H_2O$<br>NaCl<br>Citric Acid<br>$KH_2PO_4$<br>$K_2HPO_4$<br>Traces Eysmondt | 4.38 g/L<br>0.25 g/L<br>0.5 g/L<br>0.25g/L<br>0.865 g/L<br>1.14 g/L<br>10 mL/L |

*Table 3. 3 Trace element solution used in this study*

| Media | Purpose | Component | Concentration |
|---|---|---|---|
| DSM 141 Traces | Medium Preparation | Nitrilotriacetic acid | 1.5 g/L |
| | | $MgSO_4*7H_2O$ | 3 g/L |
| | | $MnSO_4*H_2O$ | 0.5 g/L |
| | | NaCl | 1 g/L |
| | | $FeSO_4*7H_2O$ | 0.1 g/L |
| | | $CoCl_2*6H_2O$ | 0.152 g/L |
| | | $CaCl_2*2H_2O$ | 0.1 g/L |
| | | $ZnSO_4*7H_2O$ | 0.18 g/L |
| | | $CuSO_4*5H_2O$ | 0.01g/L |
| | | $KAl(SO_4)_2*12H_2O$ | 0.02 g/L |
| | | $H_3BO_3$ | 0.01 g/L |
| | | $Na_2MoO_4*2H_2O$ | 0.01 g/L |
| | | $NiCl_2*6H_2O$ | 0.03 g/L |
| | | $Na_2SeO_3*5H_2O$ | 0.3 mg/L |
| | | $Na_2WO_4*2H_2O$ | 0.4 mg/L |
| Eysmondt Traces | Medium Preparation | $FeSO_4x7H_2O$ | 27.58 g/L |
| | | $COCl_2x6H_2O$ | 6.2 g/L |
| | | $Na_2MoO_4x2H_2O$ | 2.42 g/L |
| | | $NiSO_4x6H_2O$ | 0.66 g/L |
| | | $ZnCl_2$ | 2.42 g/L |
| | | $MnCl_2x4H_2O$ | 0.2 g/L |
| | | $CuCl_2x2H_2O$ | 0.004 g/L |
| | | $H_3BO_3$ | 0.012 g/L |
| | | Nitrilotriacetic Acid | 4.78 g/L |
| | | $NaSeO_3x5H_2O$ | 0.026 g/L |
| | | $Na_2WoO_4x2H_2O$ | 0.033 g/L |

## 3.2. Trace elements solution and Moon medium preparation

Trace elements solution (TE) is prepared in 1 L stocks for continued use in media preparation. Preparation of the stock begins with nitriloacetic acid, which acts as a stabilizing agent in trace element solutions and is dissolved in distilled water by titrating with 1 M KOH setting the pH to 6.5 multiple times over a magnetic stirrer, once the Nitriloacetic acid is completely dissolved, the remaining compounds can be added to the solution, table 3.3. can be referred to for the composition. The last two compounds $Na_2SeO_3*5H_2O$ and $Na_2WO_4*2H_2O$ are required in exceptionally low quantities and are difficult to accurately measure on the scale, 1000X stock solutions therefore are prepared in advance. After every compound is added to

the solution the pH is set to 7 using KOH. The TE solution can be kept stable in the fridge over the course of many months after preparation.

The Moon Medium (MM) was then prepared by adding the compounds to distilled water over a magnetic stirrer. The anaerobic nature of the experiments makes an indicator of dissolved $O_2$ a necessity and Resazurin was used for this purpose. Once all the components are added to the solution except for Cysteine-HCl*H2O, the pH is set to 7.4 using 5M KOH solution table 3.2. can be referred to for the composition. In case the media is to be dispensed in serum bottles it was gassed with $N_2/CO_2$ (80/20) for 40 minutes in order to reach anoxic conditions, after which the Cysteine-HCl*$H_2O$ is added to the media to consume the remaining $O_2$ in the medium. After the color of the medium turned indicating the $O_2$ concentration was low enough approximately 20 minutes later, the medium was dispensed into serum bottles.

In the case of fermentations, the preparation of the media was modified. Required medium for the precultures, batch phase, and continuous operation were all prepared together. This was necessary to notice any errors in media preparation as early as the preculture phase and to ensure that the cells have a smooth transition through the aforementioned phases. $KHCO_3$ was not added to this solution which enables flushing the media with $N_2$ alone, reducing the cost of each fermentation and providing ease of operation. Once the media was prepared, the desired volume was dispensed to serum bottles and autoclaved at 120 °C and 205 kPa. However, the necessary volume for batch and feed bottles was sterile filtered into the corresponding bottles and was not autoclaved.

### 3.2.1. Modified Moon Medium Preperation

A modified version of the Moon Medium was prepared in a single batch to accommodate each part of the Experiment 3, ensuring the same conditions throughout the process. Two 5L concentrated stocks were prepared with one containing the phosphate buffer and the other containing the rest of the salts. Trace elements and Resazurin were not included in the medium until later in further preparation phases. Table 3.4. can be referred to for the exact concentrations.

**Table 3. 4 Modified Moon Medium**

| Species | C [g/mL] |
|---|---|
| $Na_2HPO_4*2H_2O$ | 7.8 |
| $NaH_2PO_4*H_2O$ | 6.9 |
| $K_2HPO_4$ | 0.21 |
| $KH_2PO_4$ | 0.16 |
| $NH_4Cl$ | 1 |
| $(NH_4)2SO_4$ | 0.225 |
| NaCl | 0.438 |
| $MgSO_4*7H_2O$ | 0.091 |
| $CaCl_2*2H_2O$ | 0.006 |
| Traces DSM141 | 10 |
| Resazurin (0,2%) | 0.5 |

For the precultures, 417 mL of each stock was removed and diluted with 800 mL $dH_2O$. 200 µL of the $FeSO_4*7H_2O$ (20 g/L) stock has been added to achieve a 2mg/L iron concentration. 10.82 g $KHCO_3$ was added, followed by 20 mL of TE stock. 1 mL of Resazurin was added as an oxygen indicator. The preculture medium was filled up to make a total of 2 L. Medium was then distributed in four, 200mL serum flasks and flushed $N_2/CO_2$ gas mix before being autoclaved.

For the batch medium, 208 mL from each stock was removed and diluted with 400 mL water before being distributed in the reactors. 0.5 mL Resazurin has been added to the reactor, which is then autoclaved. 10 mL of TE solution, 100 µL of $FeSO_4$ (20 g/L), as well as Glucose stocks, have been sterile filtered into the reactors to provide a 5 g/L Glucose concentration.

As for the feed medium, 2.08 L of each stock solution has been mixed with 4 L of water. 100 mL trace element solution has been added with 5 mL Resazurin before filling up to 10 L. The pH of the feed medium has been controlled at this point before sterile filtering the medium into an autoclaved bottle. The medium is flushed with $N_2$ for an hour. 15.3 mL of the 20 g/L iron solution ($FeSO_4*7H_2O$) has been added to each to provide 30.6 mg/L iron. 13.18 µL of 400 g/L L-Cys-HCl*$H_2O$ stock solution has been added to remove any remaining oxygen dissolved in the feed medium, finishing the medium preparation.

## 3.3. Equipment for Anaerobic Conditions

### 3.3.1. Serum Bottes

**Table 3. 5 Gas mixes used in this study**

| Gas Mix | Composition |
|---|---|
| Low CO | 9% $CO_2$, 58% $H_2$, 30% CO, 3 $N_2$ |
| High CO | 21% $CO_2$, 24% $H_2$, 52% CO, 3 $N_2$ |
| $H_2/CO_2$ | 80% $H_2$, 20% $CO_2$ |

In this study, 200 mL and 1 L serum bottles were used to be filled with 20 mL and 200 mL, respectively. 200 mL bottles were used for serum bottle experiments and pre-precultures while the 1 L bottles were mainly used for precultures before fermentations. Once the medium was prepared, it was dispensed in serum bottles while the bottles were still being flushed using a dispenser (Poulten & Graf, Germany) and crimped with self-healing stoppers. After crimping to prevent gas transfer through the septum, the bottles were autoclaved to ensure sterility, and any remaining $O_2$ in the medium was consumed during autoclaving. Once autoclaved, serum bottles could be kept stable at room temperature for over the course of months. When used for experiments or precultures the serum bottles were brought into either an anaerobic tent or an anaerobic chamber for inoculation. In order to ensure the longevity of the stoppers, 0.5 mm needles were used to add any liquid substrates, compounds, and cells for inoculation, as well as take samples through the septum. If the culture was meant to be grown on a gas mix, the bottles are then brought to the gassing station and were first flushed with the desired gas composition ensuring at least three volume changes occur in the bottle. Table 3.5. can be referred to for typical gas concentrations used. Once flushed the bottles were further pressurized to 1 bar (gauge) and set in a waterbed shaker (Memmert, Germany) at 66 ˚C where the cultivation takes place.

### 3.3.2. Hungate Tubes

Hungate tubes have been preferred instead of serum bottles for experimentations that require numerous different conditions and determinations, due to the smaller space requirement in the shaker and material demand. Hungate tubes, stoppers, and caps were autoclaved empty before being dried at 75 ˚C. Tubes, stoppers, and caps were transferred into the anaerobic chamber several hours before the start of an experimental procedure in

order to ensure there was no adsorbed $O_2$ remaining. After which serum bottles were carried in the anaerobic chamber where they were de-crimped, and the medium was distributed in the tubes via pipetting before adding necessary substrates and compounds, and inoculating.

If gas mixtures were required for the cultivation the same procedure as the serum bottles was used.

### 3.3.3. Anaerobic Tent and Chamber

An anaerobic tent (Coy Lab Products, USA) was used for most serum bottle procedures due to its lower gas requirements in comparison to the chamber. The airlock was built to house a vacuum compressor and a gas inlet, which were used to flush the airlock twice with $N_2$ before finally flushing it with forming gas. Upon completion of which, the inner door of the airlock could be accessed. It was however not possible to work with the tent in cases where the medium was in direct contact with the atmosphere, as was the case with Hungate tubes since there is always a certain amount of $O_2$ inside the tent.

The anaerobic chamber (Rieger, Austria) was used for cases where the medium was in direct contact with the atmosphere, such as preparing cryos or working with Hungate tubes. The sleeves of the chamber were continuously gassed with $N_2$, ensuring anoxic conditions. Additionally, an automatic flushing sequence was available at the airlock. The chamber further acts as a laminar flow hood providing ease when sterility was a concern. The gas demands of the chamber were significantly higher, however, making each operation more costly.

### 3.3.4. Gassing Station

The gassing station was connected to $N_2$, $CO_2$, and $H_2$ bottles through pressure controllers and MFCs (BROOKS Instrument, USA). A Control Box (BROOKS Instrument, USA) was used for setting the flow rates. In addition to the built-in $H_2$ sensors in the laboratory, a personal $H_2$ sensor (Dräger, Germany) was also worn while working with $H_2$ to be able to detect any leak earlier on, therefore mitigating any potential danger or inconvenience. The $H_2$ line was

kept closed when not in active use for the same reason. The tubes connected to the MFCs were mixed into a single line that holds one last valve to stop and start the gas flow, this valve however was not a pressure controller, and therefore the pressure started building up in accordance with the flow rates once it was closed. This situation can cause a rupture in the joints or cause an unwanted spike in the pressure once the valve was opened, therefore caution had to be exercised while working with the gassing station. The inlet line was attached to a male luer connector to which a sterile filter and a serum needle could be fixed, the sterile filters could be removed to connect the serum needles to the gas line directly in cases where sterility was not a concern. The needles were used to go through the septum and flush the desired container. The outlet line did not include any additional equipment and was connected to the main off-gas line in the lab therefore relieving higher than atmospheric pressures in the containers.

The CO bottles were always kept in a fume hood due to the toxic, asphyxiating, and explosive nature of the gas and had a smaller-scale gassing station attached to them that included only a pressure reducer and a needle valve. The same flushing procedures and safety measures were applied with the gassing station in addition to the fume hood.

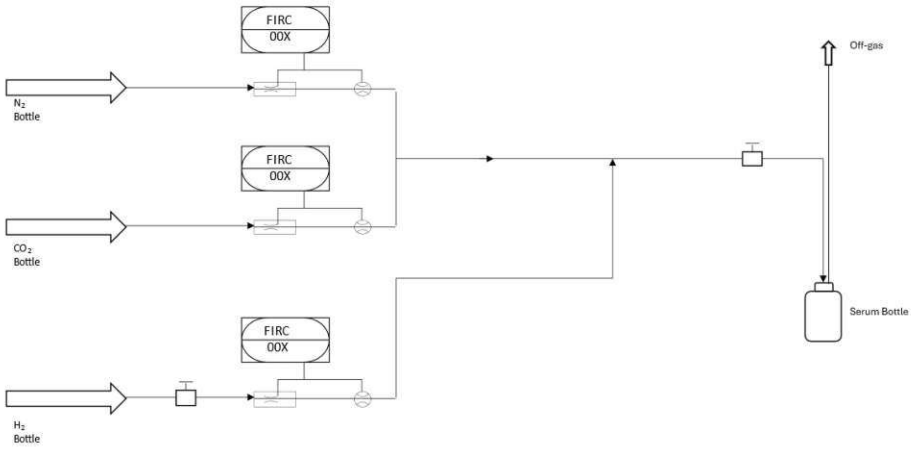


**Figure 3. 1 Gassing Station**

## 3.4. Bioreactors

### 3.4.1. Applikon Bioreactors

Two 1.5 L bioreactors (Applikon, The Netherlands) were used for gas fermentations in this study. Each bioreactor was coated with a heating sleeve that is connected to a thermostat (Lauda, Germany). The lid could be removed for cleaning and changing parts. Each reactor was equipped with a pH sensor and amplifier (Mettler Toledo, Austria), a temperature probe, a sparger for gassing, impellers, and baffles to ensure gas transfer, and a cross-flow off-gas water cooler. Furthermore, ports for feed, harvest, and base inlet for pH control and sampling were in place, in addition to which a septum was used for inoculation. For the feed, harvest, and base inlet peristaltic pumps (LAMBDA Laboratory Instruments, Czech Republic), and for the gas inlet MFCs for each gas bottle, were used. The harvest was set to keep a certain volume in the reactor during continuous fermentations, 0.6L for the purpose of this study, at all times. The weights of the reactor, the feed, base, and waste bottles were monitored at all times through scales (Sartorius, Germany) and each was placed in a tray deep enough to hold the liquid in case of a leak. The off-gas lines of the two reactors were connected to close valves which alternate the flow of each reactor between the off-gas line or GC (Thermo Fisher Scientific, USA) which was used to analyze the off-gas composition. The process control was achieved through Lucullus (TU Wien, Austria) through which several parameters could be monitored and controlled providing a high level of flexibility for operation. The setup for the Applikon reactor system can be seen in Fig. 3.2.

Before each fermentation, all the necessary components were connected to the lid and clamped off. The sparger was equipped with a sterile filter to prevent contamination in the system. The pH probe was calibrated between pH values of 4 and 7 before it was assembled. After the setup was complete the reactor was autoclaved with $dH_2O$ to prevent damage to the pH sensor. The bolts holding the lid in place were loosened to prevent pressure buildup and the sterile filter was clamped off from the reactor and covered with aluminum foil to prevent steam from entering and potentially blocking the filter.

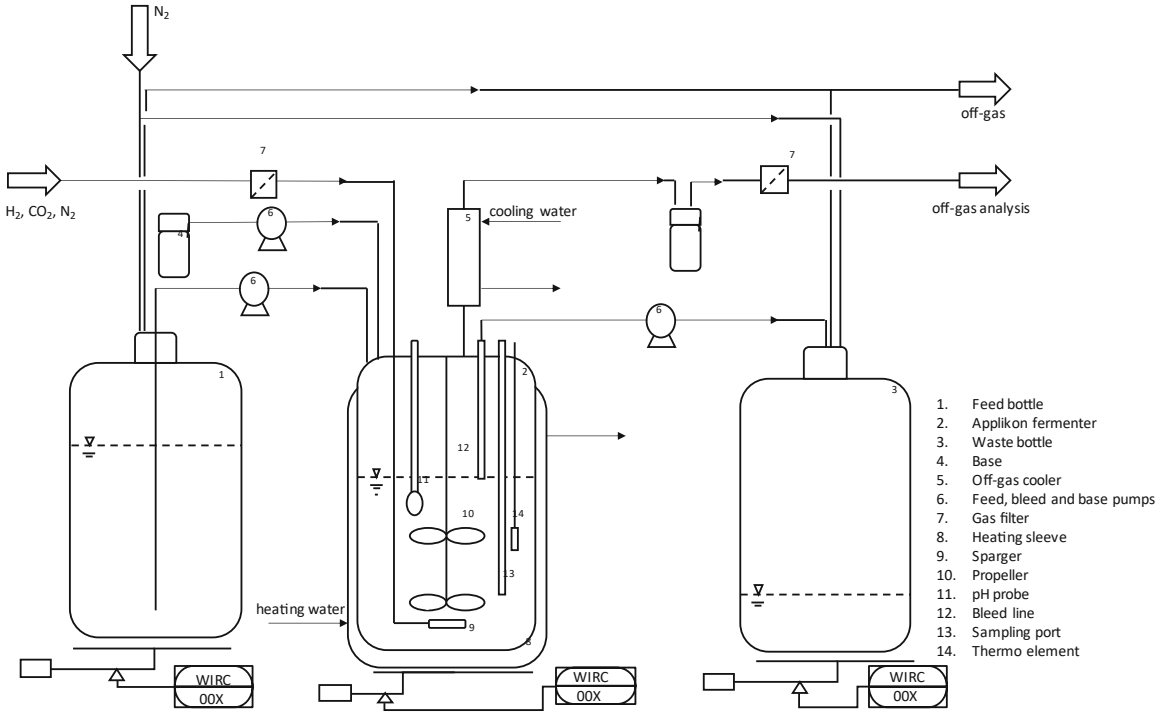


**Figure 3. 2 Applikon Bioreactor Setup**

After the autoclave, the batch medium could be sterile filtered into the reactor, and all the lines were connected. The feed and base pumps were calibrated. At this stage, it was paramount to ensure that the reactor does not have any gas leaks. This was accomplished by either a pressure holds or a flow test.

For the pressure hold test the entire line starting from the pressure reducer after the bottle, to the off-gas line, or GC if it was to be used, was pressurized with $N_2$. Once this was done the pressure is measured with a barometer, typically through the septum on the reactor, in case there was no drop in the pressure after several hours, the fermentation could proceed.

For the flow test on the other hand a flowmeter (Mesa Labs, USA) was used to measure volumetric flow rates, first before the reactor and then just before the GC or the off-gas, the results of which needed to match with one another.

Should there be a leak in the reactor or the pneumatic connections, these leaks were found and sealed before repeating the aforementioned tests. After ensuring there were no leaks in the system, the gassing was turned on with the desired gas mixture, usually a mixture of $H_2$, $CO_2$, and $N_2$ for the purposes of this study. Once the gassing is started the lab was monitored

with personal $H_2$ sensors for approximately half an hour as an additional safety measurement. Lucullus operation was started with the desired operating parameters.

Before inoculation, glucose was added to the reactors through the septum. At this point, the reactors were inoculated with enough volume from the 200 mL precultures to ensure the starting OD at 600 nm of the reactor would be a minimum of 0.15 to provide the batch phase with adequate cell density.

Once the fermentation started samples were taken at regular intervals to monitor the cell growth. This was achieved by taking a 2 mL sample through the sampling port, which was to be discarded to remove any contamination in the tube, before taking another 5 mL to be kept in a falcon tube. 2 mL of the samples were centrifuged (Heraeus, Germany) at 14000 rpm and 4 ˚C to separate the supernatant which was kept frozen at -20 ˚C to be further analyzed with HPLC. The remaining 3 mL was then used to determine the cell density through triple determination with the $OD_{600}$ and logged. As the desired cell density was reached the feed was turned on and the continuous phase was started. For the duration of the continuous operation, the same sampling procedure was applied.

As the experimentation ends the gassing was turned off and the entire system was flushed with $N_2$. Lucullus operation was stopped, and all the inlets and outlets were clamped. The lines connecting the reactor were separated and rinsed to prevent clogging before being closed off. The reactor itself with its contents was dirty autoclaved, the waste bottle was treated with NaOH and afterward, the contents of both alongside any remaining feed were discarded. The reactor was cleaned and was prepared to start another fermentation.

### 3.4.2. DASbox Mini Bioreactor System

A DASbox Mini Bioreactor System (Eppendorf, Germany) was used in this study to establish continuous cultures. The system housed four 250 mL autoclavable bioreactors each equipped with a sparger, stirrer, pH, and temperature sensor and each off-gas line was equipped with an electrical cooler. As the temperature range of the DASbox itself was limited to 60 ˚C, an external water bath was used for the growth conditions desired. The top compartment of the DASbox was equipped with 8 peristaltic pumps that were used for feed

and base inlets, an external pump was used for the harvest. There were four gas inlets in the middle compartment of the system which was set to air, $N_2$, $O_2$, and $CO_2$ by default, however, were connected to $N_2$, $CO_2$, and $H_2$ lines. The bottom compartment was the off-gas analyzer which was predominantly used to measure the $CO_2$ concentration in the off-gas, the off-gas line was further connected to the GC. Process control was achieved through DASware (Eppendorf, Germany) control software which provided more straightforward calibration and operation in addition to graphical representations, sacrificed however the flexibility offered by the Lucullus software. The setup for the DASbox system can be seen in Fig. 3.3.

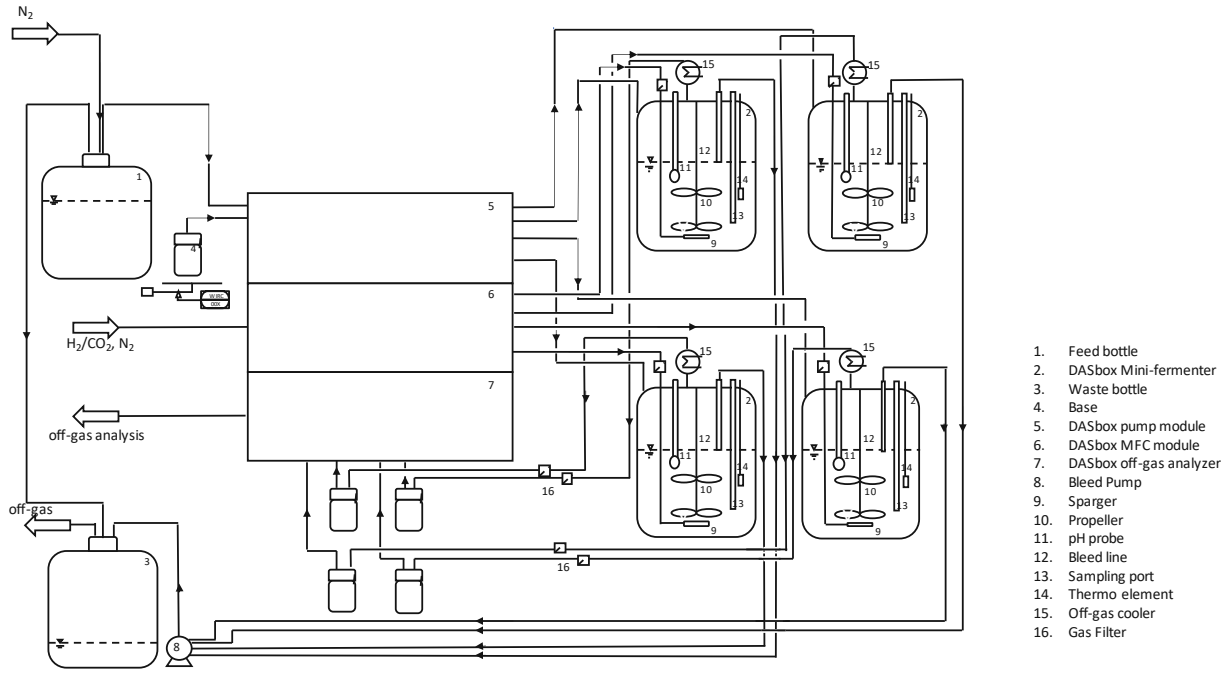


**Figure 3. 3 DASbox Mini Bioreactor System Setup**

The fermentation and sampling procedure was carried out in a similar fashion to the Applikon system, with minor differences.

### 3.4.3. Bubble Column

A 15 L bubble column (Möstl Anlagenbau, Austria) was used for establishing a batch fermentation for its scalability and lack of propellors. The bubble column was equipped with a pH sensor, temperature sensor, and a recirculation pump. Gassing was accomplished from the bottom of the column promoting mixing throughout the column height. The liquid discharge was located at the bottom of the column. The off-gas line was cooled with a cross-flow water cooler and directed to the GC for gas analysis before being burned off in the flare. The process control was achieved through Lucullus software. Fig. 3.4. can be referred to for the setup of the bubble column.

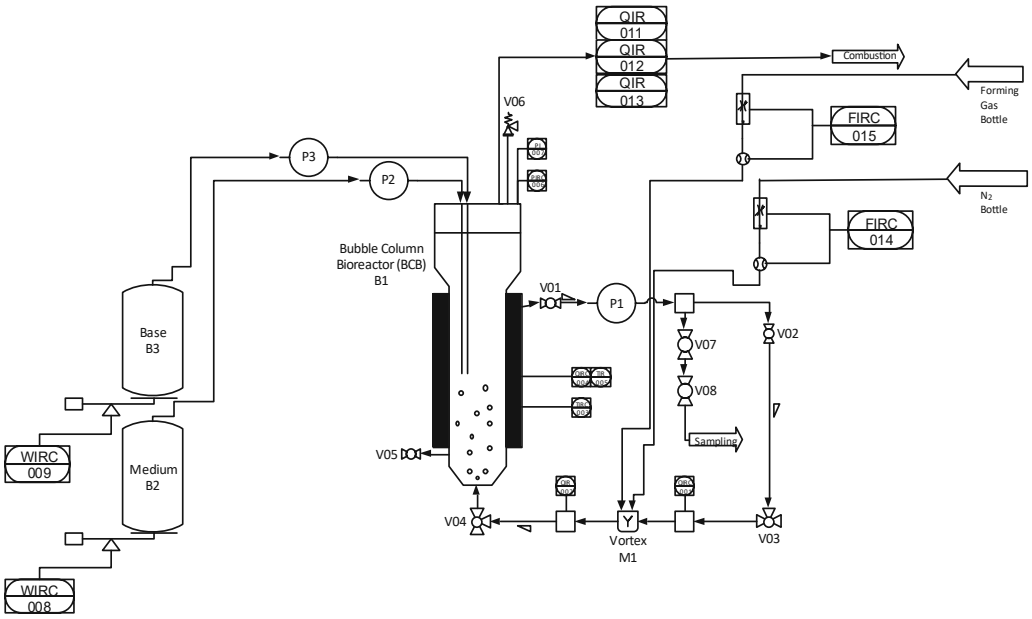


**Figure 3. 4 Bubble Column System Setup**

Operating the bubble column required it to be filled with the medium and its lid sealed off. The pressure hold test was made in the same fashion as the Applikon and DASbox systems. Once the calibrations were made and the temperature was set, the inoculation was made. The sampling process was carried out in a similar fashion albeit with a higher volume typically between 10 and 40 mL.

As the bubble column provides a higher cell amount due to the working volume, CDM values have also been measured by centrifuging 15 mL reactor broth for 10 minutes at 8000 G and washing with physiological NaCl solution before centrifuging once again.

## 3.5. Quantitative Measurements

### 3.5.1. Cell Density

Cell density was measured by Optical Density at 600nm ($OD_{600}$) and cell dry weight (CDW).

$OD_{600}$ was used to measure turbidity for estimating the concentration of cells in the samples. The OD spectrophotometer was set to zero with $dH_2O$ in a plastic cuvette. Samples were then mixed in a vortex mixer (VWR International, Austria) and 0.8-1 mL of the sample was pipetted into plastic cuvettes. The cuvettes themselves were mixed one more time to ensure the cells were uniformly dispersed in the sample before the $OD_{600}$ measurement was made. Should the OD be higher than 0.600, the samples were diluted further to ensure the accuracy of the measurement. Three different cuvettes were measured for each sample to ensure precision.

As $OD_{600}$ was a method of approximation and can be influenced by many factors, cell dry weight was also measured at the end of each fermentation. The sample volume needed to be much larger than the required volume for the $OD_{600}$ as the anaerobic bacteria tends to form cultures of little density. For the measurement clean and dried tubes were weighed on a sensitive scale to provide beginning weight. The samples were then centrifuged at 14000 rpm and 4 °C. The supernatant was removed from the tube and the cells were resuspended in 0.9% NaCl solution and centrifuged in the same conditions once again. The supernatant was discarded, and the pellets were dried at 75 °C before being weighed once again to determine the net weight difference.

### 3.5.2. CEDEX and HPLC

Cedex was used for determination of certain concentrations. The appropriate kit was selected and was placed among the cassettes, therefore only the selected compounds were measured. Every kit had a certain concentration range where measurements could be made

and should dilutions be necessary, they were automatically carried out by the CEDEX, this however was often bypassed by making manual dilutions in the desired range. Eppis produced by Eppendorf, Germany were used exclusively and were filled with the supernatant to be measured. The lid was then removed before putting the sample in the rack. Once the operation was set up using the CEDEX software, the rack could be inserted back into the CEDEX and the measurement began automatically.

450 µL of the supernatant from the centrifuged samples was mixed with 50 µL of 40 mM $H_2SO_4$ for HPLC measurements. 4 mM $H_2SO_4$ as a running buffer and 20% ethanol (or isopropanol) to flush the sampling needle was used and therefore connected to the HPLC. Once prepared the samples were put in the HPLC rack alongside desired standards for calibration and MQ water. The operation was then set up and the rack was inserted back into the HPLC. The measuring process started automatically. The results were analyzed on Chromeleon Software (Thermo Fischer Scientific, USA).

### 3.5.3. Gas Chromatography (GC)

Gas chromatography (Thermo Fisher Scientific, USA) was used to make off-gas analyses. Argon was used as a carrier gas for the GC. The carrier gas alongside the off-gas line was connected to the GC, and the off-gas samples were injected into the carrier gas in an alternating fashion. The chemicals were electronically detected at the end of the column. The device was turned on by setting the furnace, and column temperatures. Once the ready-to-use signal was lit the GC operation was automated using the Lucullus software.

# 4. Results

## 4.1. Starting Point and Overview of the Experiments

Before the start of this study, multiple adaptations to *T. kivui* were established. The adaptations, made through transferring multiple generations of cultures in certain conditions, have been made to include adaptations to grow on CO, $H_2/CO_2$ gas mix and glucose.

The $H_2/CO_2$ adapted strain has been used previously in a DASBox experiment, however, the transition to a continuous mode of operation has not been successful.

The following experiments have been conducted to establish a successful and repeatable transition to continuous operation and measure the different behaviors of *T. kivui* under changing conditions.

**Experiment 1: Evaluation of Operational Parameters for Continuous Gas Fermentation**

Investigation of the effects of medium types, iron concentrations, stirrer speeds, and dilution rates on the performance of continuous gas fermentation in Continuous Stirred Tank Reactors (CSTR).

**Experiment 2: Strain Selection and Growth Profiling Under Different Gaseous Substrates**

Assessment of the growth rates and cell densities of different *T. kivui* strains under different gaseous substrate compositions to identify the most suitable strain for further experiments.

**Experiment 3: Impact of Glucose on Continuous Gas Fermentation Performance**

Comparison of the effects of glucose vs. no glucose supplementation on growth, metabolic activity, and product formation during continuous gas fermentation, including off-gas analysis.

**Experiment 4: Scalability and Performance in a Bubble Column Reactor**

Examination of the growth profiles and scalability potential of *T. kivui* in a bubble column reactor compared to CSTRs.

**Experiment 5: Effect of pH and Acetate Concentration on Growth of CO1 strain**

Testing of the growth profiles of the CO1 strain under varying pH levels and acetate concentrations with gaseous substrates.

**Experiment 6: Growth and Adaptability of *T. kivui* with Formate as the Sole Substrate**

Evaluation of the growth profile and adaptability of the CO1 strain when formate is used as the sole substrate.

## 4.2. Experiment 1: Evaluation of Operational Parameters for Continuous Gas Fermentation

The aim of this experiment was to identify critical parameters to establish a steady state continuous culture with *T. kivui*. Multiple parameters were altered to showcase the following cariables during the experimental procedure. The experiment was carried out in DASbox Minibioreactor System.

- Growth response (Section 4.2.2 & 4.2.4);

  Feeding strategies were altered between autotrophic and heterotrophic.

  Different mediums were utilized (Moon Medium and Eysmondt medium) as were as iron concentration in the medium.

  Stimulatory supplements were pulsed during the experimental procedure (yeast extract, peptone, Ca-Pantothenate).
- Gas-liquid mass transfer (Section 4.2.3);

  Stirrer speeds were altered between 150 RPM and 1200 RPM.
- Specific growth rates (Section 4.2.3);

  Dilution rates were altered between 0.025 and 0.15 $h^{-1}$.

The starting conditions of each reactor are presented in Table 4. 1. The HPLC results and $OD_{600}$ measurements as well as the interventions are presented in Figures 4.1-4.4 and in Tables 4.2-4.5 respectively.

***Table 4. 1*** **Experiment 1 starting conditions**

| Reactor | Strain used for inoculation | Initial $OD_{600}$ measurements | Medium | Gassing at 0.25 VVM |
|---|---|---|---|---|
| R1 | $H_2/CO_2$ adapted | 0.09 | Moon Medium | $H_2$, $CO_2$, $N_2$ 58:12:30 |
| R2 | $H_2/CO_2$ adapted | 0.09 | Moon Medium | $H_2$, $CO_2$, $N_2$ 58:12:30 |
| R3 | Glucose adapted | 0.09 | Moon Medium with 10 g/L glucose | $N_2$ |
| R4 | Glucose adapted | 0.09 | Moon Medium with 10 g/L glucose | $N_2$ |

### 4.2.1. Experiment 1 Results

**Figure 4. 1 Experiment 1 Reactor 1 fermentation results at 66 ˚C and pH 6.4 including HPLC data**

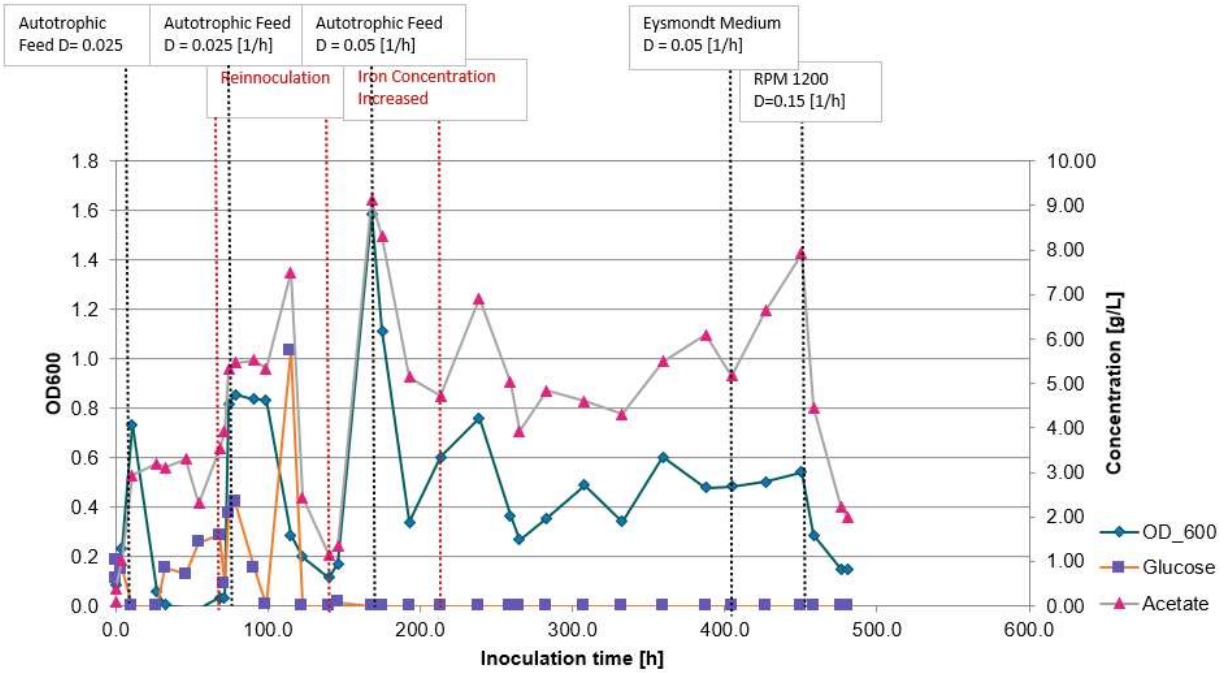


***Table 4. 2* Experiment 1 Reactor 1 overview of parameters changed**

| Inoculation Time [h] | Intervention | Stirrer Speed [RPM] | Dilution Rate [$h^{-1}$] |
|---|---|---|---|
| 10.7 | Feed turned on with Moon Medium | 600 | 0.025 |
| 27.0 | Feed turned off, glucose pulsed to 1 g/L to recover biomass | 600 | 0 |
| 32.7 | Reinoculated with 3 ml of original preculture | 600 | 0 |
| 46.0 | Reinoculated with 5ml inoculum from R2 | 600 | 0 |
| 71.5 | Reinoculated with 50 mL inoculum from bubble column (Strain CO1), stirrer speed lowered | 150 | 0 |
| 74.5 | Feed turned on with Moon Medium | 150 | 0.025 |
| 90.8 | Dilution Rate increased | 150 | 0.05 |
| 115.0 | Stirrer speed increased | 600 | 0.05 |
| 122.5 | Yeast extract added to 2 g/L to recover biomass | 600 | 0.05 |
| 140.0 | Feed turned off, reinoculated with 5mL inoculum from R3 and Peptone added to 2 g/L to assist growth | 600 | 0 |
| 168.0 | Feed turned on and Ca-Pantothenate added to 1 mg/L to assist growth | 600 | 0.05 |
| 193.0 | Peptone added to 2 g/L, stirrer speed lowered | 300 | 0.05 |
| 213.3 | Added 33 mg/L $FeSO_4*7H_2O$ (approximately) to feed | 300 | 0.05 |
| 404.5 | Feed switched to Eysmondt medium | 300 | 0.05 |
| 450.5 | Stirrer speed and dilution rate increased | 1200 | 0.15 |

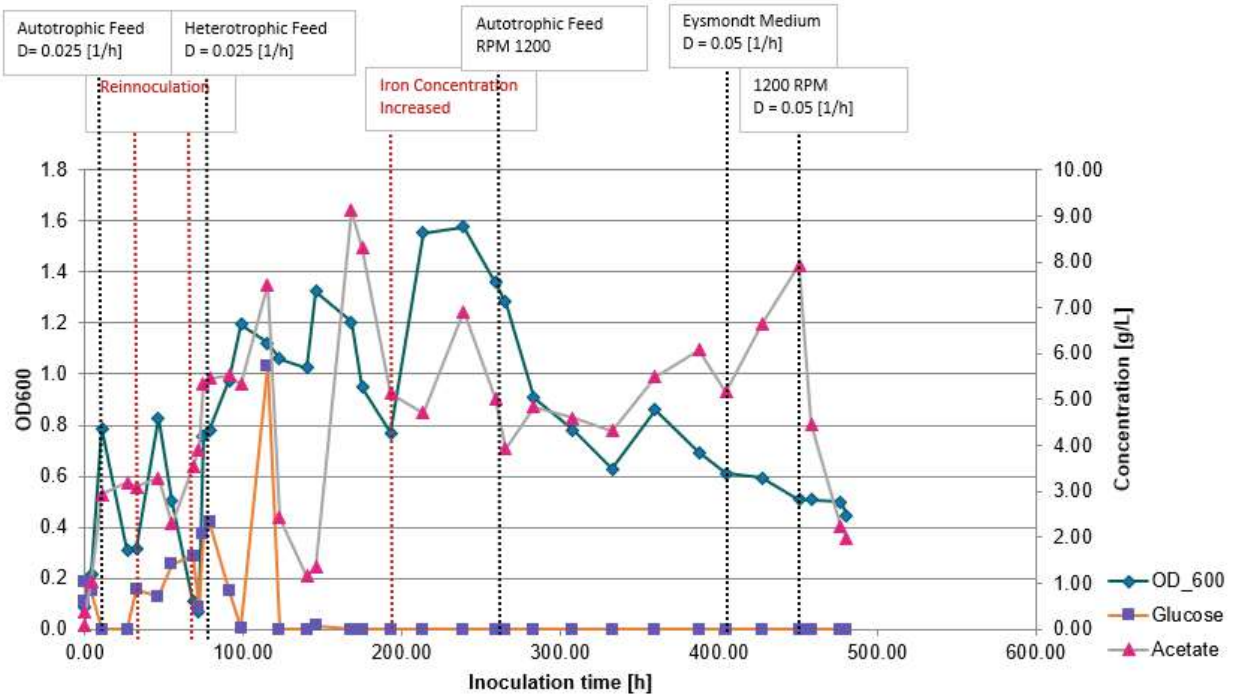


***Figure 4. 2*** **Experiment 1 Reactor 2 fermentation results at 66 ˚C and pH 6.4 including HPLC data**

***Table 4. 3*** **Experiment 1 Reactor 2 overview of parameters changed**

| Inoculation Time [h] | Intervention | Stirrer Speed [RPM] | Dilution Rate [$h^{-1}$] |
|---|---|---|---|
| 10.7 | Feed turned on with Moon Medium | 600 | 0.025 |
| 27.0 | Feed turned off, glucose pulsed to 1 g/L to recover biomass | 600 | 0 |
| 32.7 | Reinoculated with 3ml of original preculture | 600 | 0 |
| 46.0 | Feed turned on with Moon Medium | 600 | 0.025 |
| 54.7 | Feed switched to medium with 10 g/L glucose to facilitate growth | 600 | 0.025 |
| 71.5 | Reinoculated with 50 mL inoculum from bubble column (Strain; CO1), stirrer speed reduced | 150 | 0 |
| 74.5 | Feed turned on with Moon Medium and 10 g/L glucose | 150 | 0.025 |
| 90.8 | Dilution rate increased | 150 | 0.05 |
| 140.0 | Yeast extract added to 2 g/L to facilitate growth | 150 | 0.05 |
| 168.0 | Stirrer speed increased | 600 | 0.05 |
| 175.0 | Ca-Panthotenate added to 1 mg/L to facilitate growth | 600 | 0.05 |
| 193.0 | $FeSO_4*7H_2O$ added to 33mg/L in the reactor | 600 | 0.05 |
| 213.3 | 10 mL Trace Elements solution pulsed to reactor | 600 | 0.05 |
| 259.0 | Stirrer speed increased | 1200 | 0.05 |
| 265.2 | Changed to feed without glucose and $Fe^{2+}$ (see R1) | 1200 | 0.05 |
| 307.8 | Stirrer speed decreased | 300 | 0.05 |
| 404.5 | Changed the feed to Eysmondt medium | 300 | 0.05 |
| 450.5 | Stirrer speed increased | 1200 | 0.05 |

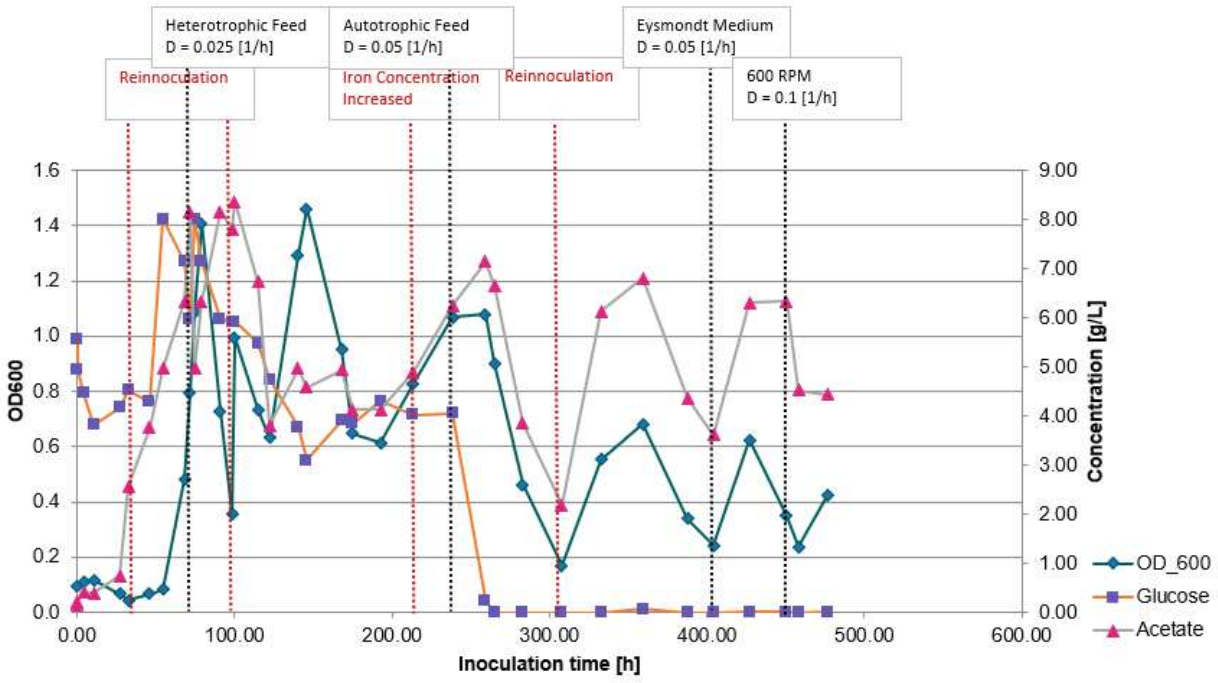


***Figure 4. 3*** **Experiment 1 Reactor 3 fermentation results at 66 ˚C and pH 6.4 including HPLC data**

**Table 4. 4 Experiment 1 Reactor 3 overview of parameters changed**

| Inoculation Time [h] | Intervention | Stirrer Speed [RPM] | Dilution Rate [$h^{-1}$] |
|---|---|---|---|
| 27.0 | Gassing switched to $H_2/CO_2$ mix. to enable growth | 600 | 0 |
| 32.7 | Reinoculated with 3ml of original preculture | 600 | 0 |
| 46.0 | Reinoculated with 5ml inoculum from R2 | 600 | 0 |
| 71.5 | Glucose added to increase concentration by 5 g/L in the reactor | 600 | 0 |
| 78.8 | Feed turned on with Moon Medium and 10 g/L glucose | 600 | 0.025 |
| 90.8 | Stirrer speed reduced | 150 | 0.025 |
| 99.8 | Added 50 mL inoculum from the bubble column (Strain; CO1) | 150 | 0.025 |
| 140.0 | Dilution rate increased | 150 | 0.05 |
| 168.0 | Added 1 mg/L Ca-Pantothenate to facilitate growth | 150 | 0.05 |
| 193.0 | 10 mL Trace Elements solution pulsed to reactor | 150 | 0.05 |
| 213.3 | $FeSO_4*7H_2O$ added to 33mg/L in the reactor, stirrer speed increased | 600 | 0.05 |
| 238.8 | Feed turned on with Moon Medium | 600 | 0.05 |
| 307.8 | Feed turned off, reinoculated with 10ml inoculum from R2, stirrer speed decreased | 150 | 0 |
| 332.7 | Feed turned on with Moon Medium | 150 | 0.05 |
| 404.5 | Feed switched to Eysmondt Medium | 150 | 0.05 |
| 450.5 | Stirrer speed and dilution rate increased | 600 | 0.10 |

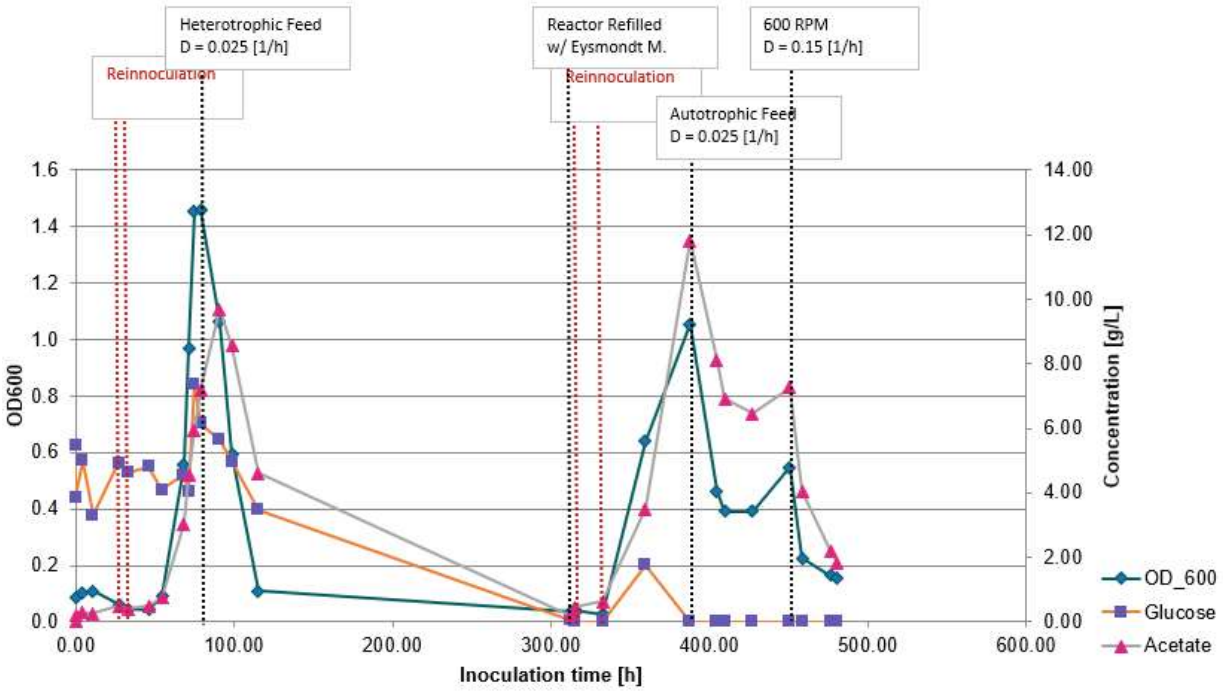


**Figure 4. 4 Experiment 1 Reactor 4 fermentation results at 66 ˚C and pH 6.4 including HPLC data**

**Table 4. 5 Experiment 1 Reactor 4 overview of parameters changed**

| Inoculation Time [h] | Intervention | Stirrer Speed [RPM] | Dilution Rate [$h^{-1}$] |
|---|---|---|---|
| 27.0 | Gassing switched to $H_2/CO_2$ mix to enable growth | 600 | 0 |
| 32.7 | Reinoculated with 3ml of original preculture | 600 | 0 |
| 46.0 | Reinoculated with 5ml inoculum from R2 | 600 | 0 |
| 71.5 | Glucose added to increase concentration by 5 g/L in the reactor | 600 | 0 |
| 78.8 | Started feed with 10 g/L glucose | 600 | 0.025 |
| 90.8 | Reduced stirrer speed | 150 | 0.025 |
| 115.0 | Culture discontinued | 150 | 0 |
| 312.5 | Reactor emptied and filled with Eysmondt medium without glucose | 150 | 0 |
| 314.5 | Reinoculated with 10 ml inoculum from R1, feed turned on with Eysmondt Medium | 150 | 0.025 |
| 332.8 | Feed turned off, glucose added to 2 g/L in the reactor, Reinoculated with 3 mL inoculum from R1 | 150 | 0 |
| 387.6 | Feed turned on with Eysmondt Medium | 150 | 0.05 |
| 450.5 | Stirrer speed and dilution rate increased | 600 | 0.15 |

### 4.2.2. Effects of Medium Composition in Establishing Steady State

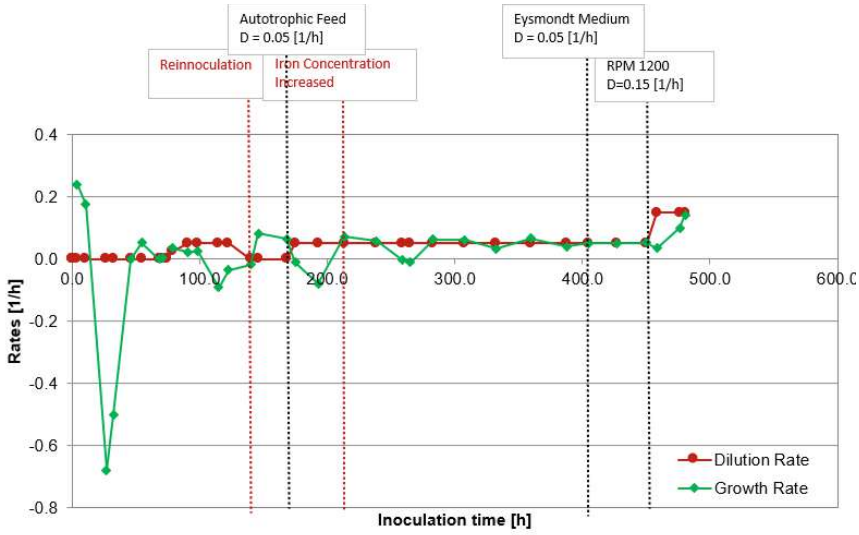


**Figure 4. 5 Experiment 1 Reactor 1 Growth Rates and Dilution Rates 66 ˚C and pH 6.4 see Table 4.2 for additional information on strains and conditions**

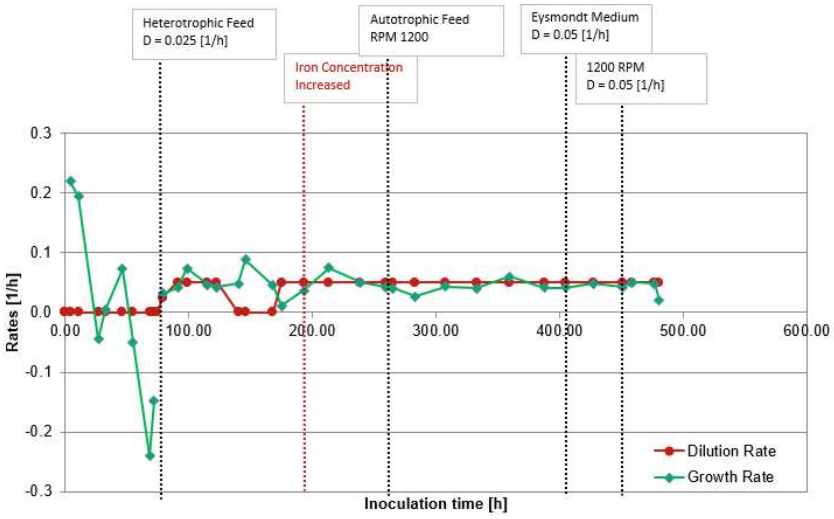


**Figure 4. 6 Experiment 1 Reactor 2 Growth Rates and Dilution Rates 66 ˚C and pH 6.4 see Table 4.3 for additional information on strains and conditions**

A steady state was successfully established in reactors 1 and 2 (Figures 4.5 & 4.6), after inoculating with CO1 strain from a previous experiment and increasing the iron concentration in the medium. From these results, it is difficult to conclude that the CO1 strain played an important role in achieving steady state, as no other strain was used in any of the reactors with an increased iron concentration in the medium (Tables 4.2-4.5).

However, it has been concluded that higher iron concentration (33 mg/L $FeSO_4*7H_2O$) is essential for transitioning to a steady state. Graphical representations of growth and dilution rates for reactors 3 and 4 can be found in the Appendix, Figures A. 1 and A. 2 respectively. The highest achieved growth rate under continuous conditions was in reactor 1 with 0.143 $h^{-1}$.

The switch to Eysmondt Medium resulted in marginal increases in productivity. After the feed was switched to Eysmondt Medium at 404.5 h of inoculation time in R1, R2, and R3, specific acetate production rates have increased steadily (Figures 4.7, 4.8, 4.9) under same stirrer speed and dilution rate (150 RPM, 0.05$h^{-1}$) with R1 and R2. The most notable increase was observed in R3, which was operated at a higher stirrer speed of 300 RPM, the reactor was not in steady state as the production increased and therefore the increase could not be solely attributed to the medium change or the increased gas transfer available due to the stirrer speed.

Effects of glucose could only be tested under batch conditions and lower iron concentrations, as the literature suggests (Table 2.1) the glucose had a stimulatory effect in establishing higher cell densities. As for the stimulatory supplements, among the tested peptone, Ca-pantothenate, and yeast extract, only the pulsing of yeast extract had a stimulatory effect on the cultures. None of the above-mentioned supplements were used in transitioning to continuous operation.

### 4.2.3. Effects of Stirrer Speeds and Dilution Rates

At the beginning of the fermentation with lower iron concentrations in the medium, the cultures were unable to make the transition to continuous mode of operation even with lower dilution rates (0.025 $h^{-1}$). Lower stirrer speeds (150 RPM) in turn have been beneficial under these “sub-optimal” conditions to maintain and promote cell growth.

Once the steady state was established, the cultures were able to survive under the highest stirrer speed and dilution rate tested (Figures 4.1, 4.5, 4.7). It is difficult however, to conclude that the growth rates would continue to match the dilution rate of 0.15 $h^{-1}$ as in

case of R1 (Figure 4.5) the growth rate gradually increased, suggesting an adaptation, and the experiment ended at the time growth rate matched the dilution rate.

For highest specific acetate productivity of 4.25 g $g_{CDM}^{-1}h^{-1}$ (43.3 mmol $g_{CDM}^{-1}$ $h^{-1}$), dilution rate of 0.15 $h^{-1}$ and stirrer speed of 600 rpm has been most beneficial with the Eysmondt Medium (Figure 4.10).

### 4.2.4. Effects of $CO_2$ in the Gas Feed

$CO_2$ is essential for the utilization of the WLP, even though *T. kivui* has the ability to produce $CO_2$ in the presence of glucose (Section 2.3.2.) this hasn't been enough to facilitate growth in batch conditions at the beginning of the fermentation process with reactor 3 and 4 as the gas feed contained only nitrogen (Figures A.1 and A.2). Growth under batch conditions was only possible after the gas feed has been switched to $H_2$:$CO_2$:$N_2$, 58:12:30 gas mixture.

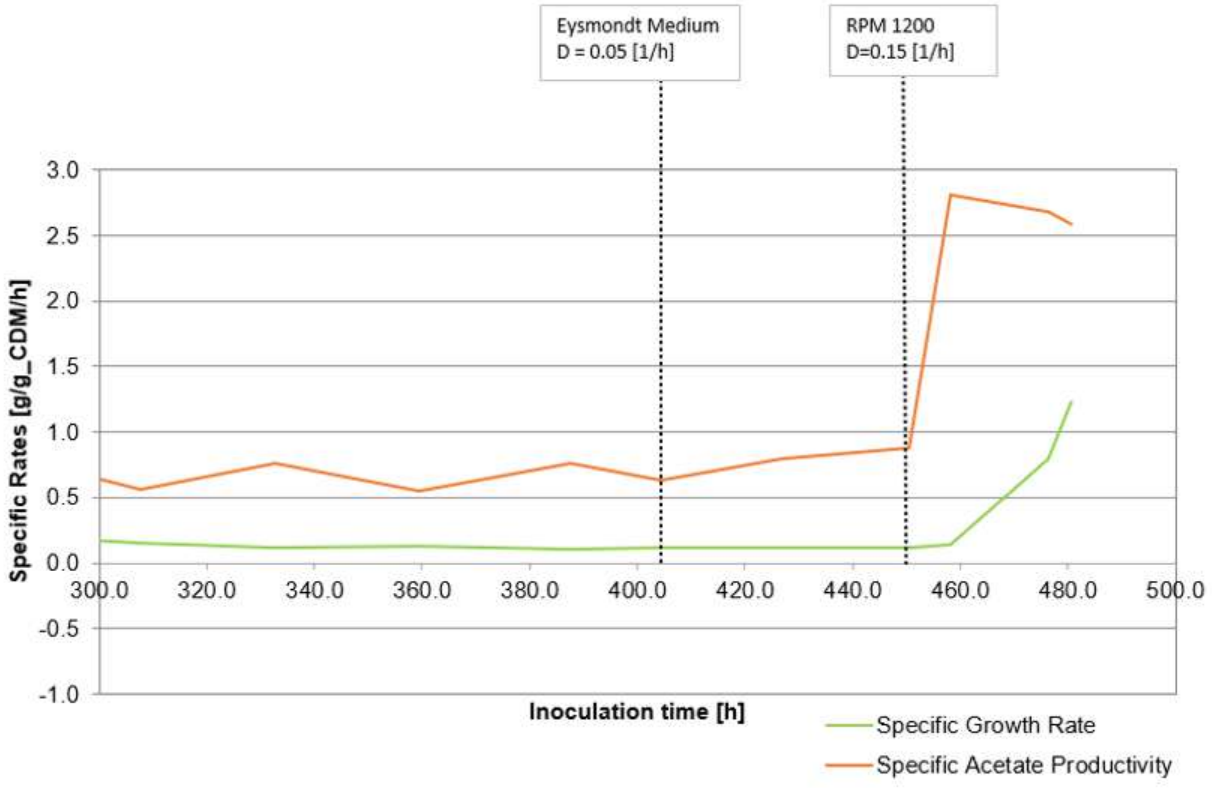


**Figure 4. 7 Experiment 1 Reactor 1 Specific Rates at 66 ˚C and pH 6.4 see Table 4.2 for additional information on strains and conditions**

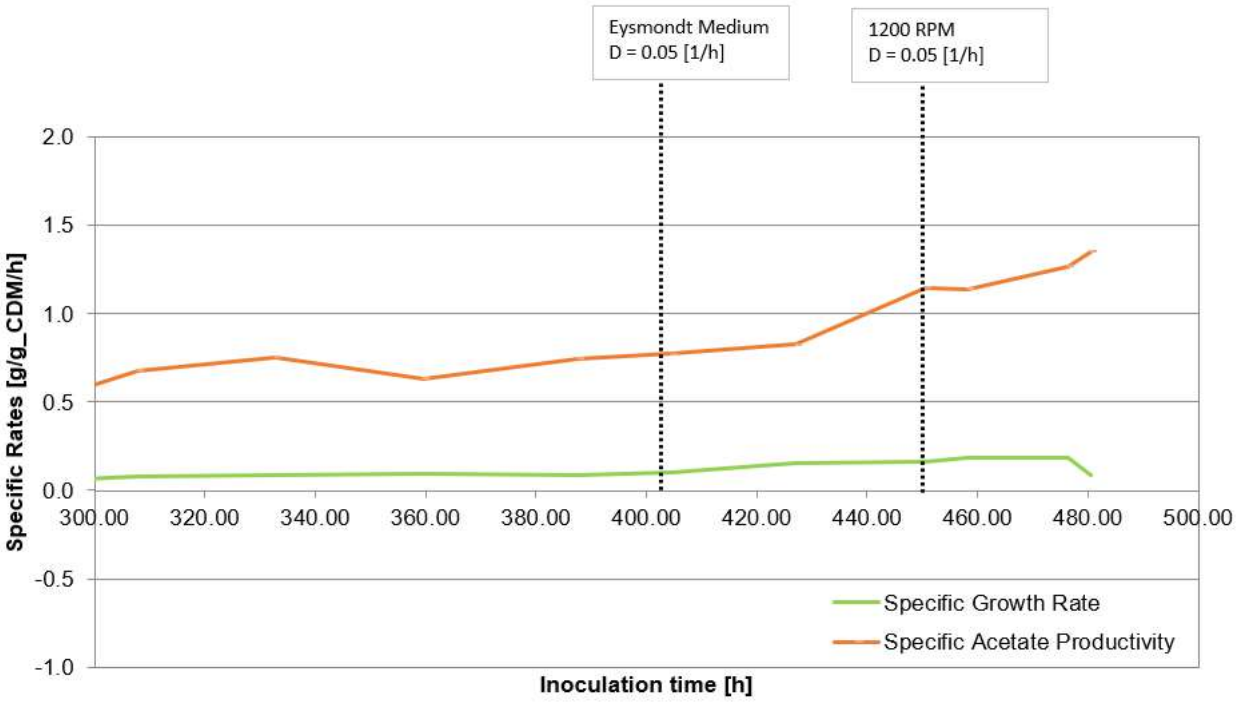


**Figure 4. 8 Experiment 1 Reactor 2 Specific Rates at 66 ˚C and pH 6.4 see Table 4.3 for additional information on strains and conditions**

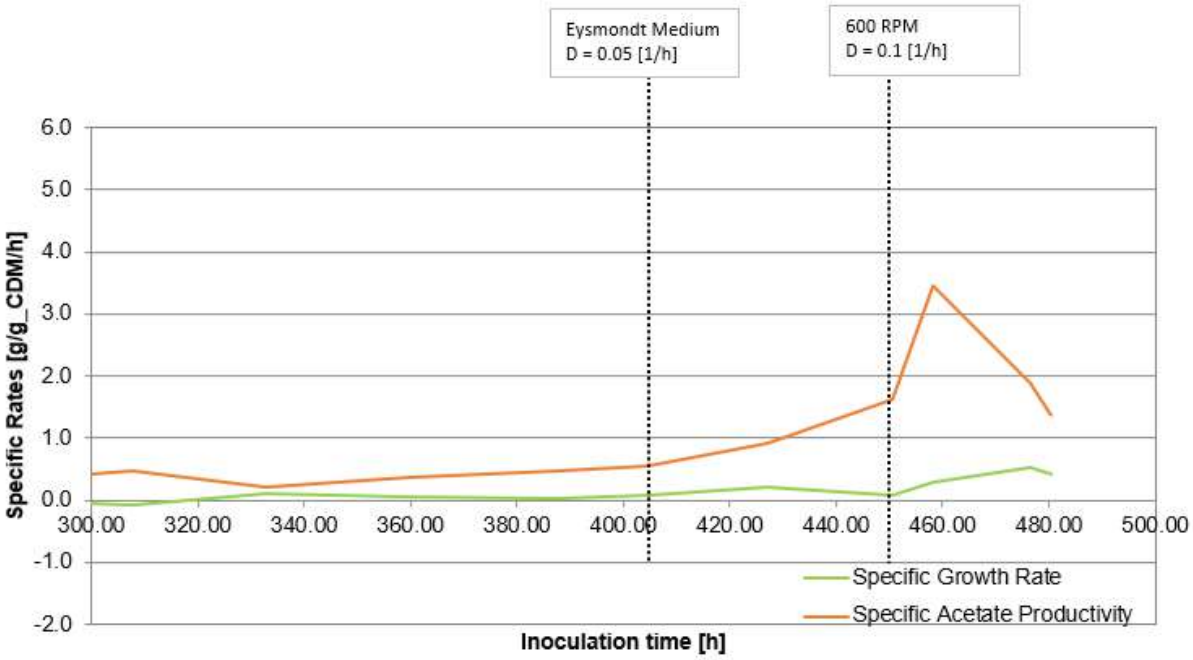


**Figure 4. 9 Experiment 1 Reactor 3 Specific Rates at 66 ˚C and pH 6.4 see Table 4.4 for additional information on strains and conditions**

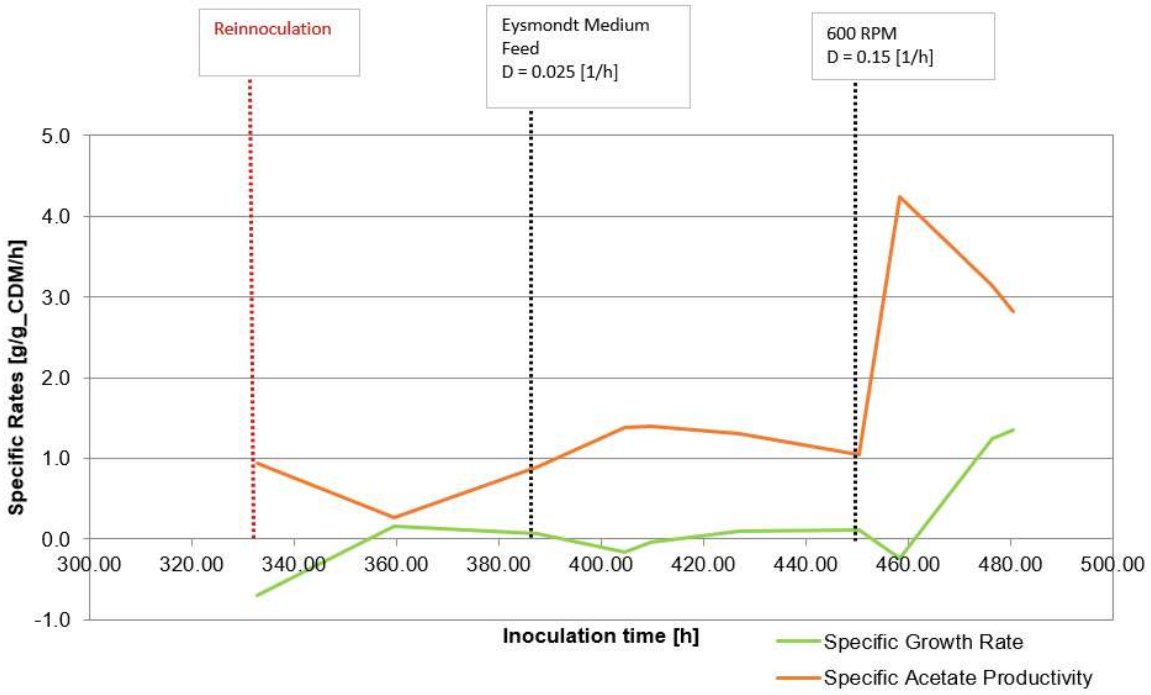


**Figure 4. 10 Experiment 1 Reactor 4 Specific Rates at 66 ˚C and pH 6.4 see Table 4.5 for additional information on strains and conditions**

### 4.2.5. Experiment 1 Results Summary

- Increasing the $FeSO_4*7H_2O$ to 33 mg/L has been beneficial in establishing a continuous culture in all of the reactors.
- The presence of $CO_2$ is beneficial for microbial growth even in the presence of glucose.
- Only CO1 strain was tested with the increased iron concentration and has made the transition to continuous mode.
- Highest growth rate ($\mu_{max}$) of 0.143 $h^{-1}$ was observed in R1with CO1 strain, Eysmondt Medium, 1200 RPM of stirrer speed and 0.15 $h^{-1}$ dilution rate.
- Highest specific acetate productivity ($q_{acetate}$) of 4.249 g $g_{CDM}^{-1}$ $h^{-1}$ (43.29 mmol $g_{CDM}^{-1}$ $h^{-1}$) was observed in R4 with CO1 strain, Eysmondt Medium, 600 RPM of stirrer speed and 0.15 $h^{-1}$ dilution rate.

## 4.3. Experiment 2: Strain Selection and Growth Profiling Under Different Gaseous Substrates

The goal of this experiment was to test the growth profiles of different strains in batch conditions and in turn determine the strain with the most potential to adapt to continuous conditions.

The experiment was carried out in serum flasks with 20 mL of Moon Medium prepared as described in Section 3.2.1. The strains used were cultivated in previous experiments, Table 4.6. can be referred to for the exact strains and their characteristics.

**Table 4. 6 Strains used in Experiment 2**

| Strain | Strain Callsign |
|---|---|
| High CO syngas adapted strain 1 | H1 |
| High CO syngas adapted strain 2 | H2 |
| High CO syngas adapted strain 3 | H3 |
| CO (100%) adapted strain clone | CO1 |
| CO (100%) adapted strain | CO population |

The strains were inoculated in the serum flasks to form triplicates, and each serum flask was flushed with either a high CO gas mix or 100% CO Table 4.7 can be referred to for more detailed information.

Growth was monitored by taking 2 mL samples through the septum with a syringe and optical density being measured.

**Table 4. 7 Gas Mixes used in flushing in Experiment 2**

| | Substrate | | |
|---|---|---|---|
| **Strain** | **High CO Syngas Mix** | **High CO Syngas Mix** | **CO (100%)** |
| **H1** | H1-1 | H1-2 | H1-3 |
| **H2** | H2-1 | H2-2 | H2-3 |
| **H3** | H3-1 | H3-2 | H3-3 |
| **CO1** | CO1-1 | CO1-2 | CO1-3 |
| **CO Population** | COP-1 | COP-2 | COP-3 |

### 4.3.1. Experiment 2 Results

Comparing the growth characteristics, unsurprisingly the highest optical densities were achieved by the CO adapted strains (CO1 and COP) in cases where substrate was 100% CO. Among the triplicates of both strains, CO1-3 achieved the highest OD of 0.15 and the highest stability during the stationary phase. However, the COP strain, and particularly the COP-3 have shown the most remarkable growth rate ($\mu_{max}$) of 3.14 $h^{-1}$ and a shorter lag phase of approximately 24 hours in comparison to CO1-3. The lack of stability in the stationary phase could have been a result of acetate accumulation in the serum bottle, as HPLC data for this experiment is not available, it cannot be concluded that this is indeed an effect of acetate accumulation.

Among the cultures grown on high CO syngas mixture, the highest ODs of 0.888 and 0.766 were achieved by the triplicates denoted as H1-1 and H2-1 respectively. Due to the longer lag phases however, over 70 hours for H1-1 and 45 hours for H2-1, these clones were deemed unsuitable for continuous gas fermentations. If H1-1 clone can adapt to have a shorter lag phase through multiple passages have not been tested. Among the cultures grown with the same gas mixture COP-2 and CO1-2 also achieved higher maximum ODs, 0.728 and 0.522 respectively, as well as showing higher stability during the stationary phase and a shorter lag phase of approximately 25 hours. Between the two clones CO1-2 have demonstrated the higher maximum growth rate ($\mu_{max}$) of 2.813 $h^{-1}$ in comparison to the maximum growth rate ($\mu_{max}$) of 2.33 $h^{-1}$ demonstrated by COP-2.

As a result, triplicate CO1-2 have been selected as the clone to be used as the biocatalyst in continuous bioreactor fermentations.

The results of this experiment are presented in Figure 4.11 and Figure 4.12.

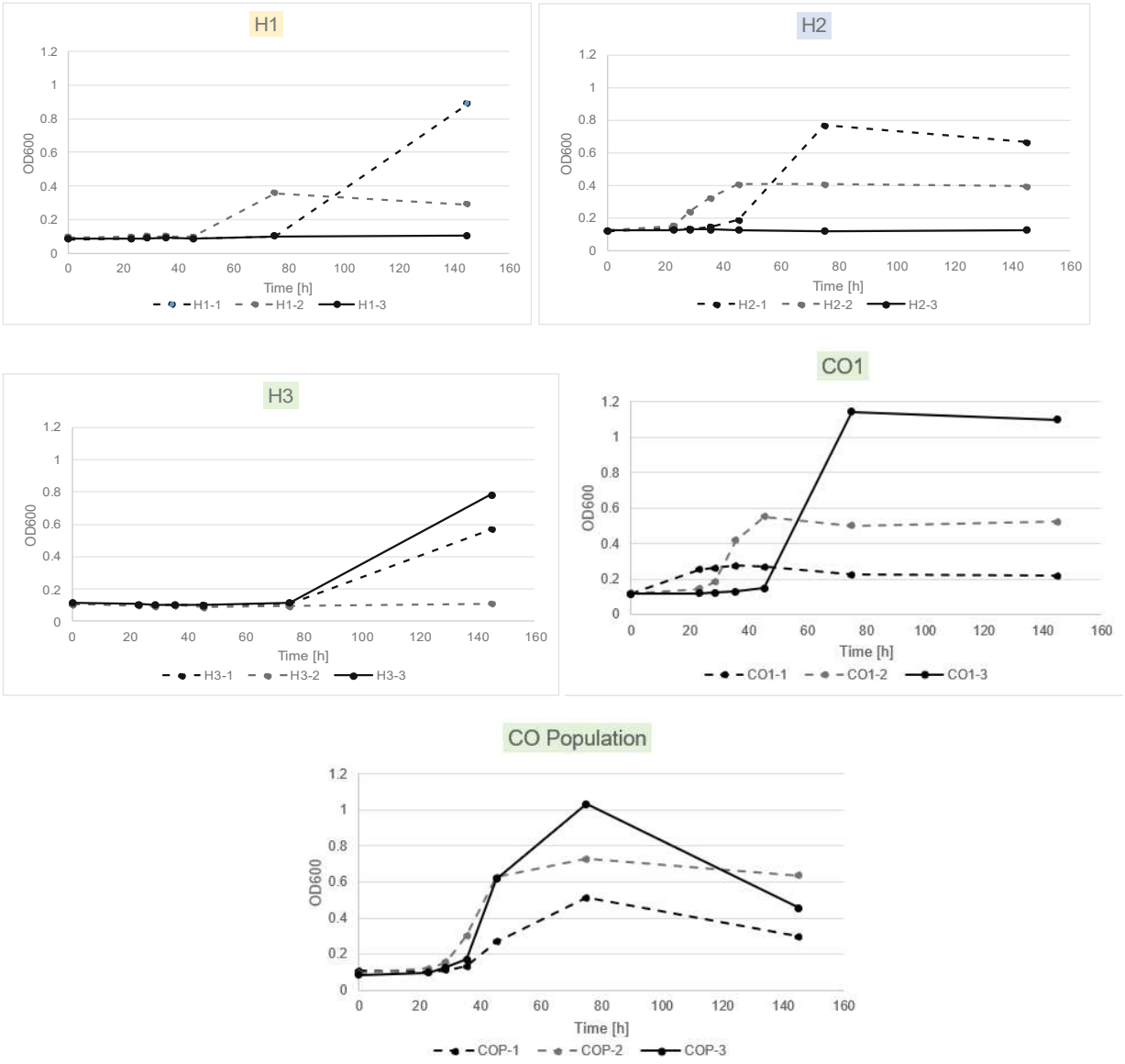


**Figure 4. 11 Experiment 2 Growth Profiles of triplicates with Moon Medium ($FeSO_4*7H_2O$, 33 mg/L), 66 ˚C, starting pH 6.4 in all cultures.**

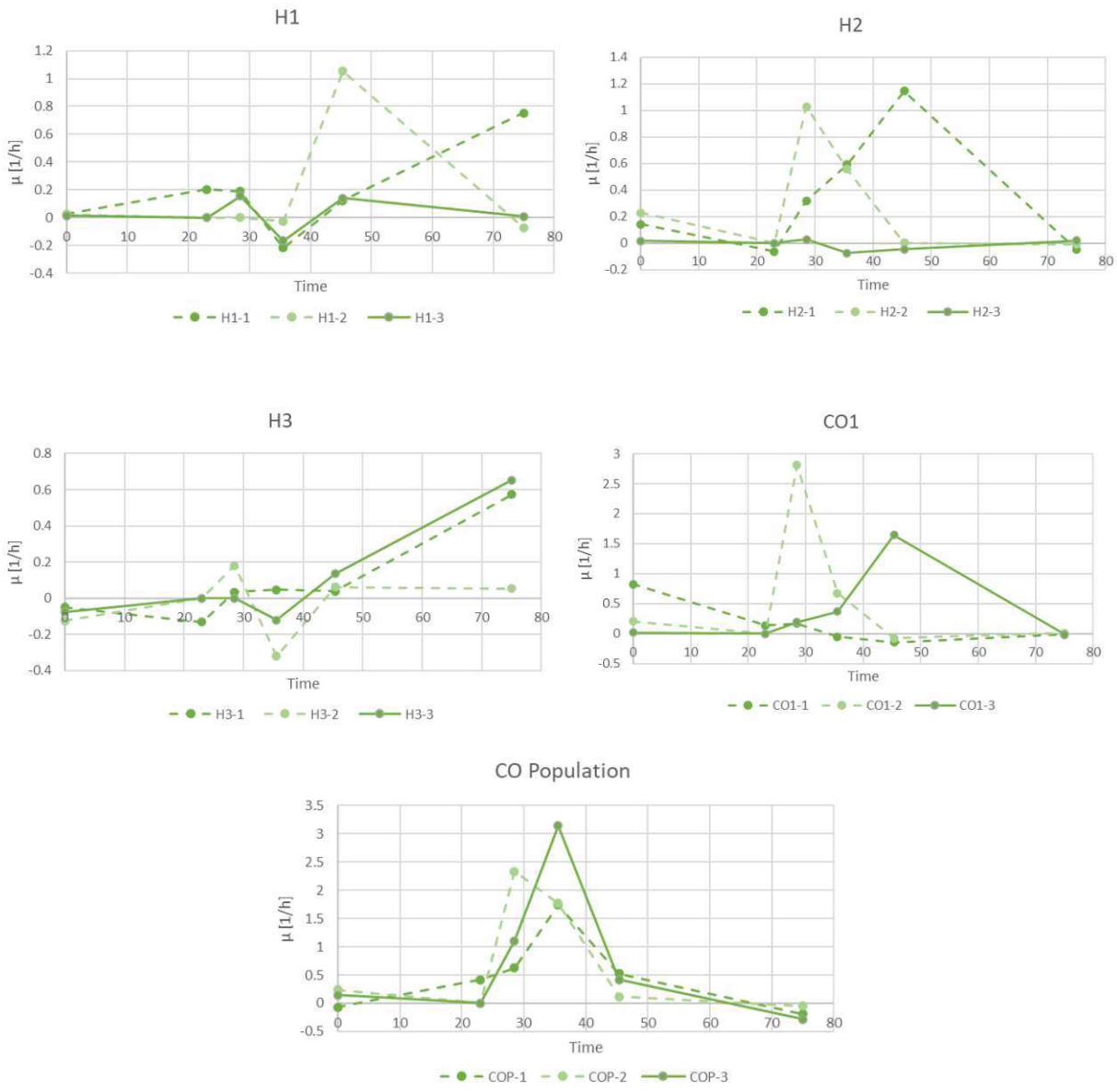


**Figure 4. 12 Experiment 2 Growth Rates of triplicates with Moon Medium ($FeSO_4$*$7H_2O$, 33 mg/L), 66 ˚C, starting pH 6.4 in all cultures.**

## 4.4. Experiment 3: Impact of Glucose on Continuous Gas Fermentation Performance

The aim of the third continuous experiment, made in the DASBox, setup was to establish a steady state in a continuous culture using the CO1 strain while taking minimal reactive actions and measuring the gas uptake rates to calculate yields and establish carbon balances for autotrophic and heterotrophic feeding regimes.

$H_2/CO_2$ gas mix was used as a substrate at 0.25 VVM and a ratio of $CO_2$:$H_2$:$N_2$ 9:58:33. Only a mild dilution rate (0.05 $h^{-1}$) have been employed in this experiment.

The medium was prepared as described in Section 3.2.1. to ensure same conditions are employed in precultures and fermentation.

All reactors have been inoculated at the same time using the CO1 strain, Table 4.8. can be referred to for initial OD600 measurements.

**Table 4. 8 Experiment 3 Initial $OD_{600}$ measurements**

| Reactor | $OD_{600}$ |
|---|---|
| R1 | 0.05 |
| R2 | 0.059 |
| R3 | 0.055 |
| R4 | 0.048 |

R1 and R2 initially contained 1 g/L glucose as opposed to R3 and R4 that have contained 10 g/L glucose to support the initial growth.

The results are displayed with R1 and R3 in succession for results under mostly autotrophic feeding in Figures 4.13 and 4.14 respectively, while R2 and R4 represent results for heterotrophic feeding in Figures 4.15 and 4.16.

### 4.4.1. Experiment 3 Results

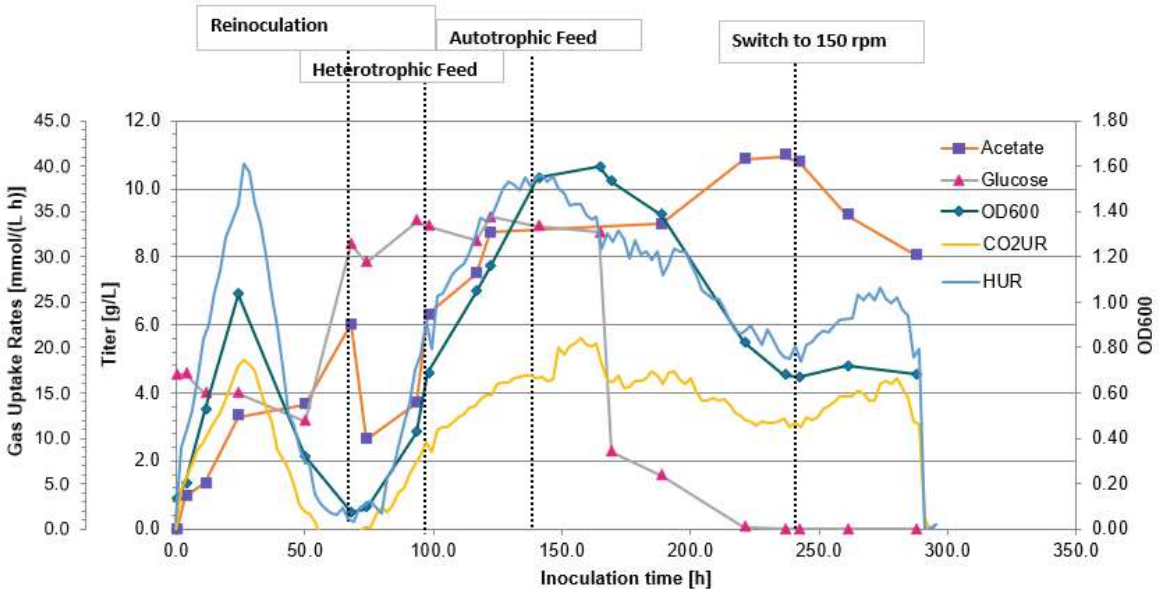


**Figure 4. 13 Experiment 3 Reactor 1 fermentation results including GC&HPLC data with CO1 strain at 66 ˚C and pH 6.4**

**Table 4. 9 *Experiment 3* Reactor 1 overview of parameters changed**

| Inoculation Time [h] | Intervention | Stirrer Speed [RPM] | Dilution Rate [$h^{-1}$] |
|---|---|---|---|
| 11.2 | Feed turned on with 10 g/L glucose | 600 | 0.05 |
| 50.1 | Stirrer speed reduced | 300 | 0.05 |
| 68.1 | Reinoculated with 10 ml inoculum from R2, feed turned off | 300 | 0 |
| 97.7 | Feed turned on with 10 g/L glucose | 300 | 0.05 |
| 140.3 | Feed switched to autotrophic | 300 | 0.05 |
| 236.5 | Stirrer speed reduced | 150 | 0.05 |
| 287.8 | pH brought down to 2 to end the experiment | | |

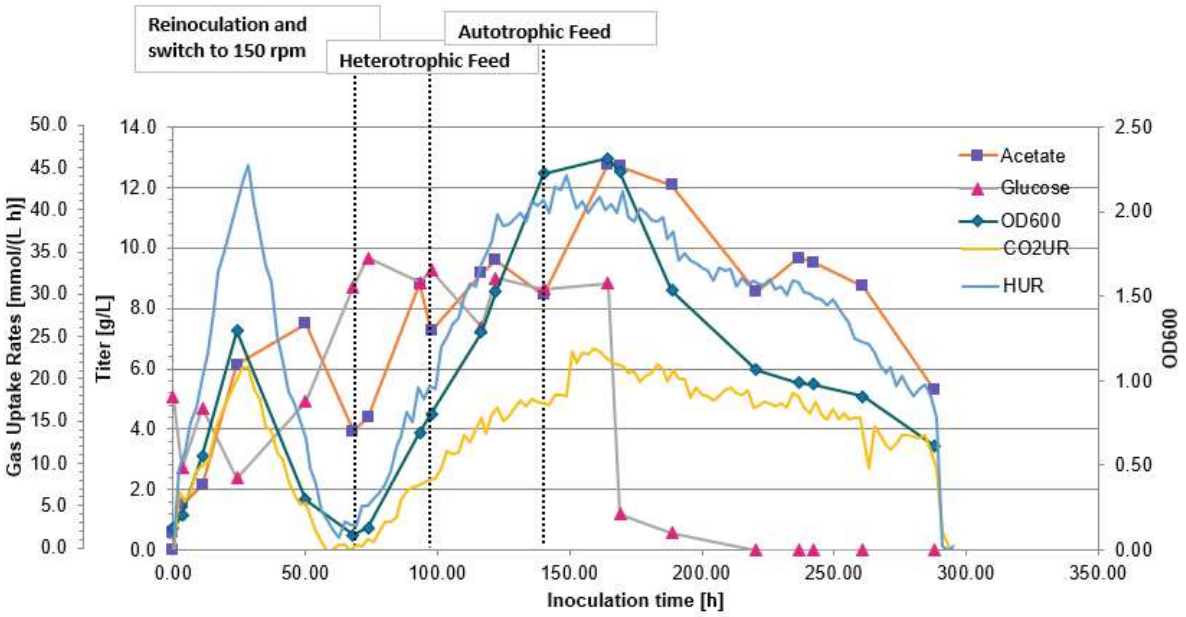


**Figure 4. 14 Experiment *3* Reactor 3 fermentation results including GC&HPLC data with CO1 strain at 66 ˚C and pH 6.4**

**Table 4. 10 Experiment 3 Reactor 3 overview of parameters changed**

| Inoculation Time [h] | Intervention | Stirrer Speed [RPM] | Dilution Rate [$h^{-1}$] |
|---|---|---|---|
| 11.2 | Feed turned on with 10 g/L glucose | 600 | 0.05 |
| 68.1 | Reinoculated with 10 ml inoculum from R2, feed turned off, stirrer speed reduced | 150 | 0 |
| 93.3 | Feed turned on with 10 g/L glucose | 150 | 0.05 |
| 140.3 | Feed switched to autotrophic | 150 | 0.05 |
| 287.8 | pH brought down to 2 to end the experiment | | |

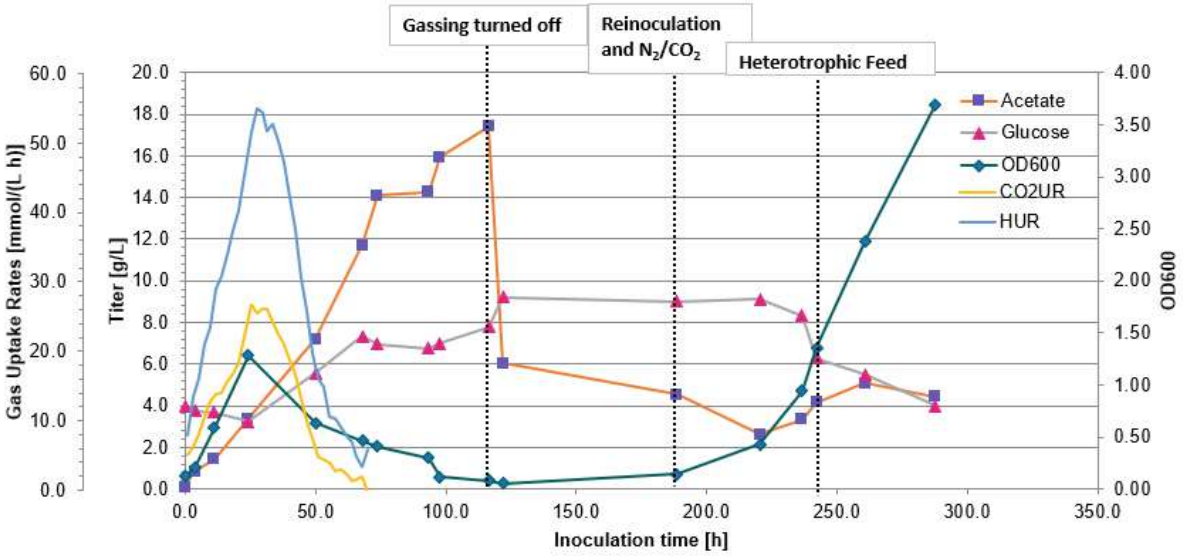


**Figure 4. 15 Experiment 3 Reactor 2 fermentation results including GC&HPLC data with CO1 strain at 66 ˚C and pH 6.4**

**Table 4. 11 Experiment 3 Reactor 2 overview of parameters changed**

| Inoculation Time [h] | Intervention | Stirrer Speed [RPM] | Dilution Rate [$h^{-1}$] |
|---|---|---|---|
| **11.2** | Feed turned on with 10 g/L glucose | 300 | 0.05 |
| **68.1** | Feed stopped due to pump failure | 300 | 0 |
| **116.5** | Turned off gassing (to make bottle last longer) | 300 | 0 |
| **188.7** | Reinoculated with 10 ml inoculum from R3, gassing switched to $N_2/CO_2$ 85:15 | 300 | 0 |
| **242.2** | Feed turned on with 10 g/L glucose | 300 | 0.05 |
| **287.8** | pH brought down to 2 to end the experiment | | |

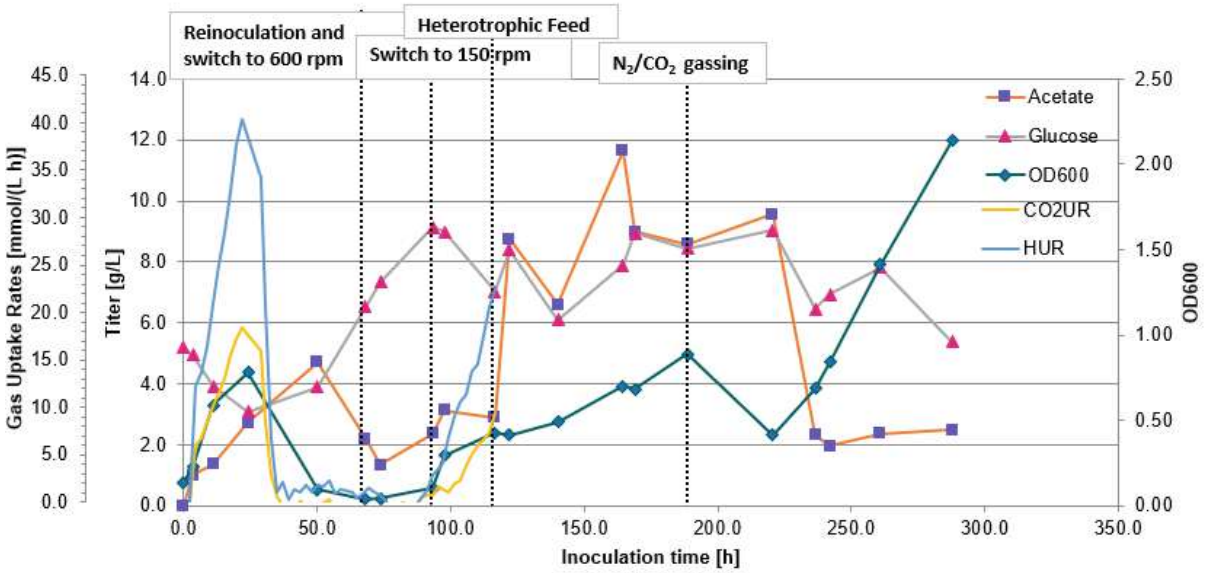


**Figure 4. 16 Experiment 3 Reactor 4 fermentation results including GC&HPLC data with CO1 strain at 66 ˚C and pH 6.4**

**Table 4. 12 Experiment 3 Reactor 2 overview of parameters changed**

| Inoculation Time [h] | Intervention | Stirrer Speed [RPM] | Dilution Rate [$h^{-1}$] |
|---|---|---|---|
| **11.2** | Feed turned on with 10 g/L glucose | 300 | 0.05 |
| **50.1** | Reinoculated with 50 mL preculture, feed turned off, stirrer speed reduced | 150 | 0 |
| **68.1** | Reinoculated with 10 ml inoculum from R2, stirrer speed increased | 600 | 0 |
| **93.3** | Stirrer speed reduced | 150 | 0 |
| **116.5** | Feed turned on with 10 g/L glucose | 150 | 0.05 |
| **188.7** | Gassing switched to $N_2/CO_2$ 85:15 | 150 | 0.05 |
| **287.8** | pH brought down to 2 to end the experiment | | |

### 4.4.2. Establishing Continuous Cultures

Unlike experiment 1, steady state under autotrophic conditions was not established in experiment 3 (figures A. 3 and A. 4). This is likely due to the accumulation of KAc in the reactors as the acetate titers in both reactors were approximately between 7-13 g/L due to the lower dilution rates.

For the reactors operated under heterotrophic conditions there are data points where the growth rates exceeding the dilution rates (figures 4.17 and 4.18), especially in case of reactor 2. In both reactors the growth rates exceed the dilution rates when the acetate titers are lower (approximately between 2 and 6 g/L), showing that a higher dilution rate would have had a positive effect on establishing steady state as mentioned in the Section 4.2.2. Transitioning to continuous cultures has been successful in all four reactors even if the steady state has not been established.

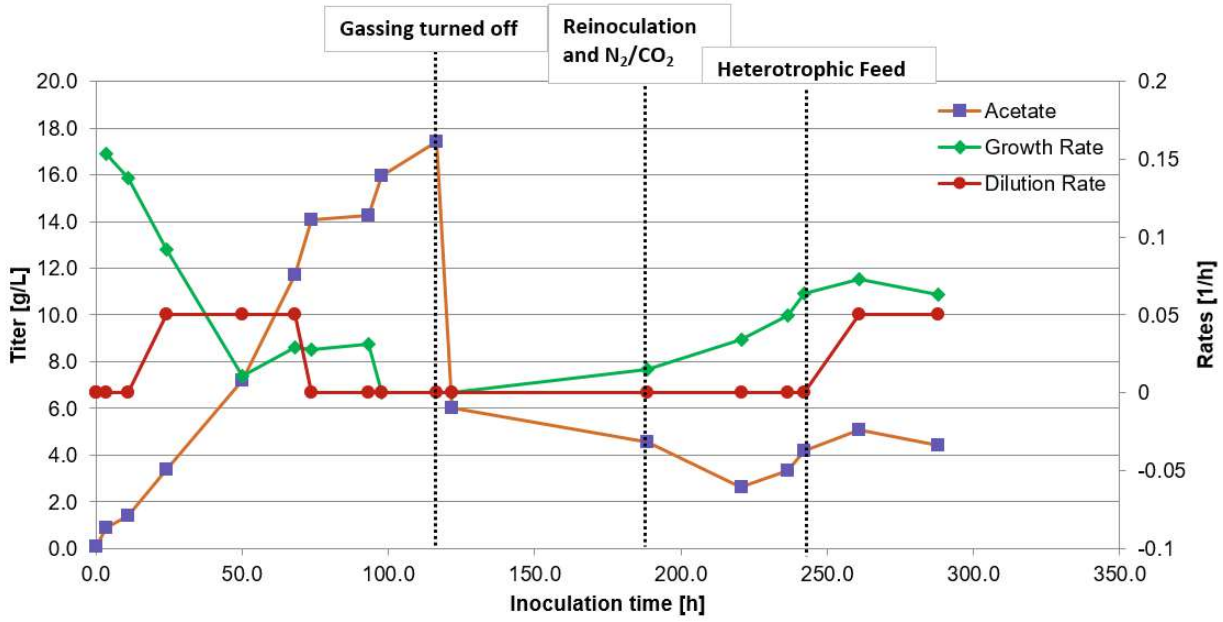


***Figure 4. 17*** **Experiment 3 Growth Rates, Dilution Rates and Acetate Titers with Modified Moon Medium, CO1 strain at 66 ˚C and pH 6.4**

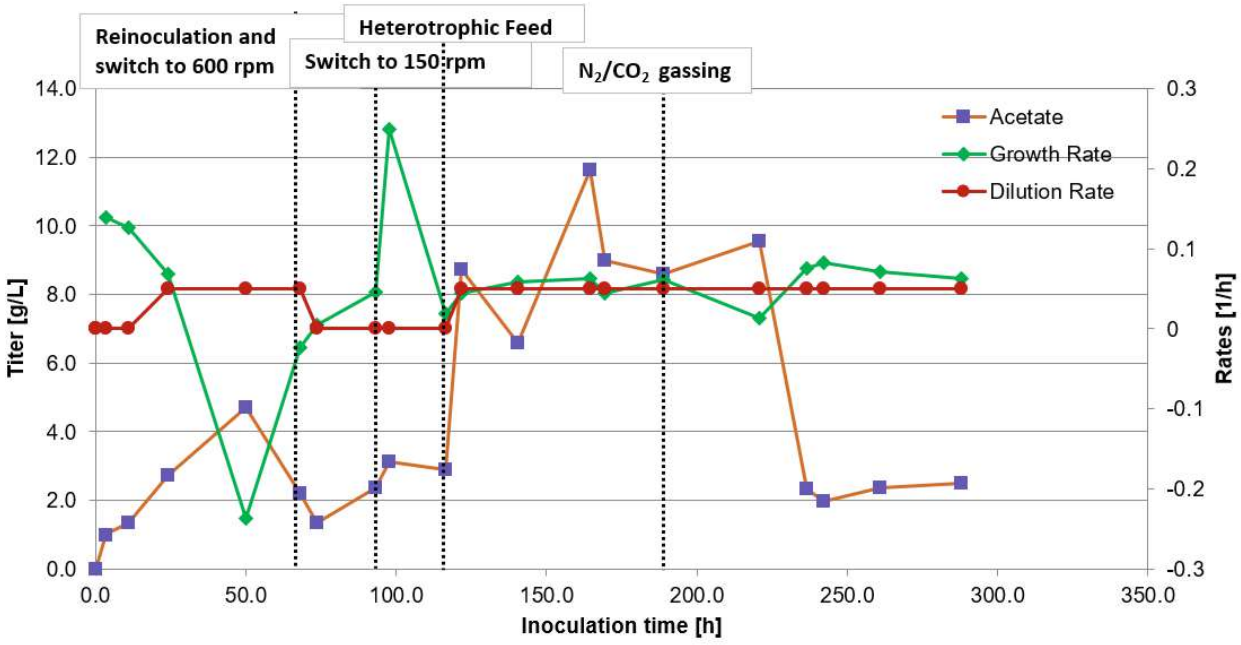


***Figure 4. 18*** **Experiment 3 Reactor 4 Growth Rates, Dilution Rates and Acetate Titers with Modified Moon Medium, CO1 strain at 66 ˚C and pH 6.4**

### 4.4.3. Optical Density to BTS Ratios

As *T. kivui* achieves lower cell densities CDW measurements can only be applied with larger sample volumes. As mentioned in Section 4.7 these samples were only taken at the end of the experimental procedure.

**Table 4. 13 Experiment 3 $OD_{600}$ to BTS (g/L) ratios**

| Reactor | $OD_{600}$/CDM |
|---|---|
| R1 | 2.71 |
| R2 | 7.63 |
| R3 | 4.12 |
| R4 | 4.08 |

As can be seen in Table 4.13 there is a significant margin of error between the measurements.

According to Leigh et al. (1981) *T. kivui* cells grown on $H_2/CO_2$ gas mixes vary in cell length between 2 - 3.5 µm while the cells grown on glucose vary between 5.5 – 7.5 µm. As optical density employs light scattering, an aggregate variable of density, opacity and granularity, and cell size is shown to be a factor in OD measurements in other species (Chioccioli et al. 2014), the average values are assumed between R1 and R3 for autotrophic conditions yielding 3.42 ± 0.7 and R2 and R4 for heterotrophic conditions yielding 5.85 ± 1.77 for purposes of calculating specific rates.

### 4.4.4. Specific Rates

Figures 4.13 and 4.14 display the $CO_2$ and $H_2$ uptake rates for reactor 1 and reactor 3 respectively. The results show that even with glucose present as a substrate, *T. kivui* still utilizes $CO_2$ and $H_2$ for metabolic needs. Under heterotrophic conditions the gas uptakes appear dependent on the cell densities in both reactors (figures 4.13, 4.14, 4.15 and 4.16). Upon glucose depletion, the specific gas uptakes increase in both reactors (figures 4.19 and 4.20) increase gradually, suggesting an adaptation.

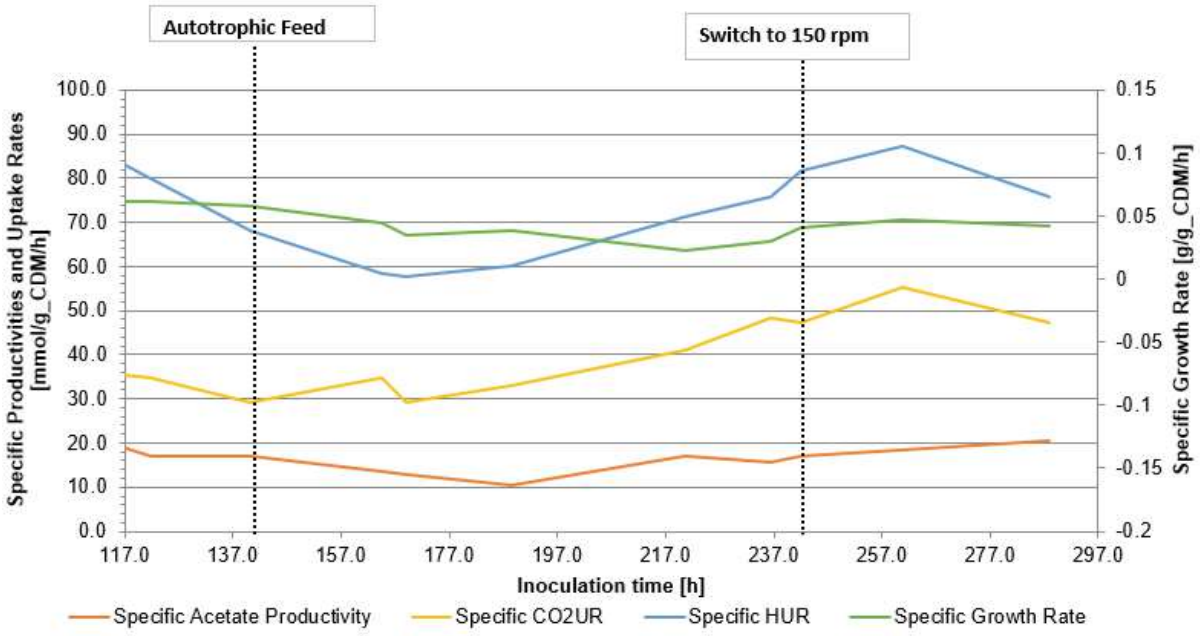


**Figure 4. 19 Experiment 3 Reactor 1 Specific Rates with Modified Moon Medium, CO1 strain at 66 ˚C and pH 6.4**

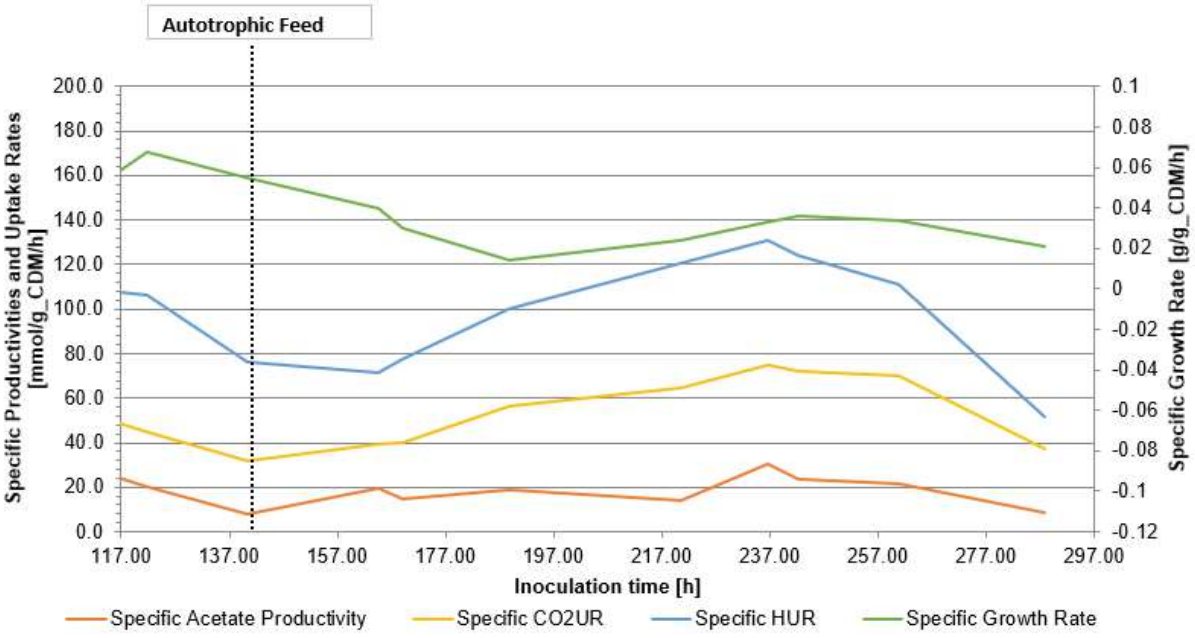


**Figure 4. 20 Experiment 3 Reactor 3 Specific Rates with Modified Moon Medium, CO1 strain at 66 ˚C and pH 6.4**

In reactor 4 under heterotrophic conditions removing $H_2$ from the feedstock results in a significant decrease in specific acetate productivity while the specific growth rates remain relatively stable (Figure 4.21). The increase in specific growth rates at 236.5 hours mark is most likely due to the reduced acetate titers in the reactor (Figures 4.16 and 4.18).

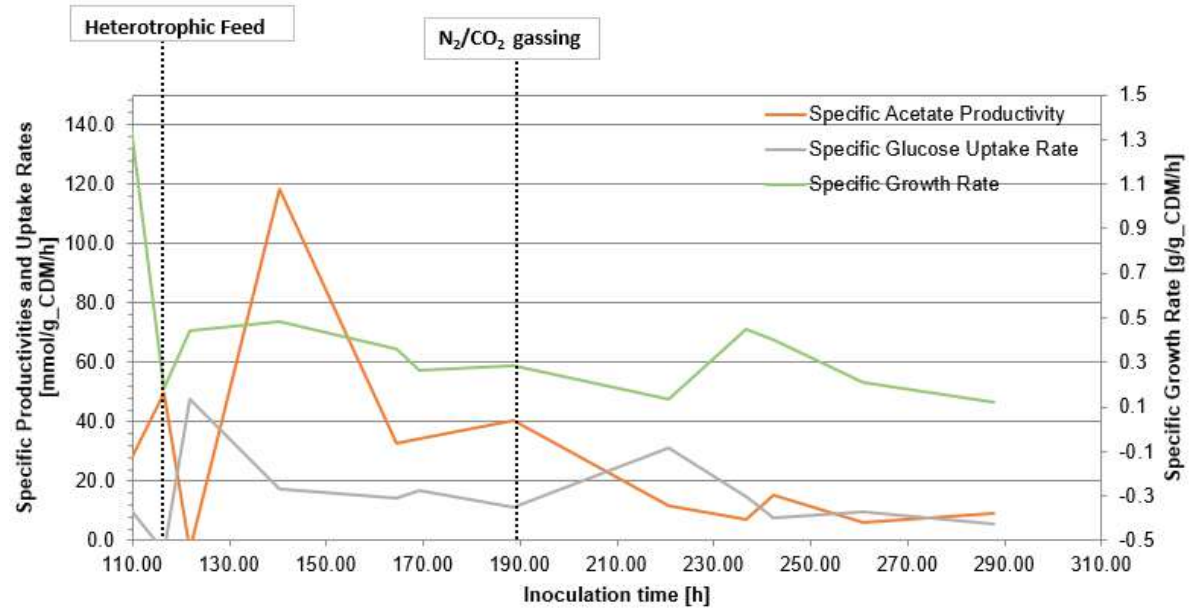


**Figure 4. 21 Experiment 3 Reactor 4 Specific Rates with Modified Moon Medium, CO1 strain at 66 ˚C and pH 6.4**

### 4.4.5. Yields and Carbon Balances

The product and biomass to substrate yields for the reactors operated under autotrophic conditions are displayed in figures 4.22 and 4.23. The average acetate/$CO_2$ yields are 0.41 in reactor 1 and 0.34, significantly lower, in reactor 3. Whereas the averages of acetate/$H_2$ yields are calculated as 0.22 and 0.18, respectively.

The yields, even though comparable, are lower than the expected value of 0.5 for $CO_2$ and 0.25 for $H_2$ in both reactors (Hess et al., 2014; Katsvy et al., 2021). This discrepancy is most likely caused by some of the acetyl-CoA produced during the WLP being utilized in anabolic pathways. The acetate titers (figures 4.13 and 4.14) didn't have any discernable effect in terms of yields as the yields are higher both in terms of biomass production and acetate formation in reactor 1, despite the higher acetate levels.

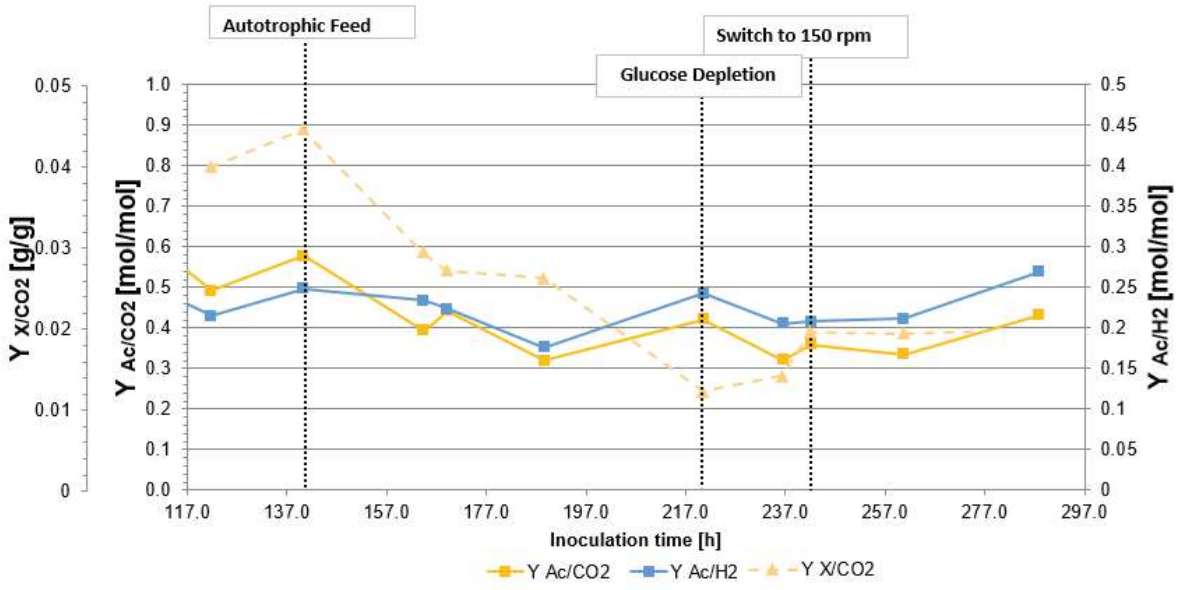


**Figure 4. 22 Experiment 3 Reactor 1 Acetate and Biomass Yields with Modified Moon Medium, CO1 strain at 66 ˚C and pH 6.4**

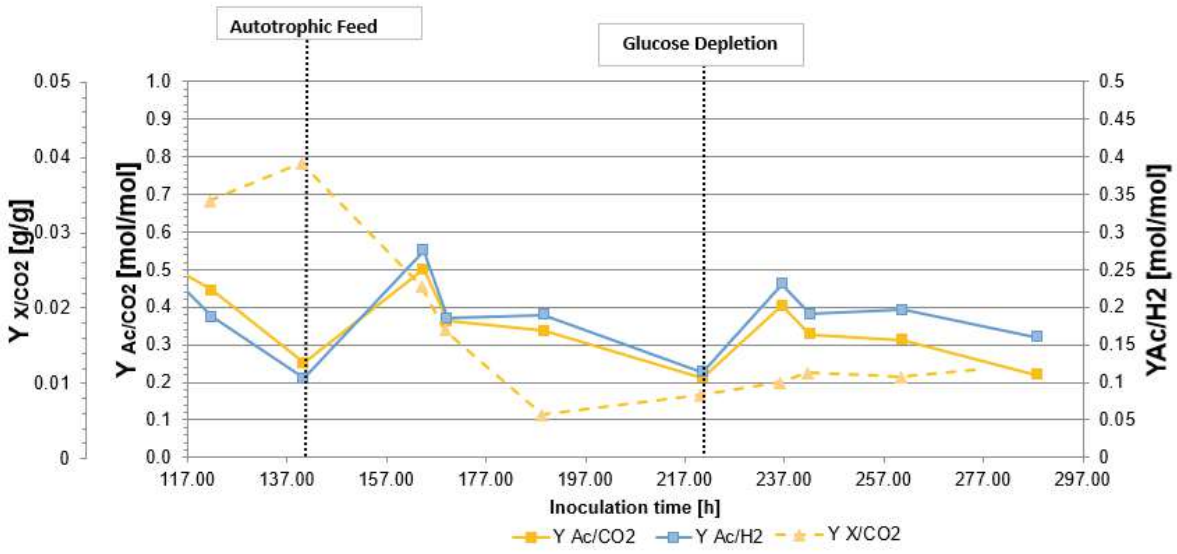


**Figure 4. 23 Experiment 3 Reactor 3 Acetate and Biomass Yields with Modified Moon Medium, CO1 strain at 66 ˚C and pH 6.4**

Carbon balances made around reactors 1 and 3 (displayed in figures 4.24 and 4.25) shows that changing the feeding strategy from heterotrophic to autotrophic ($CO_2/H_2$) causes a change in the product formation in favor of acetate. On average even when glucose is available as a substrate, 73.58 ± 1.9% of the carbon consumed by the biocatalyst originates from $CO_2$ and 82.7 ± 0.3% of the consumed carbon is converted to acetate.

Carbon recovery in acetate under these conditions is comparable the average 84% demonstrated by Leigh et al., (1981) with glucose under $N_2/CO_2$ atmosphere. Upon glucose depletion the conversion of the consumed carbon to acetate increases to 91 ± 1.2% approximately 10% lower than the demonstrated 101% (Leigh et al., 1981), 100% carbon recovery in acetate would be unrealistic for continuous cultures with $CO_2$ as the sole carbon source, as some growth is necessary to keep the biomass in the reactors with the existence of dilution rates.

The increased growth rates when glucose is present, could potentially be caused by glucose more easily being converted into pyruvate in comparison to $CO_2$, or more likely the improved bioenergetics when glucose is available as a substrate (Katsvy et al., 2021).

Biomass production is assumed in the carbon balances with respect to total consumption of carbon and acetate formation. It is more than likely that some of the carbon that is consumed would have been unrecovered, reducing the total amount of carbon used for biomass synthesis. Establishing an elementary analysis of both glucose and $H_2/CO_2$ grown cells would provide more information in terms of biomass synthesis, as the cell size and cell inclusions differ depending on the substrate (Leigh et al., 1981) and could have an effect on the total carbon content of the cells.

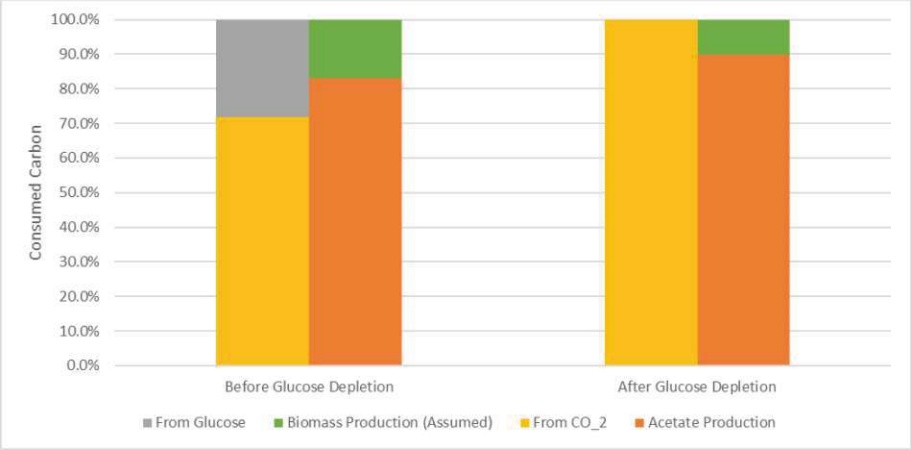


**Figure 4. 24 Experiment 3 Reactor 1 Carbon Balance with Modified Moon Medium, CO1 strain at 66 ˚C and pH 6.4, biomass production is assumed with respect to total consumed carbon and acetate formation.**

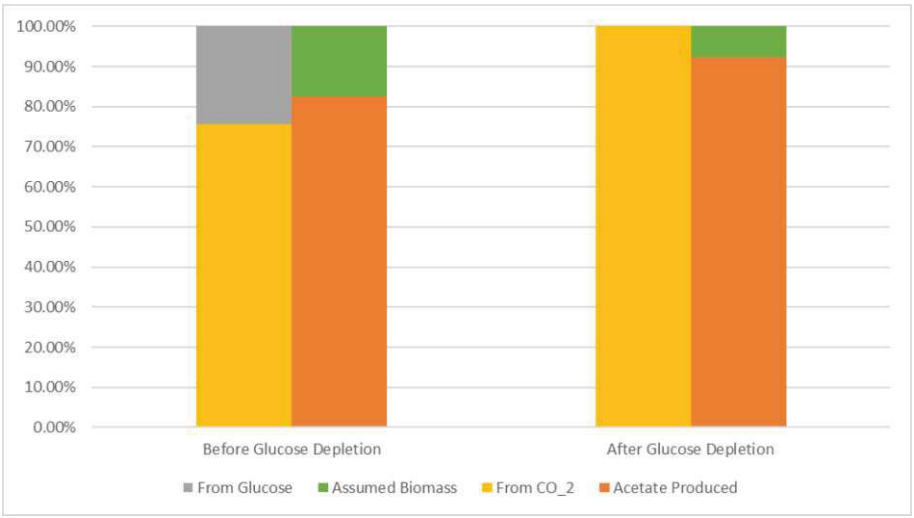


**Figure 4. 25 Experiment 3 Reactor 3 Carbon Balance with Modified Moon Medium, CO1 strain at 66 ˚C and pH 6.4, biomass production is assumed with respect to total consumed carbon and acetate formation.**

### 4.4.6. Experiment 3 Results Summary

- The acetate accumulation in the reactors is a determining factor in establishing a steady state fermentation. Higher dilution rates are beneficial in this regard especially under autotrophic conditions.
- $H_2$ in the feedstock is not necessary for growth when glucose is available as a substrate, however the acetate productivity suffers probably due to limited Ech function.
- Highest growth rate ($\mu_{max}$) of 0.054 $h^{-1}$ was observed in R1 (CO1 strain, 150 RPM and 0.05 $h^{-1}$ dilution rate) under autotrophic conditions, and 0.082 $h^{-1}$ in R4 (CO1 strain, 150RPM, 0.05 $h^{-1}$ dilution rate) under heterotrophic conditions.
- Highest specific acetate productivity ($q_{acetate}$) of 1.67 g $g_{CDM}^{-1}$ $h^{-1}$ (17.02 mmol $g_{CDM}^{-1}$ $h^{-1}$) was observed in R3 (CO1 strain, 150 RPM and 0.05 $h^{-1}$ dilution rate) under autotrophic conditions, and 0.83 g $g_{CDM}^{-1}$ $h^{-1}$ (8.46 mmol $g_{CDM}^{-1}$ $h^{-1}$) under heterotrophic conditions.
- Highest specific $CO_2$UR of 62.1 mmol $g_{CDM}^{-1}$ $h^{-1}$ was observed in R3 (CO1 strain, 150 RPM and 0.05 $h^{-1}$ dilution rate) under autotrophic conditions.
- Highest acetate/$CO_2$ yield of 0.43 mol/mol was observed in R1 (CO1 strain, 150 RPM and 0.05 $h^{-1}$ dilution rate) under strictly autotrophic conditions.
- Switching the feeding regime from heterotrophic to autotrophic in case of $H_2$/$CO_2$ causes a switch in product formation in favor of acetate. Using CO as the substrate could result in higher cell densities and therefore higher overall carbon utilization and product formation due to improved bioenergetics (Katsvy et al., 2021).

## 4.5. Experiment 4: Scalability and Performance in a Bubble Column Reactor

The aim of this experiment was to establish a batch fermentation using a bubble column setup to gauge industrial scalability with a syngas mixture using CO1 strain.

Moon medium has been used without increased iron concentration. Glucose concentration has been brought up to 1 g/L to provide the cells with an initial growth boost.

CO1 strain has been used for inoculation and a low CO syngas mixture (Table 4.14) was used as the substrate for showing industrial applicability. The experiment has been prepared as described in sections 3.4. and 3.4.3 without any additional steps taken. The initial OD600 after inoculation was 0.055.

**Table 4. 14 Low CO Syngas Mix**

| Gas | Fraction |
|---|---|
| $CO_2$ | 0.1111 |
| CO | 0.2667 |
| $H_2$ | 0.5156 |
| $N_2$ | 0.1111 |

### 4.5.1. Experiment 4 Results

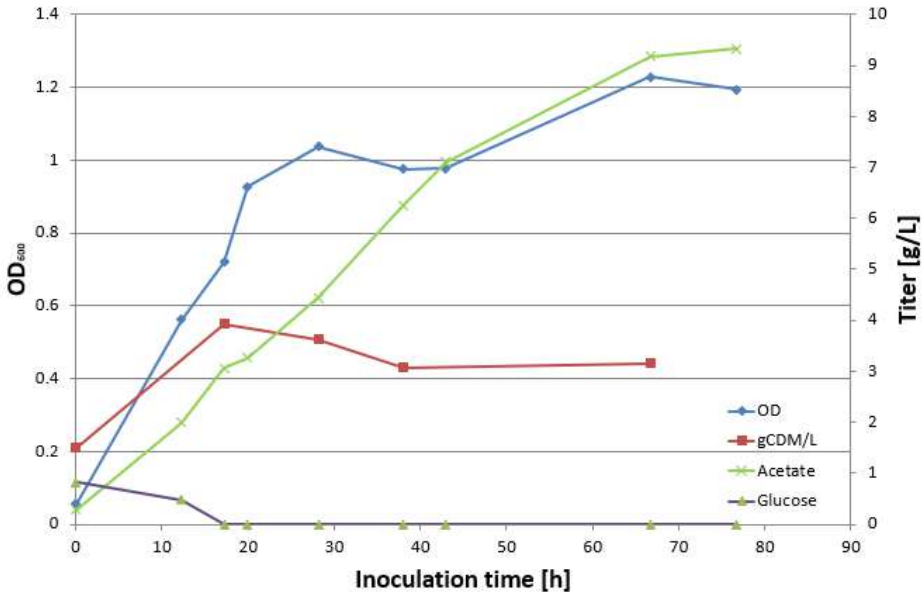


**Figure 4. 26 Bubble Column Batch Fermentation Results Moon Medium, CO1 strain at 66 ˚C and pH 6.4**

In the bubble column fermentation experiment (Figure 4.26), the results demonstrate *T. kivui* is able to grow in such conditions with syngas as its sole substrate. Notably, the maximum optical density achieved reaches approximately 1.21, a notably higher value compared to any other cultivation method under autotrophic feeding. The $OD_{600}$ results indicates that cells undergo an adaptation to the conditions between 28 and 42 hours after inoculation, although this adaptation is not mirrored in the measurements of Cell Dry Mass (CDM). Regardless, a stationary phase is observed, a phenomenon not previously encountered in Continuous Stirred-Tank Reactor (CSTR) setups.

The higher volume samples allowed for comparing CDM measurements in most of the samples with optical densities. The results show that even under autotrophic conditions the ratio between CDM and optical densities are prone to change. The average $OD_{600}$/BTS values are observed to be 2.1 ± 0.31 under autotrophic conditions (figure 4.27).

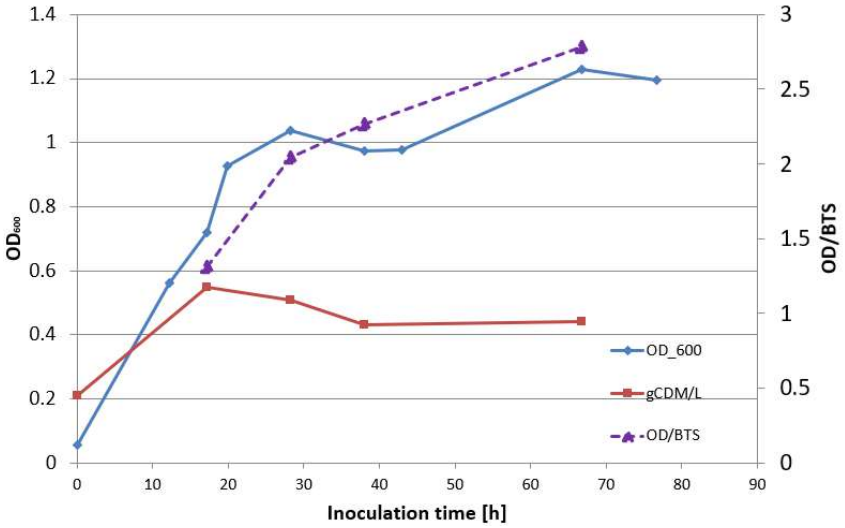


**Figure 4. 27 Bubble Column Batch Fermentation comparison of $OD_{600}$ to CDM measurements Moon Medium, CO1 strain at 66 ˚C and pH 6.4**

Growth rates and acetate productivities that are displayed on figure 4.28, reveals that cultures exhibit a preference towards either growth or energy conservation through acetate production. The growth rates (μ) undergo a very steep decrease to a negligible level when the glucose is consumed (0.0029 ± 0.0038 $h^{-1}$). The achieved rates are much lower in comparison to previous experiments (sections 4.2.3 and 4.4.2), as well as the specific acetate productivities ($q_{Acmax}$= 4.34 mmol $g_{CDM}^{-1}h^{-1}$). Even though GC data is not available for this experiment, it is very likely that the bubble column provides more limited gas to liquid mass transfer in comparison to the CSTR setups. The difference between acetate productivity and growth rates suggests that *T. kivui* favors catabolic routes for energy production in case of substrate limitation.

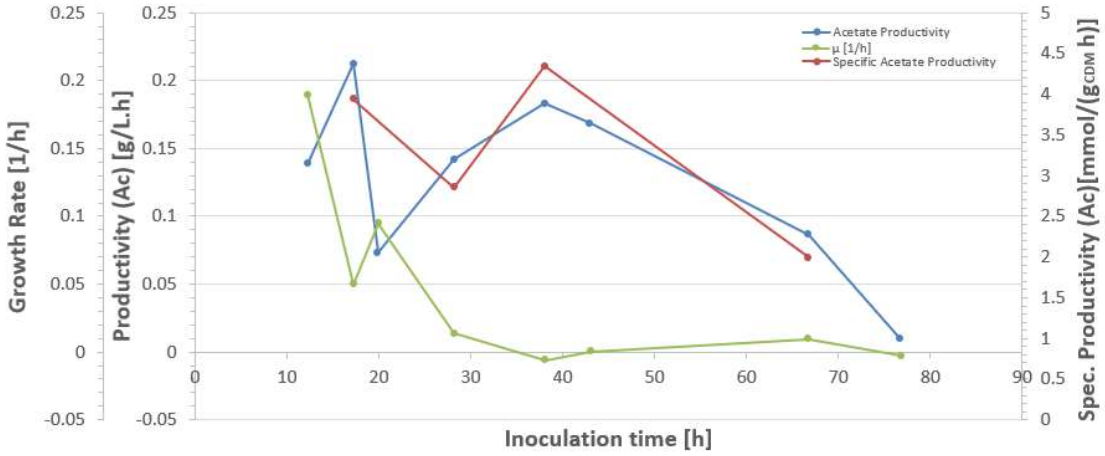


**Figure 4. 28 Bubble Column Batch Fermentation Rates Moon Medium, CO1 strain at 66 ˚C and pH 6.4**

## 4.6. Experiment 5: Effect of pH and Acetate Concentration on Growth of CO1 strain

**Table 4. 15 Starting pH and Acetate Concentrations**

| Name | pH | KAc [g/L] | OD600 |
|---|---|---|---|
| LpH_Ac0a | 5.8 | 0 | 0.224 |
| LpH_Ac0b | 5.7 | 0 | 0.212 |
| LpH_Ac10a | 5.5 | 10 | 0.047 |
| LpH_Ac10b | 5.5 | 10 | 0.05 |
| MpH_Ac0a | 6.5 | 0 | 0.495 |
| MpH_Ac0b | 6.6 | 0 | 0.314 |
| MpH_Ac10a | 6.6 | 10 | 0.213 |
| MpH_Ac10b | 6.1 | 10 | 0.166 |
| HpH_Ac0a | 7 | 0 | 0.559 |
| HpH_Ac0b | 7 | 0 | 0.458 |
| HpH_Ac10a | 6.9 | 10 | 0.125 |
| HpH_Ac10b | 6.8 | 10 | 0.22 |

The experiment was conducted in serum bottles to test the resistance of *CO1* strain to different pH levels and K-Acetate concentrations under autotrophic conditions using $H_2/CO_2$ gas mix as a substrate. Duplicates have been used for each data point. The Moon Medium was modified by differentiating the concentration of K-salts in the phosphate buffer to create three distinct starting pH levels. K-Phosphate concentration at the start of the experiment has been alternated between 0 g/L for the lower point and 10 g/L for the high. Table 4.15 can be referred to for the exact starting conditions.

The difference in starting pH values effected the reaction with the Resazurin resulting in different colorations during the sampling, possibly affecting the $OD_{600}$ values. This effect has been taken into consideration for the calculation of final $OD_{600}$ values.

### 4.6.1. CO1 Strain Growth Profiles with Starting pH 5.8-7 and KAc 0-10 g/L Results

The results presented in Figures 4.29 through 4. 31 show that both pH and K-Ac concentrations play a significant role in cell reproduction.

The cultures established at lower pH of 5.5-5.8 have shown no signs of growth in presence of 10 g/L K-acetate according to the $OD_{600}$ measurements while the pH values decreased from 5.5 to 5.35 suggesting some metabolic activity occurred in between the time first two OD measurements. Without the presence of KAc, the $OD_{600}$ measurements increased from 0.063 ± 0.002 to a maximum value of 0.155 ± 0.006 after 24 hours as the pH decreased from 5.75 ± 0.05 to 4.475 ± 0.025. The cell densities according to OD measurements have remained stable for another 24 hours before decreasing to 0.085 ± 0.004 in the next day. The $\mu_{max}$ was 0.052 ± 0.002.

The cultures with both medium and higher starting pH values of 6.35 ± 0.25 and 6.85 ± 0.05, showed similar growth profiles with the presence of KAc (MpH_Ac10, HpH_Ac10). A longer lag phase was observed in both cultures with final established OD values of 0.28 ± 0.1 for MpH_Ac10 and 0.36 ± 0.04 for HpH_Ac10 while the pH values of both cultures decreased to a final value of 5.5. The maximum growth rates were 0.026 ± 0.007 for MpH_Ac10 and 0.04 ± 0.008 for HpH_Ac10.

In the cultures established in the abovementioned pH range without KAc, the cultures with higher starting pH (7) have achieved higher cell densities as the $OD_{600}$ values reached 0.8 ± 0.04 after 48 hours while the pH decreased to 5.07 ± 0.02. As for the cultures with the medium starting pH (6.55 ± 0.05) have achieved OD of only 0.51 ± 0.02 while the pH decreased to 4.88 ± 0.025 in the same time frame. Whereas the maximum growth rates were 0.053 ± 0.008 for MpH_Ac0 and 0.064 ± 0.006 for HpH_Ac0.

The minimum pH where *T. kivui* can grow significantly is determined to be 5.2 by Leigh et al. (1981) and even though this particular pH was not tested the results suggest that this is approximately correct for the CO1 strain as well.

According to Klepms et al., (1987) however, wildtype *T. kivui* can achieve an $OD_{660}$ of 4 even with a starting 32 g/L KAc concentration. The results of this experiment show that with a starting pH of 7, and 10 g/L KAc starting concentration the growth is less then 50% of the cultures that include no starting KAc in case of the CO1 strain while the growth rate is approximately 60% in the cultures that contains starting KAc as opposed to the ones that do not. This limitation on the growth rates are very detrimental for continuous fermentations by imposing limitations on dilution rates.

Such concentrations are achieved even in continuous mode of operation with milder dilution rates (0.05 $h^{-1}$) in fermentations (Figure 4.2). Supporting the advantages of higher dilution rates earlier on in the fermentation processes already mentioned in Section 4.2.2.

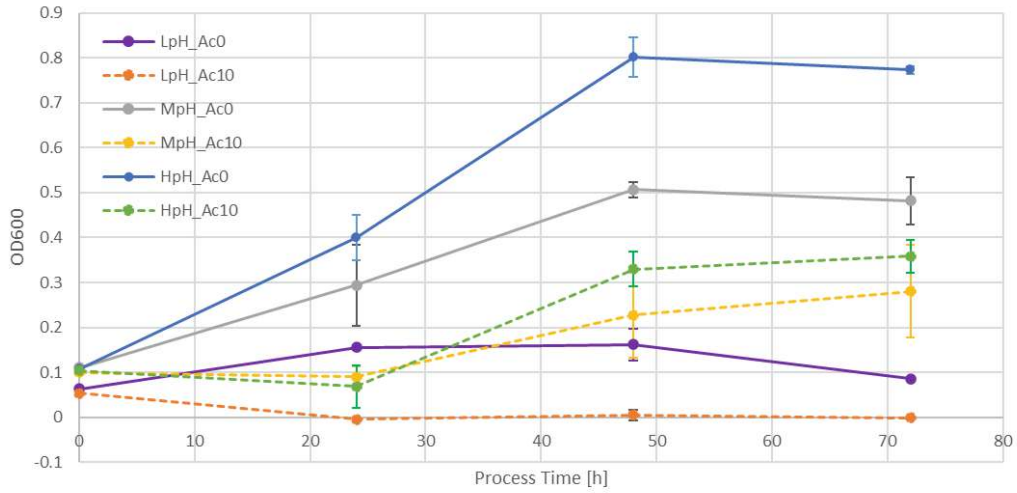


**Figure 4. 29 Growth Profiles of CO1 strain with different starting pH values (5.5 – 7) and sodium acetate concentrations (0-10 g/L) at 66 ˚C, the mean values of duplicates are displayed.**

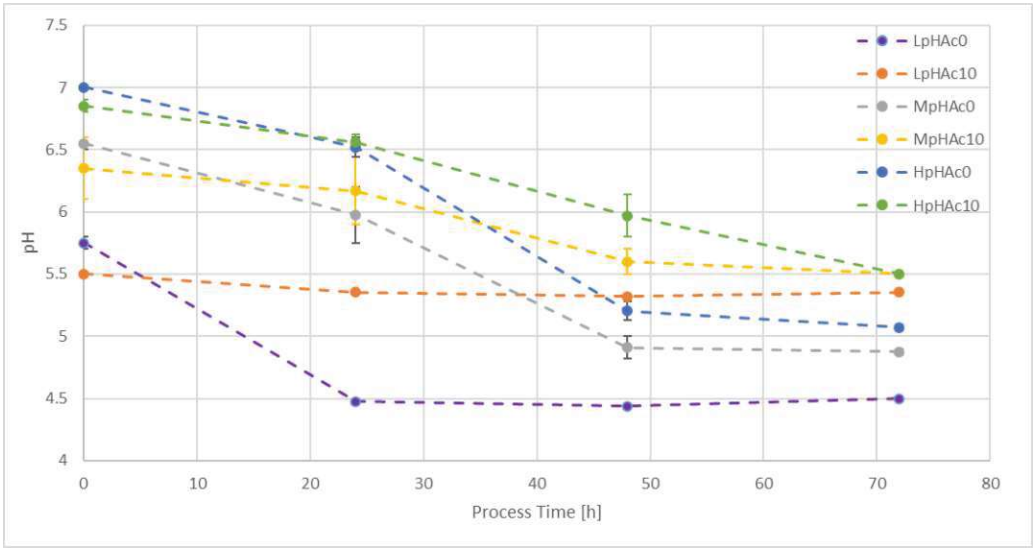


**Figure 4. 30 pH change CO1 strain during growth with different starting pH values (5.5 – 7) and sodium acetate concentrations (0-10 g/L) at 66 ˚C, the mean values of duplicates are displayed.**

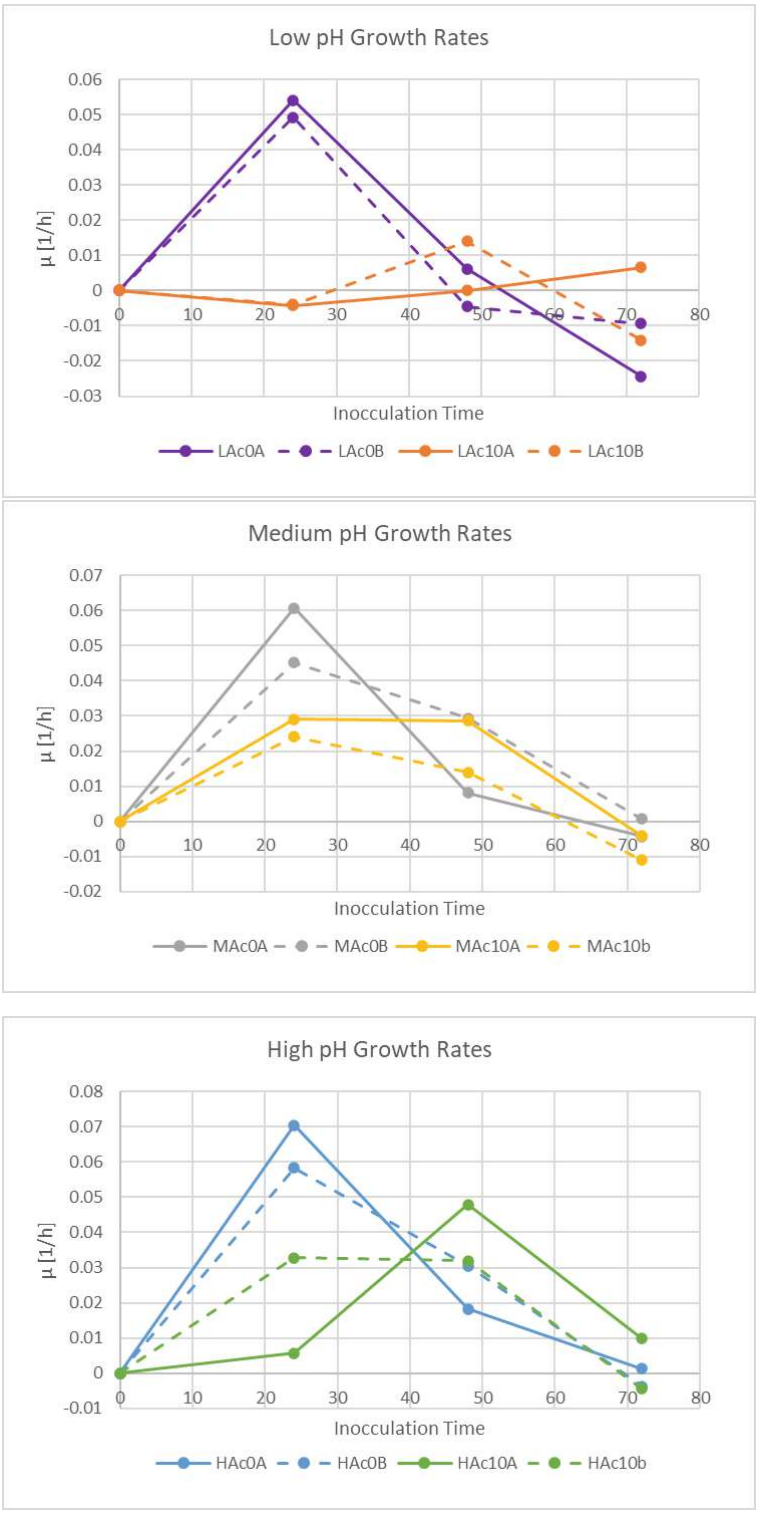


**Figure 4. 31 Growth Rates of CO1 strain with different starting pH values (5.5 – 7) and sodium acetate concentrations (0-10 g/L) at 66 ˚C**

## 4.7. Experiment 6: Growth and Adaptability of *T. kivui* with Formate as the Sole Substrate

This experiment aimed to examine the possibility of using formate as a substrate instead of the $H_2/CO_2$ gas mixture for the CO1 strain.

Even though formate is a natural part of the WLP, the initial attempts to grow CO1 with formate have not been successful in the previous experiments.

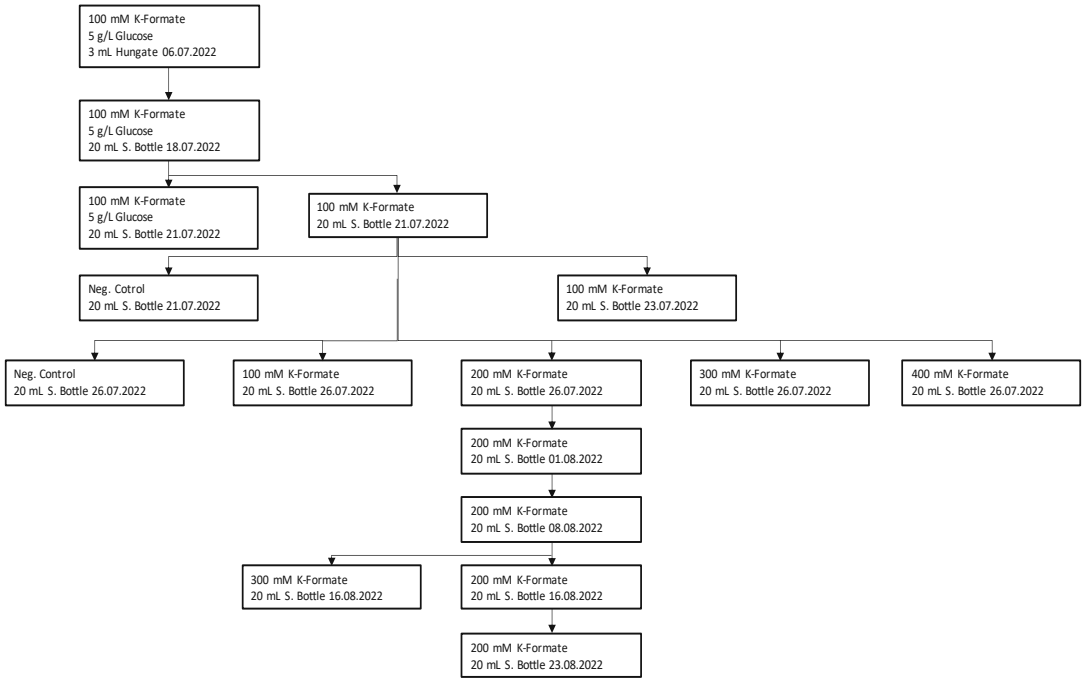


**Figure 4. 32 Chart of Passages for Formate Adaptation**

The series of experiments for formate adaptation started with a single Hungate tube experiment to gauge the possibility of growth with CO1 strain. As opposed to the previous experiments the cell density has risen within 12 days from 0.7 to 0.15 in optical density. The experiment therefore has been carried over to a 20 mL serum bottle under the same conditions where similar results have been achieved. As growth has been recorded on the second step of the passage, two additional serum bottles were inoculated under the same conditions, in this passage however glucose has been excluded from one to see if the growth was possible solely due to the presence of glucose.

The serum flask containing formate has already shown signs of growth within three days of inoculation. As third passage has been successful, an additional passage was carried out including a negative control.

As similar results have been achieved in the serum bottle with the 100 mM formate and no sign of growth has been recorded in the negative control, an additional passage was made this time including a negative control and four different K-Formate concentrations being 100, 200, 300 and 400 mM.

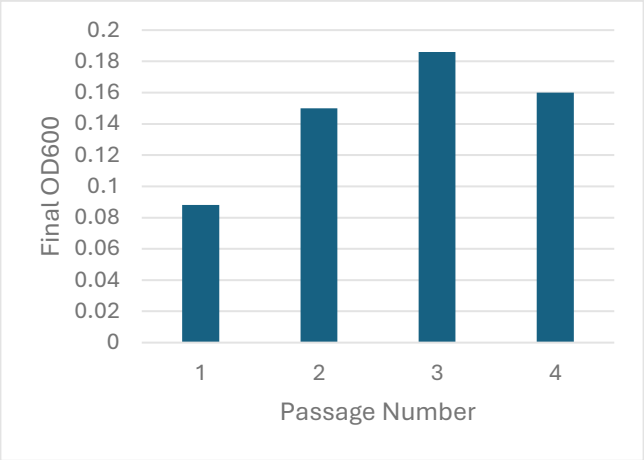


***Figure 4. 33*** **Final $OD_{600}$ values for 200mM formate as sole substrate with CO1 strain at 66 ˚C and starting pH of 6.4**

Between all the serum flasks, only 100 mM and 200 mM formate-containing bottles showed growth, while the 400 mM serum bottle showed signs of precipitation, suggesting 400 mM K-Formate hindering the stability of the Moon Medium under given conditions.

Multiple passages have been carried out in 20 mL serum bottles containing 200 mM K-Formate following this to facilitate the adaptation of *T. Kivui* to grow on formate. Figure 4.32. can be referred to for the chart showing the passages carried out. Figure 4.33. can be referred to for the final $OD_{600}$ results for the last four passages.

The cell densities achieved are not high enough to establish continuous fermentations. This could be explained by either the cells favoring $H_2/CO_2$ production as outlined by Burger et al., (2022) in presence of formate, or the fact that adaptation of *T. kivui* may require further passages.

However, cryo cultures have been prepared for the successful cultures. The cryo cultures that have been established have successfully been able to grow in serum bottles with the presence of 200 mM K-Formate and anaerobic conditions.

# 5. Discussion and Outlook

The idea behind this study was that continuous gas fermentation with syngas can be used to produce bio-commodities with *T. kivui* as the biocatalyst. In this study, methods for establishing continuous cultures utilizing *T. kivui* have been explored.

The methodologies employed in this study encompassed a diverse array of approaches, including the evaluation of cellular responses to potential growth-enhancing compounds such as Ca-pantothenate, peptone, and yeast extract, alongside the investigation of various growth environments characterized by distinct reactor setups, stirrer speeds, dilution rates, mediums and feedstocks.

A significant milestone was achieved through the successful initiation of steady state cultures with CO1 strain subsequent to the supplementation of iron concentrations ($FeSO_4*7H_2O$) within the Moon Medium, raising it to 3.3 mg/L and later switching to the Eysmondt Medium. The ensuing cultures, presented in sections 4.2.2, demonstrate a robustness that renders them amenable to prospective omics analyses, presenting an exciting avenue for further investigation.

- **Potential Benefits of Higher Dilution Rates**

The accumulation of acetate in the reactors presents a more important factor then initially considered. In almost every continuous culture established higher acetate titers prevented the transition to a steady state by limiting the growth rates, as the operating conditions are kept stable at 66 ˚C and pH 6.4.

High concentrations of acetic acid are known to inhibit growth in bacteria in varying degrees (Lasko et al., 2000). The most widespread explanation for this inhibition is the uncoupling effect the organic acid (Pinhal et al., 2019). Acetic acid, the protonated form of acetate, is known to diffuse freely across the cell membrane (Grime et al., 2008). However, the dissociation of HAc within the cell into acetate ions and $H^+$ makes the expulsion of excess protons from the cell a necessity in order to maintain the membrane potential, as according to Katsvy et al., (2021) maintaining the proton gradient is necessary for ATP production as

well as reducing Fd in *T. kivui* with $H_2/CO_2$ as feedstock, at the cost of energy expenditure in terms of ATP, proving detrimental to growth (Pinhal et al., 2019). This effect can be particularly severe in acetogens as acetate is the final product of the WLP, causing higher intracellular concentrations as opposed to extracellular concentrations.

- **Limitations of $OD_{600}$ Measurements**

$OD_{600}$ measurements are a very practical way to estimate the cell densities and growth rates during the fermentation process due to their ease and speed. However as optical density of the cultures is dependent not only on cell densities but also other variables such as density, opacity and granularity of the medium, as well as cell size, changing conditions that are very common in such long fermentations reduce the accuracy of these measurements independent of the precision involved. Since these measurements influence the decisions in terms of operating conditions such as dilution rates and stirrer speeds, the inaccurate measurements are prone to hinder the transitions to steady state operations. It could be beneficial to take KOH titers or acetate titers measured through CEDEX into consideration especially when a decision to change the dilution rate is to be made.

- **Effects of Stirrer Speeds**

Stirrer speeds are an important parameter as they facilitate the gas to liquid mass transfer at the cost of increased sheer forces. Even though the cultures that successfully transitioned to a steady state can accommodate higher stirrer speeds (i. e. 1200 RPM), at the earlier stages of the fermentation the detrimental effects of the increased sheer forces hindering microbial growth could be affecting the fermentation process negatively. Increasing the stirrer speeds gradually during fermentation may be a more suitable strategy for long term fermentations.

However, the complexity of microbial systems necessitates acknowledgment of the challenges inherent in pinpointing the precise optimal working conditions amidst the interplay of multiple factors. In this regard, the employment of Design of Experiments (DOE) methodology in experimentation may be helpful in determining the “optimum” operating conditions.

- **CO1 Strain and Adaptations**

It is difficult to conclude that the CO1 strain has been superior to other *T. kivui* strains as no other strains were tested with the improved medium compositions under continuous conditions.

However, in each fermentation the transition to continuous conditions has been successful only after a reinoculation from a successful reactor was made. Even when a culture from a previous fermentation is used as inoculum as is the case of Experiment 3 suggesting the certain adaptations during fermentation may be necessary to successfully establish a steady state fermentation.

- **Availability of Glucose in Parallel to Gas Mixtures**

The availability of glucose during fermentation results in higher cell densities in almost every case, due to anabolic routes being favored, as demonstrated in section 4.4.5. Establishing higher densities of the biocatalyst is particularly desirable, especially in industrial applications, as it can lead to increased product formation, provided that gas/liquid mass transfer is sufficient to meet the metabolic demands of the cells. However, the growth observed with a $CO_2/H_2$ gas mixture alone is currently insufficient to achieve the necessary cell density in fermenters, making the inclusion of glucose a necessity to boost biomass production. Alternatively, CO could be a preferred substrate, as it is known to enhance bioenergetics (Katsvy et al., 2021), potentially leading to higher cell densities and improved overall process efficiency.

- **Industrial Feasibility**

*T. kivui* (CO1 strain) exhibits a favorable response to cultivations conducted in bubble column, especially when glucose is available as a substrate. Lack of sheer forces created by the stirrers allow the cells to function for longer durations utilizing syngas as a primary feedstock. However, the gas/liquid mass transfer provided by a bubble column appear inadequate for industrial applications (section 4.5.1). This could potentially be overcome by considering a different bioreactor setup, possibly a trickle bed reactor for increased surface areas and therefore enhancing the gas/liquid mass transfer. Consequently, rendering the process more scalable to industrial applications.

- **Formate as an alternative feedstock**

The cell densities achieved during serum bottle experiments show that the CO1 strain can indeed grow on formate to a certain extent. However, the cell densities achieved are too low to establish a continuous fermentation using formate alone as a feedstock.

According to Burger et al., (2022) *T. kivui* wild type, produces $H_2$ and $CO_2$ in presence of formate with a yield of ($Y_{H2/formate}$) 0.86 mol $mol^{-1}$. If CO1 strain behaves in a similar fashion, resting cells cultivated with another substrate can be used for producing $H_2$, greatly enhancing the potential of $H_2$ as an energy carrier by enabling an alternative storage strategy.

- **Challenges**

The primary challanges, on the other hand, in utilizing *T. kivui* as a biocatalyst stem from the complexities involved in achieving a consistent state in continuous fermentations and addressing the economic viability of the process. Persistent challenges have been encountered in each attempt to establish continuous cultures with the existing strains. Furthermore, once established, the stability of these continuous cultures proves highly susceptible to even minor fluctuations in conditions. Failure to establish standardized operational procedures hampers broader applications, particularly in industrial settings.

Regarding economic considerations, the use of syngas as a feedstock remains economically unfavorable due to its high value and diverse applications in the energy production sector. The production of acetate as a product renders the process economically less viable compared to current applications, particularly when factoring in downstream processing requirements.

# 6. Conclusion

This study aimed to develop techniques and strategies for implementing continuous gas fermentation using *T. kivui* to conduct further analyses as well as showcasing the scalability and feasibility of industrial applications.

The continuous gas fermentation has been successfully established at 66˚C and 6.4 pH over the course of this study by:

(i) Increasing the $FeSO_4*7H_2O$ concentration to 33 mg/L in the Moon Medium.

(ii) Selecting the most successful strain of CO1 under batch conditions.

(iii) Facilitating successful adaptation of the selected strain to continuous fermentation.

Established continuous cultures exhibited the following properties:

(i) Maximal growth rate ($\mu_{max}$) of 0.143 $h^{-1}$.

(ii) Maximal specific $CO_2UR$ of 62.1 mmol $g^{-1}_{CDM}$ $h^{-1}$ and specific HUR of 108 mmol $g^{-1}_{CDM}$ $h^{-1}$.

(iii) Maximal specific acetate production rate ($q_{Ac}$) of 43.29 mmol $g_{CDM}^{-1}$ $h^{-1}$.

For demonstrating industrial applications:

(i) CO1 strain has been adapted to grow on formate.

(ii) Batch fermentation in a bubble column has been established, showcasing a maximal growth rate ($\mu_{max}$) of 0.190 $h^{-1}$ with glucose, and a stationary phase.

In conclusion, the methodologies employed in this study facilitated the successful implementation of continuous cultures, opening avenues for further analyses. The rates demonstrated by *T. kivui* are marginally higher than those demonstrated by *A. woodii* ($\mu_{max}$ 0.1±0.03 $h^{-1}$, $CO_2UR$ 40.3±0.4 mmol $g^{-1}_{CDM}$ $h^{-1}$, HUR 84.1±4.2 mmol $g^{-1}_{CDM}$ $h^{-1}$, $q_{Ac}$ 21.1±2.0 mmol $g_{CDM}^{-1}$ $h^{-1}$) in similar continuous cultivations reported by Novak et al., (2021). The study highlights the strengths and limitations of continuous gas fermentation using *T. kivui*, emphasizing the need for further research to develop more robust strains and enable the formation of value-added products.

## 7. References


Alsarhan, L. M., Alayyar, A. S., Alqahtani, N. B., Khdary, N. H., (2021), 'Circular Carbon Economy (CCE): A Way to Invest $CO_2$ and Protect the Environment, a Review', *Sustainability*, vol. 13, no. 21

Appel, A. M., Bercaw, J. E., Bocarsly, A. B., Dobbek, H., DuBois, D. L., Dupuis, M., Ferry, J. G., Fujita, E., Hille, R., Kenis, P. J. A., Kerfeld, C. A., Morris, R. H., Peden, C. H. F., Portis, A. R., Ragsdale, S. W., Rauchfuss, T. B., Reek, J. N. H., Seefeldt, L. C., Thauer, R. K., Waldrop, G. L., (2013), 'Frontiers, Opportunities, and Challenges in Biochemical and Chemical Catalysis of $CO_2$ Fixation', *Chemical Reviews*, vol. 113, no. 8

Asimakopoulos, K., Gavala, H. N., Skiadas, I. V., (2018), 'Reactor Systems for Syngas Fermentation Processes: A Review', *Chemical Engineering Journal*, vol. 348, pg. 732-744

Bajracharya, S., Sarkar, O., Krige, A., Matsakas, L., Rova, U., Christakapoulos, P., (2022), 'Current Developments in Biotechnology and Bioengineering', *Elsevier*, pg. 321-351

Basen, M., Geiger, I., Henke, L., Müller, V., (2017), ‚A Genetic System for The Thermophilic Acetogenic Bacterium Thermoanaerobacter Kivui', *Applied and Environmental Microbiology*, vol. 84, no. 3

Bengelsdorf, F. R., Beck, M. H., Erz, C., Hoffmeister, S., Karl, M. M., Riegler, P., Wirth, S., Poehlein, A., Weuster-Botz, D., Dürre, P., (2018), , Chapter Four - Bacterial Anaerobic Synthesis Gas (Syngas) and $CO_2$ + $H_2$ Fermentation', *Advances in Applied Microbiology*, vol. 103

Bertsch, J., Müller, V., (2019), 'Bioenergetic Constraints for Conversion of Syngas to Biofuels in Acetogenic Bacteria', *Biotechnology for Biofuels*, vol. 8, no. 210

Biegel, E., Müller, V., (2010), 'Bacterial $Na^+$-Translocating Ferredoxin:$NaD^+$ Oxidoreductase', *PNAS*, vol. 107, no. 42

Brandon, N. P., Kurban, Z., (2017), 'Clean Energy and Hydrogen Economy', *Philosophical Transactions of the Royal Society A: Mathematical, Physical, and Engineering Sciences*, vol. 375, no. 2098

Burger, Y., Schwarz, F. M., Müller, F., (2022), ‚Formate-Driven $H_2$ Production By Whole Cells of Thermoanaerobacter Kivui', *Biotechnology for Biofuels and Bioproducts,* vol. 15, no. 48

Capaldi, R. A., Aggeler, R., (2002), 'Mechanism of The $F_1F_0$-Type ATP Synthase, a Biological Rotary Motor', *Trends in Biochemical Sciences*, vol. 27, no. 3

Chen, Y., Cheng, J., Hu, P., Wang, H., (2008), ‚Examining the Redox and Formate Mechanisms for Water–Gas Shift Reaction on Au/$CeO_2$ Using Density Functional Theory', *Surface Science*, vol. 602, no. 17

Chioccioli, M., Hankamer, B., Ross, I. L., (2014), 'Flow Cytometry Pulse Width Data Enables Rapid and Sensitive Estimation of Biomass Dry Weight in the Microalgae Chlamydomonas Reinhardtii and Chlorella Vulgaris', *PLoS One*, vol. 9, no. 5

Claassens, N. J., (2021), 'Reductive Glycine Pathway: A Versatile Route for One-Carbon Biotech', *Trends in Biotechnology*, vol. 39, no. 4

Daniel, J., Köpke, M., Simpson, S. D., (2012), 'Commercial Biomass Syngas Fermentation', *Energies*, vol. 5, no. 12

Dutta, S., Gavala, H. N., Skiadas, I. V., (2023), 'Expressing Variable Mass Transfer Coefficients for Gas Fermentation In Trickle Bed Reactors', *Chemical Engineering Journal,* vol. 475

Fast, A. G., Schmidt, E. D., Jones, S. W., Tracy, B. P., (2015), ‚Acetogenic Mixotrophy: Novel Options for Yield Improvement in Biofuels and Biochemicals Production', *Current Opinion in Biotechnology*, vol. 33, pg. 60-72

Furdui, C., Ragsdale, S. W., (2000), ‚The Role of Pyruvate Ferredoxin Oxidoreductase in Pyruvate Synthesis During Autotrophic Growth by the Wood-Ljungdahl Pathway', *The Journal of Biochemical Chemistry,* vol. 275, No. 37

Gleizer, S., Bar-on Y. M., Ben-Nissan, R., Milo, R., (2020), , Engineering Microbes to Produce Fuel, Commodities, and Food From $CO_2$', *Cell Reports Physical Science*, vol.1, no. 10

Grime, J. M., Edwards, M. A., Rudd, N. C., (2008), 'Quantitative Visualization of Passive Transport Across Bilayer Lipid Membranes', *PNAS*, vol. 105

Gong, F., Cai, Z., Li, Y., (2016), 'Synthethic Biology for $CO_2$ Fixation', *Science China*, vol. 59, no. 11

Hawkins, A. S., McTernan, P. M., Lian, H., Kelly, R. M., Adams M. W. W., 'Biological Conversion of Carbon Dioxide and Hydrogen into Liquid Fuels and Industrial Chemicals', *Current Opinion in Biotechnology*, vol. 24, no. 3

Hess, V., Poehlein, A., Weghoff, M.C., Daniel, R., Müller, V., (2014), ‚A Genome-Guided Analysis of Energy Conservation in the Thermophilic, Cytochrome-Free Acetogenic Bacterium Thermoanaerobacter Kivui', *BMC Genomics*, 15:1139

J. Rockström, W. Steffen, K. Noone, Å. Persson, S. Chapin, E. F. Lambin, T. M. Lenton, M. Scheffer, C. Folke, J. Schellnhuber, B. Nykvist, C. A. DeWit, T. Hughes, S. van der Leeuw, H. Rodhe, S. Sörlin, P. K. Snyder, R. Costanza, U. Svedin, M. Falkenmark, L. Karlberg, R. W. Corell, V. J. Fabry, J. Hansen, D. Liverman, K. Richardson, P. Crutzen, J. Foley, (2009), 'A Safe Operating Space for Humanity.', *Nature*, no. 461, pg. 472–475

Jain, S., Dietrich, H. M., Müller, V., Basen, M., (2020), ‚Formate is Required for Growth of the Thermophilic Acetogenic Bacterium Thermoanaerobacter Kivui Lacking Hydrogen-Dependent Carbon Dioxide Reductase (HDCR)', *Frontiers in Microbiology*, vol. 11, no. 59

Jin, S., Bae, J., Song, Y., Pearcy, N., Shin, J., Kang, S., Minton, N., Soucaille, P., Cho, B. K., (2020), 'Synthethic Biology on Acetogenic Bacteria for Highly Efficient Conversion of C1 Gases to Biochemicals', *International Journal of Molecular Sciences*, vol. 21, no. 20

Kaiser, S. C., Werner, S., Jossen, V., Blaschczok, K., Eibl, D., (2018), ‚Power Input Measurements in Stirred Bioreactors at Laboratory Scale', *Journal of Visualized Experiments*, vol. 135

Katsvy, A., Jain, S., Basen, M., Müller, V., (2021a), ‚Electron Carriers Involved in Autotrophic and Heterotrophic Acetogenesis in the Thermophilic Bacterium *Thermoanaerobacter Kivui*', *Extremophiles*, vol. 25, pg. 513-526

Katsvy, A., Müller, V., (2020), 'Overcoming Energetic Barriers in Acetogenic C1 Conversion', *Frontiers in Bioengineering and Biotechnology*, vol. 8

Katsvy, A., Schoelmeric, M. C., Basen, M., Müller, V., (2021b), ‚The Pyruvate:Ferredoxin Oxidoreductase of the Thermophilic Acetogen, *Thermoanaerobacter Kivui*', *FEBS openbio*, vol. 11, no. 5

Kim, S., Lindner, S. N., Aslan, S., Yishai, O., Wenk, S., Schann, K., Bar-Even, A., (2020), 'Growth of E. Coli on Formate and Methanol via the Reductive Glycine Pathway', *Nature Chemical Biology*, vol. 16, pg. 538-545

Klemps, R., Schoberth, S.M., Sahm, H., ‚Production of Acetic Acid by *Acetogenium Kivui*', *Applied Microbiology and Biotechnology*, vol. 27, pg. 229-234

Köpke, M., Simpson, S. D., (2020), 'Pollution to Products: Recycling of 'Above Ground' Carbon by Gas Fermentation', *Current Opinion in Biotechnology*, vol. 65, pg. 180-189

Kuhns, M., Trifunovic, D., Huber, H., Müller, V., (2020) ‚The rnf Complex is a $Na^+$ Coupled Respiratory Enzyme in a Fermenting Bacterium, Thermotoga Maritima', *Communications Biology*, vol. 3, no. 431

Kuzuyama, T., (2002), 'Mevalonate and Nonmevalonate Pathways for the Biosynthesis of Isoprene Units', *Bioscience, Biotechnology, and Biochemistry*, vol. 66, no. 8

Lasko, D. R., Zamboni, N., Sauer, U., (2000), ‚Bacterial Response to Acetate Challenge: A Comparison of Tolerance Among Species', *Applied Microbiology and Technology*, vol. 54, pg. 243-247

Leigh, A., Mayer, F., Wolfe, R. S., (1981), 'Acetogenium Kivui, a New Thermophilic Hydrogen-Oxidizing, Acetogenic Bacterium', *Archives of Microbiology*, 129: 275-180

Liew, E. F., Köpke, M., Simpson, S. D., (2013), 'Gas Fermentation for Commercial Biofuels Production', *Liquid, Gaseous and Solid Biofuels - Conversion Techniques*, InTech

Liu, S., (2017), 'Bioprocess Engineering: Kinetics, Sustainability, and Reactor Design', *Elsevier*, pg. 700-732

Müller, V., (2003), 'Energy Conservation in Anaerobic Bacteria', *Applied and Environmental Microbiology*, vol. 69, no. 11

Müller, V., (2019), 'New Horizons in Acetogenic Conversion of One-Carbon Substrates and Biological Hydrogen Storage', *Trends in Biotechnology*, vol. 37, no. 12

Müller, V., Chowdhury, N. P., Basen, M., (2018), 'Electron Bifurcation: A Long-Hidden Energy-Coupling Mechanism', *Annual Review of Microbiology*, vol. 72, pg. 331-353

Nguyen, H. K., Minato, T., Moniruzzaman, M., Kiyasu, Y., Ogo, S., Yoon, K. S., (2023), 'Selective Formate Production from $H_2$ And $CO_2$ Using Encapsulated Whole-Cells Under Mild Reaction Conditions', *Journal of Bioscience and Bioengineering*, vol. 136, no. 3

Novak, K., Neuendorf, C. S., Kofler, I., Kieberger, N., Klamt, S., Pflügl, S., (2021), ‚Blending Industrial Blast Furnace Gas with $H_2$ Enables Acetobacterium Woodii to Efficiently Co-Utilize CO, $CO_2$ And $H_2$', *Bioresource Technology*, vol. 323

Onyenwoke, R. U., Wiegel, J., (2015), ‚Thermoanaerobacter', *Bergey's Manual of Systematics of Archea and Bacteria*, pg. 14

Park, S. H., Park, C., Lee, J. Y., Lee, B., (2017), 'A Simple Parameterization for the Rising Velocity of Bubbles in a Liquid Pool', *Nuclear Engineering and Technology*, vol. 49, no. 4

Pavan, M., Reinments, K., Garg, S., Mueller, A. P., Marcellin E., Köpke, M., Valgepea, K., (2022), 'Advances in Systems Metabolic Engineering of Autotrophic Carbon Oxide-Fixing Biocatalysts Towards a Circular Economy', *Metabolic Engineering*, vol. 71, pg. 117-141

Pinhal, S., Ropers, D., Geiselmann, J., Jong, H., (2019), 'Acetate Metabolism and the Inhibition of Bacterial Growth by Acetate', *Journal of Bacteriology*, vol. 201, no. 13

Ragsdale, S. W., Pierce, E., (2008), 'Acetogenesis and The Wood-Ljungdahl Pathway Of $CO_2$ Fixation', *Biochimica et Biophysica Acta – Proteins and Proteomics*, vol. 1784, no. 12

Raworth, K. (2012), 'A Safe and Just Space for Humanity: Can We Live Within the Doughnut?', *Oxfam Discussion Papers*

Redl, S., Diender, M., Jensen, T. Ø., Sousa, D. Z., Nielsen, A. T., (2017), ‚Exploiting the Potential of Gas Fermentation', *Industrial Crops and Products*, vol. 106, pg. 21-30

Richardson, K., Steffen, W., Lucht, W., Bendtsen, J., Cornell, S.E., Donges, J.F., Drüke, M., Fetzer, I., Bala, G., Rockström, J., (2023), 'Earth Beyond Six of Nine Planetary Boundaries', *Science Advances*, vol. 9, no. 37

Ross, M. B., De Luna, P., Li, Y., Dinh, C. T., Kim, D., Yang, P., Sargent, E. H., (2019), 'Designing Materials for Carbon Dioxide Recycling', *Nature Catalysis*, vol. 2, pg. 648-659
Saptura, R., Khalid, M., Walvekar, R., Pariatamby, A., (2022), 'Chapter 15 – Circular Carbon Economy', Emerging Carbon Capture Technologies Towards a Sustainable Future, *Elsevier*, pg. 427-462

Schmidt, G. A., Ruedy, R., Miller, R,. Lacis, A., (2010), ‚Attribution of the Present-Day Total Greenhouse Effect', *Journal of Geophysical Research-Atmospheres*, vol. 115, no. D20

Schoelmerich, M. C., Müller, V., (2019), ‚Energy Conservation by a Hydrogenase-Dependent Chemiosmotic Mechanism in an Ancient Metabolic Pathway', *PNAS*, vol. 116, no.13

Schuhmann, K., Müller, V., (2012), 'A Bacterial Electron-Bifurcating Hydrogenase', *The Journal of Biological Chemistry*, vol. 287, no. 37

Schuhmann, K., Müller, V., (2014), 'Autotrophy at the Thermodynamic Limit of Life: A Model for Energy Conservation in Acetogenic Bacteria', *Nature Reviews Microbiology*, 12, 809-821

Schwarz, F. M., Müller, V., (2020), ‚Whole-Cell Biocatalysis for Hydrogen Storage and Syngas Conversion to Formate Using a Thermophilic Acetogen', *Biotechnology for Biofuels*, vol. 13, no. 32

Schwarz, F. M., Schuhmann, K., Müller, V., (2018), , Hydrogenation of $CO_2$ at Ambient Pressure Catalyzed by a Highly Active Thermostable Biocatalyst', *Biotechnology and Biofuels*, vol. 11, no. 237

Sokic-Lazic, D., Rodrigues de Andrade, A., Minteer, S. D., (2011), 'Utilization of Enzyme Cascades for Complete Oxidation of Lactate in an Enzymatic Biofuel Cell', *Electrochimica Acta*, vol. 56, no.28

Tan, X., Huang, X., Zou, Y., Yu, T., Zhao, Y., Huang, X., (2018), 'Synthesis and Characterization of Co-Doped Brookite Titania Photocatalysts with High Photocatalytic Activity', *Transactions of Tianjin University*, vol. 24, pg. 111-122

Tokiwa, Y., Calabia, B. P., Ugwu, C. U., Aiba, S., (2009), 'Biodegradability of Plastics', *International Journal of Molecular Sciences*, vol. 10, no. 9

Ulmer, U., Dingle, T., Duchesne, P. N., Morris, R. H., Tavasoli, A., Wood, T., Ozin, G. A., (2019), 'Fundamentals and Applications of Photocatalytic CO2 Methanation', *Nature Communications*, vol. 10, no. 3169

Wang, S., Huang, H., Kahnt, J., Mueller, A. P., Köpke, M., Thauer, R. K., (2013 b), , NADP-Specific Electron-Bifurcating [FeFe]-Hydrogenase in a Functional Complex with Formate

Dehydrogenase in Clostridium Autoethanogenum Grown on CO', *Journal of Bacteriology*, vol. 195, no. 19

Wang, S., Huang, H., Kahnt, J., Thauer, R. K., (2013 a), , A Reversible Electron-Bifurcating Ferredoxin- and Nad-Dependent [FeFe]-Hydrogenase (HydABC) in Moorella Thermoacetica', *Journal of Bacteriology*, vol. 195, no. 6

Weghoff, M. C., Müller, V., (2016), ‚CO Metabolism in the Thermophilic Acetogen Thermoanaerobacter Kivui', *Applied and Environmental Microbiology*, vol. 82, no. 8

Whitman, W. G., (1962), 'A Preliminary Experimental Confirmation of the Two Film Theory of Gas Absorption', *International Journal of Heat and Mass Transfer*, vol. 5, no. 5

Wood, H. G., Ragsdale, S. W., Pezacka, E., (1986), ‚The Acetyl-CoA Pathway: A Newly Discovered Pathway of Autotrophic Growth', *Trends in Biochemical Sciences*, vol. 11, no. 1, pg. 14-18

Yilmaz, F., Al Shehri, T., Luomi, M., Alturki, F. M., (2023), ‚Enhancing the G20's Climate Change Policy Agenda with the Circular Carbon Economy Index', *T20 Policy Brief*

Zhao, R., Ding, P., Wei, P., Zhang, L., Liu, Q., Luo, Y., Li, T., Lu, S., Shi, X., Gao, S., Asiri, A. M., Wang, Z., Sun, X., (2021), 'Recent Progress in Electrocatalytic Methanation of $CO_2$ at Ambient Conditions', *Advanced Functional Materials*, vol. 31, no. 13

Zhou, Y., Han, L. R., He, H. W., Sang, B., Yu, D. L., Feng, J. T., Zhang, X., (2018), 'Effects of Agitation, Aeration and Temperature on Production of a Novel Glycoprotein GP-1 by Streptomyces Kanasenisi ZX01 and Scale-Up Based on Volumetric Oxygen Transfer Coefficient', *Molecules*, vol. 23, no. 1

# 8. Appendix

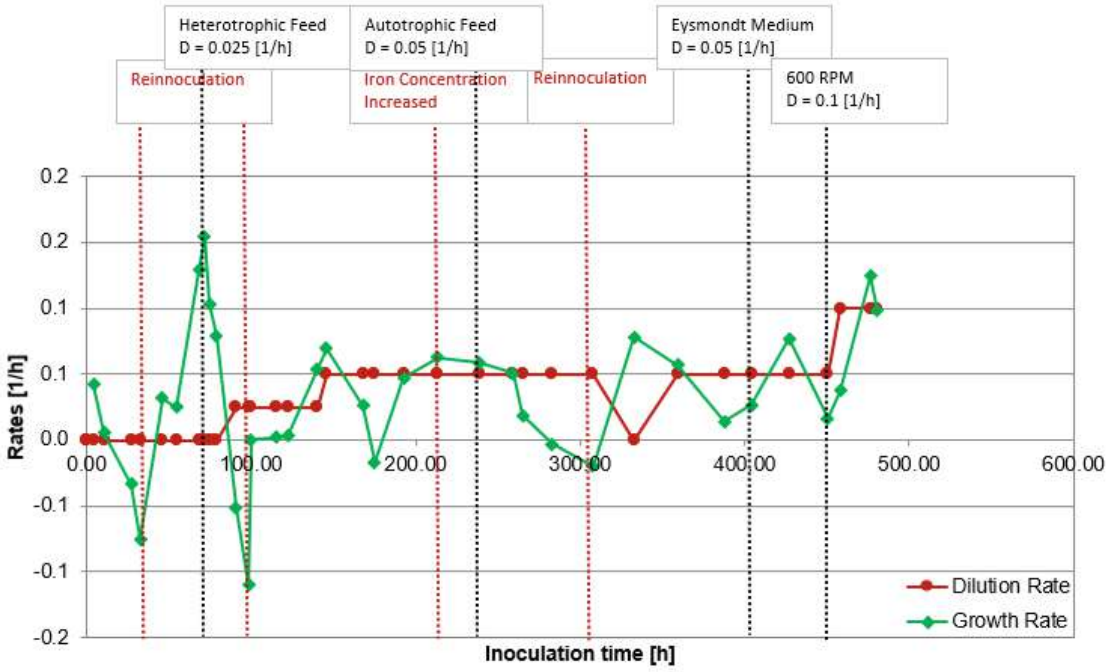


***Figure A. 1 Experiment 1*** **Reactor 3 Growth Rates and Dilution Rates at 66 ˚C and pH 6.4 see Section 4.2 for information on Mediums and Strains**

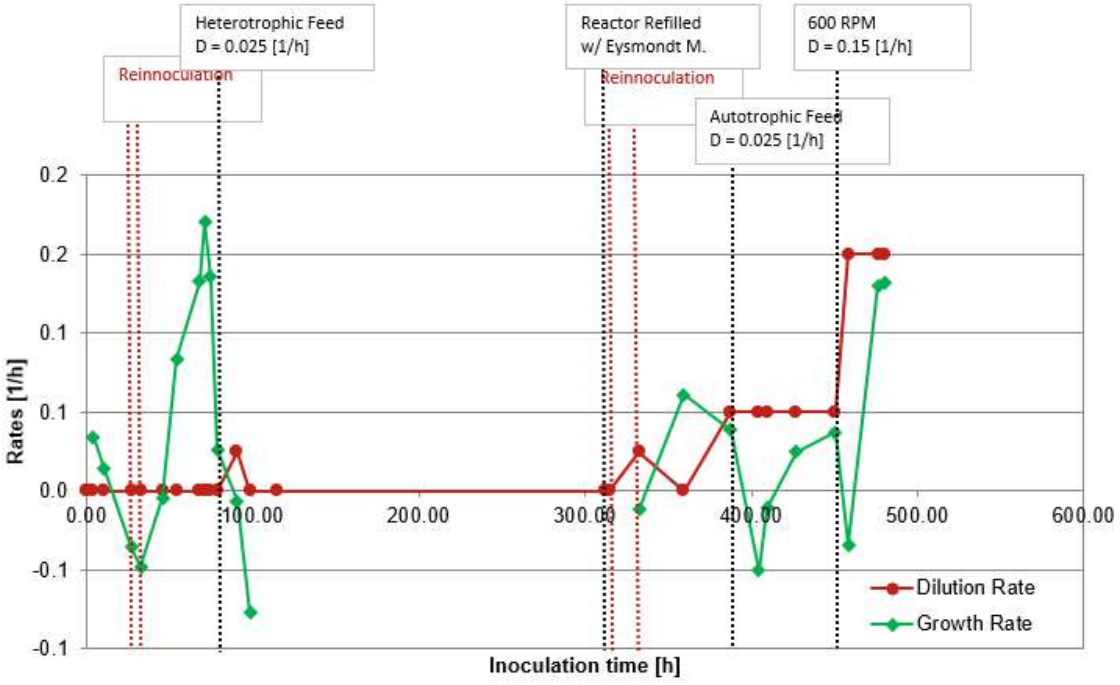


***Figure A. 2*** **Experiment 1 Reactor 4 Growth Rates and Dilution Rates at 66 ˚C and pH 6.4 see Section 4.2 for information on Mediums and Strains**

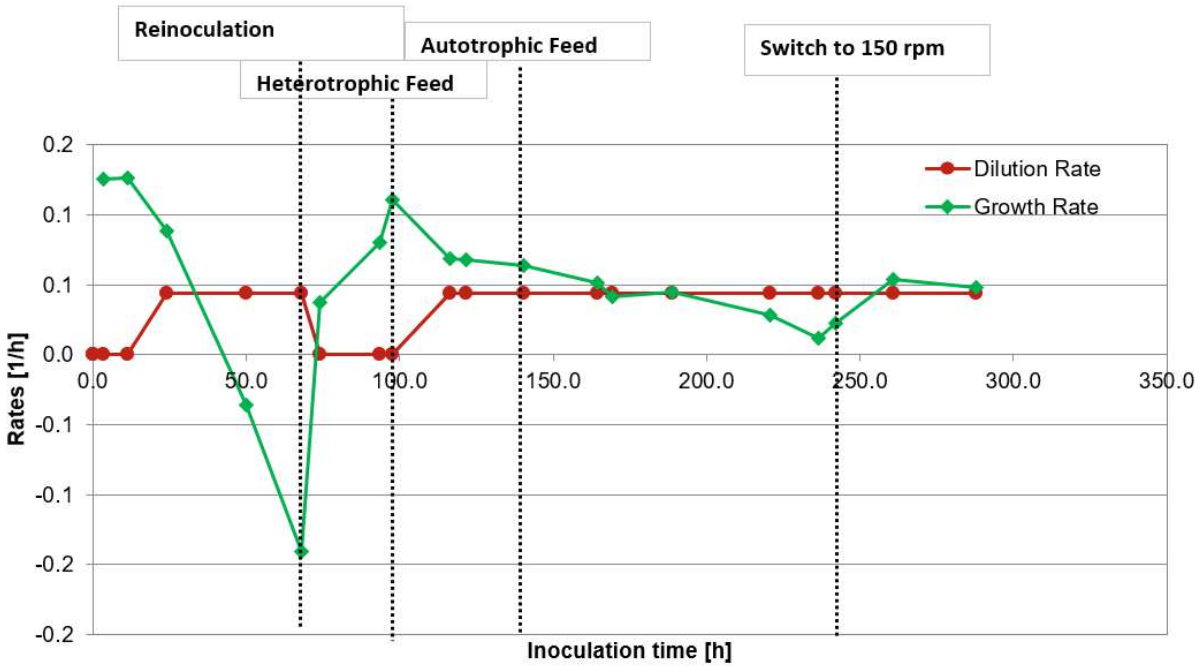


**Figure A. 3 Experiment 3 Reactor 1 Growth Rates and Dilution Rates, Modified Moon Medium, CO1 strain at 66 ˚C and pH 6.4**

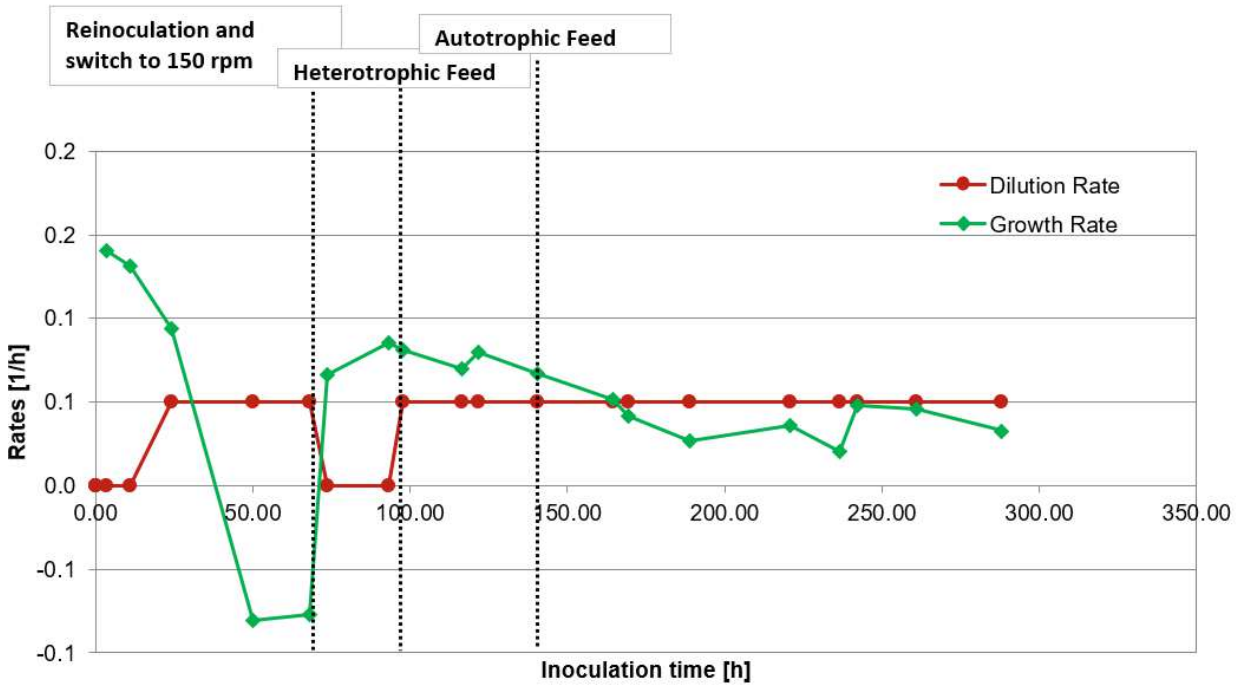


**Figure A. 4 Experiment 3 Reactor 3 Growth Rates and Dilution Rates, Modified Moon Medium, CO1 strain at 66 ˚C and pH 6.4**

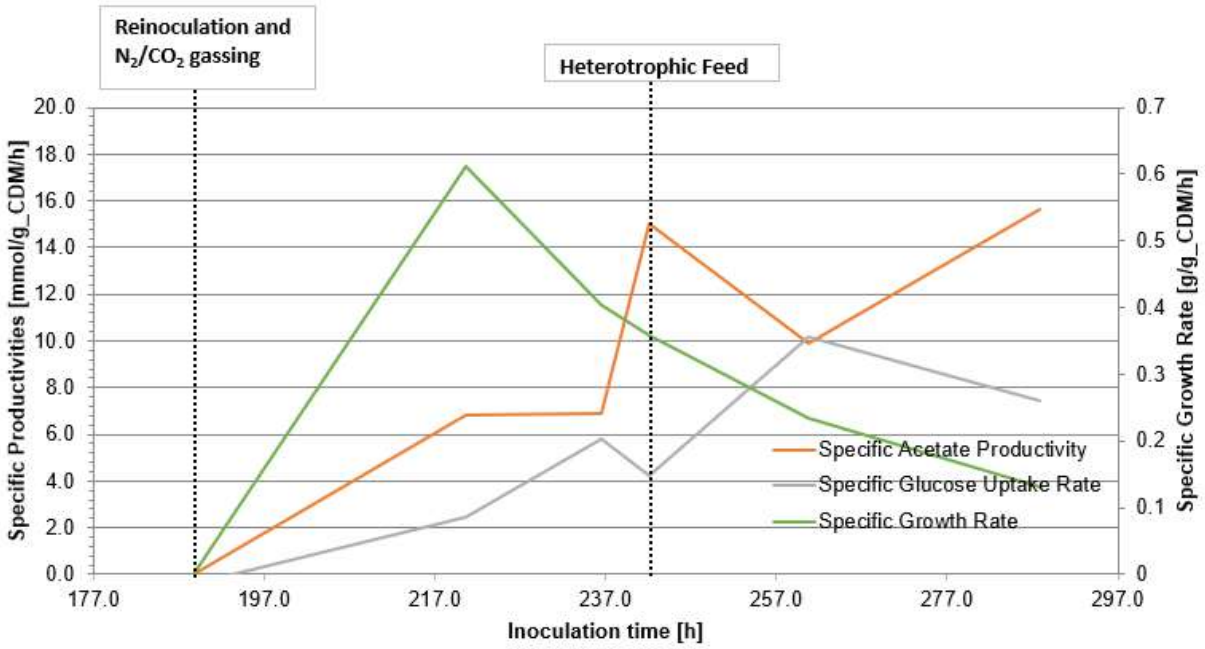


**Figure A. 5 Experiment 3 Reactor 2 Specific Rates with Modified Moon Medium, CO1 strain at 66 ˚C and pH 6.4**